



HAL
open science

Experimental study of the edge radial electric field in different drift configurations and its role in the access to H-mode at ASDEX Upgrade

U. Plank, D. Brida, G. Conway, T. Happel, A. Hubbard, T. Pütterich, C. Angioni, M. Cavedon, R. Dux, T. Eich, et al.

► To cite this version:

U. Plank, D. Brida, G. Conway, T. Happel, A. Hubbard, et al.. Experimental study of the edge radial electric field in different drift configurations and its role in the access to H-mode at ASDEX Upgrade. *Physics of Plasmas*, 2023, 30 (4), 10.1063/5.0102763 . hal-04276326

HAL Id: hal-04276326

<https://hal.science/hal-04276326>

Submitted on 9 Nov 2023

HAL is a multi-disciplinary open access archive for the deposit and dissemination of scientific research documents, whether they are published or not. The documents may come from teaching and research institutions in France or abroad, or from public or private research centers.

L'archive ouverte pluridisciplinaire **HAL**, est destinée au dépôt et à la diffusion de documents scientifiques de niveau recherche, publiés ou non, émanant des établissements d'enseignement et de recherche français ou étrangers, des laboratoires publics ou privés.

This is the author's peer reviewed, accepted manuscript. However, the online version of record will be different from this version once it has been copyedited and typeset.

PLEASE CITE THIS ARTICLE AS DOI: 10.1063/5.0102763

AIP/POP22-AR-DPP63-00854R

Experimental Study of the Edge Radial Electric Field in Different Drift Configurations and its Role in the Access to H-mode at ASDEX Upgrade

U. Plank,¹ D. Brida,¹ G. D. Conway,¹ T. Happel,¹ A. E. Hubbard,² T. Pütterich,¹ C. Angioni,¹ M. Cavedon,³ R. Dux,¹ T. Eich,¹ R. Fischer,¹ P. Hennequin,⁴ and the ASDEX Upgrade Team^{1, a)}

¹⁾*Max-Planck-Institut für Plasmaphysik, Boltzmannstraße 2, 85748 Garching, Germany*

²⁾*Plasma Science and Fusion Center, MIT, Cambridge, Massachusetts 02129, USA*

³⁾*Dipartimento di Fisica “G. Occhialini”, Università di Milano-Bicocca, 20126 Milano, Italy*

⁴⁾*Laboratoire de Physique des Plasmas, CNRS, Sorbonne Université, Ecole polytechnique, Institut Polytechnique de Paris, 91120 Palaiseau, France*

(*Electronic mail: Ulrike.Plank@ipp.mpg.de)

(Dated: 13 March 2023)

This is the author's peer reviewed, accepted manuscript. However, the online version of record will be different from this version once it has been copyedited and typeset.

PLEASE CITE THIS ARTICLE AS DOI: 10.1063/5.0102763

The formation of the equilibrium radial electric field (E_r) has been studied experimentally at ASDEX Upgrade (AUG) in L-modes of 'favourable' (ion ∇B -drift towards primary X-point) and 'unfavourable' (ion ∇B -drift away from primary X-point) drift configuration, in view of its impact on H-mode access, which changes with drift configuration. Edge electron and ion kinetic profiles, impurity velocity and mean-field E_r profiles across the separatrix are investigated, employing new and improved measurement techniques. The experimental results are compared to local neoclassical theory as well as to a simple 1D scrape-off layer (SOL) model. It is found that in L-modes of matched heating power and plasma density the upstream SOL E_r and the main ion pressure gradient in the plasma edge are the same for either drift configuration, whereas the E_r well in the confined plasma is shallower in unfavourable compared to favourable drift configuration. The contributions of toroidal and poloidal main ion flows to E_r , which are inferred from local neoclassical theory and the experiment, cannot account for these observed differences. Furthermore, it is found that in L-mode the intrinsic toroidal edge rotation decreases with increasing collisionality and it is co-current in the banana-plateau regime for all different drift configurations at AUG. This gives rise to a possible interaction of parallel Pfirsch-Schlüter flows in the SOL with the confined plasma. Thus, the different H-mode power threshold for the two drift configurations can not be explained in the same way at AUG as suggested by LaBombard *et al.* for Alcator C-Mod¹. Finally, comparisons of E_r profiles in favourable and unfavourable drift configuration at the respective confinement transitions show that also there the E_r gradients are all different, which indirectly indicates a different type or strength of the characteristic edge turbulence in the two drift configurations.

^{a)}See U. Stroth *et al.* 2022 (<https://doi.org/10.1088/1741-4326/ac207f>) for the ASDEX Upgrade Team.

I. INTRODUCTION

The underlying mechanism for the transition from L- to H-mode confinement (L-H transition) has been of interest since the discovery of the H-mode on the ASDEX tokamak². The equilibrium radial electric field, E_r , at the plasma edge is often considered to be responsible for the transition into H-mode, as its gradients are connected to a background $E \times B$ shear flow, which can stabilize the underlying edge turbulence³. The condition for the H-mode access is then that the shearing-rate of the $E \times B$ velocity ($v_{E \times B}$) is large enough to suppress the characteristic turbulence at the plasma edge. At ASDEX Upgrade (AUG) it has been found in experiments in standard configuration (lower single-null favourable drift configuration) that the minimum of $v_{E \times B}$, which is a proxy for its shear in these conditions, is constant at the L-H transition for a wide range of densities, magnetic field strengths and different isotopes (D and H)⁴. This finding indicates not only that $v_{E \times B}$ and its connected shear play a crucial role for the confinement transition, but also suggests indirectly that the underlying edge turbulence may be unchanged for this parameter range.

On a macroscopic scale the transition into H-mode occurs if sufficient auxiliary heating power is applied. The so called H-mode power threshold (P_{LH}) exhibits many dependencies that are not always consistent between the different tokamaks⁵. However, one robust observation that has been made on several devices is that P_{LH} changes by more than a factor of two if either the toroidal magnetic field is reversed or if the configuration is switched from lower single-null (LSN) to upper single-null (USN)^{2,6-9}. A magnetic configuration in which the ∇B -drift of the main ions ($v_{\nabla B, i}$) points *towards* the primary X-point exhibits a lower P_{LH} than one in which $v_{\nabla B, i}$ points *away* from the primary X-point. For this reason, the first one is termed 'favourable' drift configuration, whereas the latter is referred to as 'unfavourable' drift configuration.

As of yet it has not been clarified unambiguously why P_{LH} alters with drift configuration, but it is considered that it is connected to changes in the local edge parameters and the resulting edge turbulence. Previous experimental observations on several tokamaks including DIII-D, AUG and WEST have consistently shown that E_r in the confined plasma edge region is different between the two drift configurations¹⁰⁻¹². The resulting differences in the E_r gradients could directly influence the criterion of turbulence suppression by $E \times B$ mean shear flows. Divertor profile measurements together with scrape-off layer (SOL) modelling

This is the author's peer reviewed, accepted manuscript. However, the online version of record will be different from this version once it has been copyedited and typeset.

PLEASE CITE THIS ARTICLE AS DOI: 10.1063/1.50102763

results also show changes of the upstream E_r in the SOL with the switch of the drift configuration^{13,14}. Modifications in the SOL E_r could also impact the strength of the $E \times B$ shear flows and, as such, lead to differences in the H-mode onset between the two drift configurations. At Alcator C-Mod it was observed that the SOL flows change with the drift direction and that they possibly set a boundary condition for the intrinsic toroidal edge rotation v_ϕ , which, in turn, influences E_r ¹. In the study of Alcator C-Mod the L-H transition occurred in both drift configurations if v_ϕ was of the same size and co-current, leading to a threshold behaviour in $v_{E \times B}$ at the L-H transition, which could then be related to the increased P_{LH} in unfavourable drift configuration. Another possible mechanism recently discussed is connected to a change in the characteristic edge turbulence with reversed ∇B -drift direction, which would also lead to the existence of the I-mode in unfavourable drift configuration¹⁵. It is conceivable that such a change in the edge turbulence leads to modified requirements for the $E \times B$ shear flow needed to suppress the characteristic edge turbulence, resulting in a higher P_{LH} in unfavourable drift configuration. Other theories deal with the differences in the parallel momentum transport due to the up-down asymmetry of the magnetic geometry, which could impact both the edge turbulence and the mean-field E_r simultaneously, but differently for the two drift configurations^{16,17}. Also ion orbit losses close to the boundary of the confined plasma¹⁸ or the interaction with neutrals penetrating into the confined plasma – both mechanisms have been found to depend on the exact magnetic configuration^{19–21} – have been considered as possible candidates for the observed differences in E_r and the altered H-mode power threshold in the two drift configurations since long.

In view of possible explanations for the altered H-mode access conditions between the different drift configurations, the here presented experimental work focuses on the characterization of the equilibrium edge radial electric field and related quantities, like the main ion pressure gradient and the edge rotation, in L-mode and at the L-H transition in the two different drift configurations. Thanks to new and improved diagnostic techniques, special emphasis can be put on the analysis of the E_r gradient across the separatrix, which connects confined plasma and SOL. The measurements are compared with predictions of local neoclassical theory in the confined plasma and with a simple 1-D model for the upstream E_r in the SOL. Based on these results it is discussed whether the theories introduced above could be valid candidates to explain the increased P_{LH} in unfavourable drift configuration. Furthermore, the current observations are brought in context with previous experimental

findings in order to identify key mechanisms important for the L-H transition in general, which then can serve for validation of theoretical models aiming to predict the L-H transition self-consistently.

The paper is organized as follows: Section II reviews the properties of the edge and SOL E_r . Section III introduces the design of the experiments and the analysis methods. Section IV compares the H-mode power threshold in the different drift configurations and Section V describes the corresponding evolution of the outer E_r gradient during the transition from L- to H-mode. Section VI compares edge and outer divertor target profiles in L-modes of different drift configurations at matched density and heating power. Section VII presents results on the behaviour of E_r in L-mode with changing density and heating power. Section VIII compares E_r profiles at the confinement transition in favourable and unfavourable drift configuration. Section IX summarizes the results from this experimental study and discusses the conclusions drawn from them.

II. PROPERTIES OF E_r FROM THE PLASMA EDGE TO THE SCRAPE-OFF LAYER

The radial electric field E_r can be determined starting with the momentum balance equation for a plasma species α :

$$m_\alpha n_\alpha \frac{d\mathbf{u}_\alpha}{dt} = q_\alpha n_\alpha (\mathbf{E} + \mathbf{u}_\alpha \times \mathbf{B}) - \nabla p_\alpha - \nabla \cdot \mathbf{\Pi}_\alpha + \mathbf{R}_\alpha. \quad (1)$$

Here m_α is the mass, n_α the number density, \mathbf{u}_α the fluid velocity, q_α the charge and p_α the scalar pressure of α . $\mathbf{\Pi}_\alpha$ is the viscous stress tensor and \mathbf{R}_α the friction force between species α and all other plasma species. \mathbf{E} and \mathbf{B} are the local electric and magnetic field, respectively.

Under stationary conditions, i.e. $m_\alpha n_\alpha d\mathbf{u}_\alpha/dt = 0$, and if friction forces are neglected, Equation 1 simplifies in the first order of the Larmor radius $r_{L,\alpha}$ to²²:

$$\nabla p_\alpha = q_\alpha n_\alpha (\mathbf{E} + \mathbf{u}_\alpha \times \mathbf{B}). \quad (2)$$

This equation has to be fulfilled by each single plasma species α , but in the following we concentrate on the relation of E_r with the properties of the main ion (i) and electron (e) species.

In the confined plasma E_r is determined by the main ion quantities and Equation 2 can be re-written as the well-known radial force balance equation:

$$E_r = \frac{\nabla_r p_i}{Z_i e n_i} + v_i \times B = \frac{\nabla_r p_i}{Z_i e n_i} - v_{\theta,i} B_\phi + v_{\phi,i} B_\theta, \quad (3)$$

with $\nabla_r \equiv \partial/\partial R$, Z_i the charge number, $v_{\theta,i}$ the poloidal and $v_{\phi,i}$ the toroidal velocity of the main ion species i and B_ϕ and B_θ the toroidal and poloidal magnetic field components (with their respective signs). Please note that we assume a right-handed (R, Θ, Φ) system, which is in accordance with the coordinate system of AUG. Further details on AUG's coordinate system and the sign conventions can be found in Appendix A. Besides this, in the present work v_ϕ is positive if it is in the same direction as I_p (i.e. co-current), unless it is stated differently.

In H-mode it is often observed that $v_i \times B$ is small^{23,24} and, thus,

$$E_r \approx \frac{\nabla_r p_i}{Z_i e n_i} < 0. \quad (4)$$

In the SOL an expression for the electric field parallel to the magnetic field lines E_{\parallel} can be derived from Equation 1²⁵:

$$E_{\parallel} = \frac{j_{\parallel}}{\sigma_{\parallel}} - \frac{1}{en_e} \nabla_{\parallel} p_e - \frac{0.71}{e} \nabla_{\parallel} T_e. \quad (5)$$

Here j_{\parallel} is the parallel current density and σ_{\parallel} is the parallel electrical conductivity. n_e , p_e and T_e are the electron density, pressure and temperature, respectively. This parallel force balance equation is also known as Ohm's law of the SOL since it connects the electric field with the current-density²⁶.

The electric potential V_{pl} at the outer mid-plane (OMP) can be obtained by integrating Equation 5 in the SOL from the outer divertor target plate (denoted with 't') upstream to the OMP. For an analytic solution, the following assumptions are made: $j_{\parallel}/\sigma_{\parallel}$ is neglected, since it is found to be small, at least in LSN favourable drift configuration L-modes^{27,28}, and $p_e = p_{e,t} \left(\frac{T_e}{T_{e,t}}\right)^a$ is assumed²⁹. This gives the following expression for V_{pl} :

$$V_{pl} = \frac{2.8}{e} T_{e,t} + V_{fl} + \frac{0.71+a}{e} (T_{e,OMP} - T_{e,t}), \quad (6)$$

where V_{fl} is the potential of the electrically floating divertor target plates and $a = \frac{0.47}{\log(T_{e,OMP}/T_{e,t})}$ at AUG²⁷. E_r in the SOL at the OMP is then calculated as:

$$E_r = -\nabla_r V_{pl}. \quad (7)$$

In the conduction-limited regime $T_{e,OMP} \gg T_{e,t}$. If also V_{fl} is small, Equation 6 simplifies with Equation 7 to²⁶:

$$E_r \approx -\frac{1}{e} \nabla_r T_{e,OMP} > 0. \quad (8)$$

Combining Equation 8 and Equation 4 shows that E_r changes sign close to or at the separatrix (i.e. at the normalized poloidal magnetic flux $\rho_{pol} = 1$). From this the following structure of E_r is expected in the plasma edge and SOL (see also Figure 2): In the confined region E_r exhibits a negative well, with its minimum ($E_{r,min}$) located near, but inside the separatrix. In the SOL, E_r has a hill structure, with $E_{r,max}$, the maximum of the hill, and a decay towards the far SOL. The negative E_r gradient, entirely located in the confined region, is termed the 'inner' E_r gradient in the following. In contrast, the 'outer' E_r gradient is the positive one at the separatrix, which connects $E_{r,min}$ and $E_{r,max}$. In the paradigm of the critical $E \times B$ shear needed to suppress the edge turbulence at the L-H transition, it has not been identified yet, whether both E_r gradients are responsible for the L-H transition or if either the inner or the outer E_r gradient is the important one. At AUG recent experimental observations indicate that the turbulence suppression starts at the location of the inner E_r gradient³⁰.

III. METHODOLOGY

In the following, the design of the experiments and the different analysis methods are introduced.

A. Discharge Design

Figure 1 shows a typical L-H transition plasma discharge at AUG (the reference discharge, # 35842). It is in LSN favourable drift configuration, with a toroidal magnetic field of $B_\phi = -2.5$ T at the geometric axis, a plasma current of $I_p = +800$ kA and a safety factor of $q_{95} = -5$ (see also Appendix A for the sign conventions of AUG). Several versions of this reference discharge were performed and analysed, with modifications of different parameters (plasma density, drift configuration, heating method).

For most of the L-H transition discharges electron cyclotron resonance heating (ECRH) power ramps were applied to trigger the transition into H-mode (see Figure 1a). For this type

This is the author's peer reviewed, accepted manuscript. However, the online version of record will be different from this version once it has been copyedited and typeset.

PLEASE CITE THIS ARTICLE AS DOI: 10.1063/1.50102763

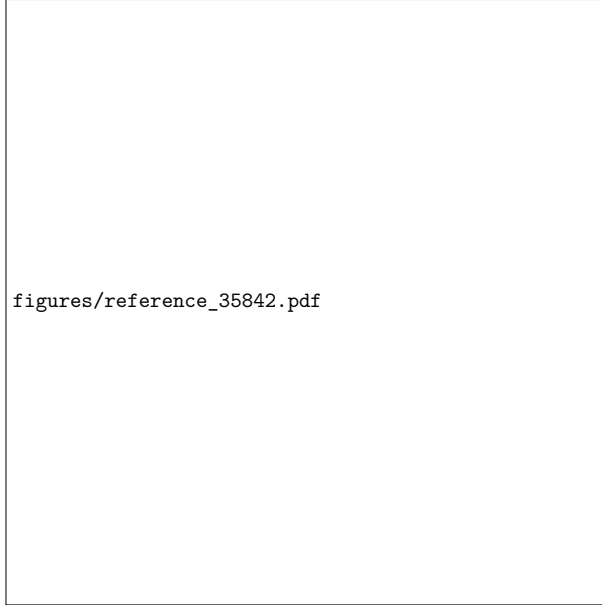


FIG. 1. *Reference L-H transition discharge in LSN favourable drift configuration.* Time traces of (a) auxiliary heating power (green, red), the net input power (blue) and main chamber radiation (purple). Time evolution of (b) the line-averaged electron density at the plasma core (black) and edge (blue) and of the stored thermal energy (green). (c) Evolution of the minimum of E_r (black) and the signal of the outer shunt current measurement (grey), which can be used as indicators of the L-H and H-L back transition. The L-H transitions and the H-L back transitions of this discharge are marked by the vertical dashed and dotted lines, respectively.

of heating scheme the label 'ECRH' is used in the following. X2 mode heating at 140 GHz was employed, which deposits the heating power near the magnetic axis. The power was stepwise increased by 200 to 300 kW to pinpoint P_{LH} . Each power step was chosen to be at least 150 ms long to reach steady-state conditions (the confinement time $\tau_E = 100 - 140$ ms in the investigated L-mode conditions). During each heating step, a slow strike-point sweep (covering approx. 2 cm in about 100 ms) along the outer divertor target was accommodated for a better coverage of Langmuir probe (LP) measurements. At the end of each heating step, a 10 ms long blip of the neutral beam injection (NBI) with a nominal power of 2.5 MW per

blip was applied for charge exchange recombination spectroscopy (CXRS) measurements on fully-stripped low-Z impurities (boron and nitrogen). Each NBI blip is a small perturbation to the plasma and increases the net input power (P_{net} , see Equation 9) by about 200 kW for approximately 50 ms. This amount of heating is within the uncertainties of the P_{LH} determination, but it was regularly observed that the additional power of the NBI blip triggered the L-H transition. However, the H-mode could then only be sustained if after the perturbation by the NBI blip sufficient additional ECRH was applied. Otherwise the plasma transited back into L-mode after the perturbation by the NBI blip. Furthermore, if no NBI blips were applied, then the plasma entered H-mode in the subsequent ECRH step, which confirms the assumption that the additional power introduced by the NBI blip is of the same size as the ECRH power steps.

In a few L-H transition experiments also dominant ion heating was applied. For these discharges the NBI was modulated and the frequency of the modulation was stepwise increased, such that effectively heating power steps of 200 to 300 kW were achieved³¹. For this heating scheme also a small amount of central ECRH (200 to 300 kW) was applied continuously. It is referred to this heating scheme as 'NBI+ECRH' in the following.

Figure 1b shows the time traces of the core and edge line-averaged densities of the deuterium cyanide laser interferometer ($\bar{n}_{e,\text{core}}$ and $\bar{n}_{e,\text{edge}}$)³², which correspond to approximate ρ_{pol} positions of 0.4 and 0.95, respectively. The target density for the reference discharge was chosen to be $\bar{n}_e \approx 4.5 \times 10^{19} \text{m}^{-3}$, as it is the density for which the L-H transition occurs at the lowest heating power in deuterium (D) plasmas in standard drift configuration at AUG ($\bar{n}_{e,\text{min}}$)³³. To achieve this density, a D fuelling rate of about 3×10^{21} el/s from the divertor was needed. In USN discharges, where the pumping efficiency is lower due to the lack of a cryostatic pump in the upper divertor, substantially lower fuelling rates are needed to get this desired density. Also, if the intrinsic B concentration was too low for CXRS measurements, small amounts of N were injected. The low-Z impurity content was monitored with the CXRS diagnostics³⁴ and found to be below 1%, leading to an average Z_{eff} of about 1.2 – 1.4³⁵.

Starting from the reference discharge several modifications were applied to it and the impact on the L-H transition power, on the density, temperature and E_r profiles at the OMP and at the outer divertor target in the vicinity of the separatrix was studied. The plasma density and the heating mix (ECRH and NBI) was altered for both favourable

and unfavourable drift configurations. Pairs of L-H transition discharges in forward and reversed magnetic field direction were performed in both LSN and USN configurations. In this way also a possible impact of the different divertor geometries (closed divertor in LSN and open divertor in USN) on P_{LH} could be addressed for either drift configuration. The exact magnetic geometries with their respective drift directions and how they can be achieved at AUG is described in more detail in Appendix A.

In the upcoming plots shades of the colour blue are used for plasmas in the LSN favourable drift configuration, purple for USN favourable drift configuration, red for LSN unfavourable drift configuration and orange for USN unfavourable drift configuration.

B. Determination of the L-H Transition Time and Power

The L-H transition time point (t_{LH}) was determined using several different diagnostic signals. One important feature of the L-H transition is the sudden increase of the edge density and the stored thermal plasma energy W_{MHD} (see Figure 1b). Further measurements employed to pinpoint t_{LH} are the shunt current measurements of the inner and outer target tiles, $I_{\text{t,i}}$ and $I_{\text{t,o}}$, and poloidal magnetic field fluctuation (\dot{B}_{θ}) measurements of two Mirnov coils located close to the primary and secondary X-points. Also the minimum of the edge radial electric field, here determined with HeII spectroscopy (HES)³⁶ (see Section III E), shows a sudden drop at the L-H transition, and is, therefore, a useful indicator of the L-H transition (see Figure 1c). A more detailed description on the use of these different diagnostics to determine t_{LH} can be found in previous AUG-related publications on the L-H transition^{4,31}. Taking into account the information of these different signals allows for a determination of t_{LH} with high precision (± 1 ms uncertainty).

In favourable drift configuration the plasma enters a dithering phase at t_{LH} , which is termed I-phase at AUG^{37–39}, and found also at other machines^{40–42}. It is regularly observed that the plasma develops from the I-phase, which exhibits periodic oscillations, into a more bursty state, which is often identified as a type-III ELMy H-mode, before the type-I ELMy H-mode is observed. Concomitant with this development a continuous increase in plasma confinement is observed. The I-phase oscillations have a frequency of a few kHz⁴³ and can be seen as a modulation on $I_{\text{t,i}}$ and $I_{\text{t,a}}$, and also on \dot{B}_{θ} . Therefore, these signals are a precise indicator of t_{LH} .

The I-phase should not be confused with the I-mode. The latter is, besides L- and H-mode, another confinement regime, which is normally observed in unfavourable drift configuration^{6,9,44}. The I-mode exhibits improved energy, but L-mode-like particle confinement^{6,9,44,45} and can be operated as a stable regime^{9,46}. The I-mode occurs and evolves, in terms of heating power, between L-mode and H-mode (see also Figure 5). Therefore, in unfavourable drift configuration, the L- to H-mode transition can be separated into a transition from L- to I-mode (L-I transition) at t_{LI} and a transition from I- to H-mode (I-H transition) at t_{IH} . For the determination of t_{LI} and t_{IH} the same diagnostics as described above for the determination of t_{LH} are used. Additional information is taken from edge temperature and reflectometer (density fluctuation) measurements, as the I-mode is characterized by a pedestal structure in T_i and T_e and the existence of a weakly-coherent mode (WCM) at approximately 100 kHz, located at the plasma edge⁹. In I-mode no or only a weak increase of the edge plasma density is observed⁴⁷, while a sharp increase of the plasma density occurs only at the H-mode onset at t_{IH} .

The definitions of t_{LH} , t_{LI} and t_{IH} here are consistent with the ones used in previous L-H transition and I-mode studies at AUG^{4,46}. If not stated differently, the edge electron density and temperature profiles (which are referred to as 'kinetic' in the following), and the E_r profiles, which are shown in this article, are taken from stable L-mode or I-mode phases. For this, the profiles were averaged over time windows of 50 – 150 ms duration. The time windows in the stable phases extend until at most 15 ms before the defined L-H, L-I or I-H transition time. The ion temperature and impurity rotation profiles are taken from the NBI blip closest to this time window, averaged over the entire length of the NBI blip.

The H-mode power threshold P_{LH} in favourable drift configuration (I- and H-mode power thresholds P_{LI} and P_{IH} in unfavourable drift configuration) is defined as the net input power P_{net} at t_{LH} (t_{LI} and t_{IH}), where

$$P_{net} = P_{heat} - \frac{dW_{MHD}}{dt} = P_{OH} + P_{aux} - \frac{dW_{MHD}}{dt}. \quad (9)$$

P_{heat} is hereby the absorbed heating power from all heating contributions, namely the Ohmic power P_{OH} introduced through the plasma current and all auxiliary heating contributions $P_{aux} = P_{NBI} + P_{ECRH}$, corrected for their respective losses^{31,48,49}. P_{net} also includes a correction for changes of the plasma stored energy dW_{MHD}/dt . The main chamber radiation $P_{rad,main}$, reconstructed from bolometer measurements⁵⁰, is not taken into account in the

calculation of P_{net} , since it has been found to show little variation at the L-H transition between the different discharges and it is also small, between 300 and 500 kW, for all investigated discharges. Time traces of P_{net} , P_{ECRH} , P_{NBI} and $P_{\text{rad,main}}$ are depicted for the reference discharge in Figure 1a.

C. Power Balance Analysis

Power balance analysis was performed in order to deduce the surface-integrated edge ion and electron heat fluxes ($Q_{i,\text{edge}}$ and $Q_{e,\text{edge}}$) at the L-H transition. For this, the transport code ASTRA was employed in an interpretive mode⁵¹. To determine the exact heat deposition profile of the ECRH, the microwave beam tracing code TORBEAM⁵² was used and for the NBI deposition profile, the real-time code RABBIT⁴⁹ was coupled to ASTRA.

Consistent with previous L-H transition studies at AUG^{31,48}, the total edge ion and electron heat fluxes were evaluated at the radial position of $\rho_{\text{pol}} \approx 0.98$, where ρ_{pol} is the normalized poloidal magnetic flux.

D. Edge Kinetic Profile Measurements and Alignment

For an exact reconstruction of the magnetic equilibrium in all investigated magnetic configurations, the Grad-Shafranov equation is coupled with the current-diffusion equation⁵³. Furthermore, other constraints on the equilibrium, e.g. the measurements of the thermal pressure profile, are taken into account in the framework of Bayesian probability theory^{32,53}. This leads to an uncertainty of about 1 cm for the separatrix position in L-mode at the outer mid-plane, which corresponds to $\Delta\rho_{\text{pol}} \approx 0.014$ for the here investigated plasma shapes⁵⁴.

The T_e and n_e profiles presented in this work were determined using integrated data analysis (IDA) of several diagnostics³². The T_e profiles were shifted radially in such a way that the prediction for $T_{e,\text{sep}}$, employing Spitzer-Härm power balancing⁵⁵⁻⁵⁷, was fulfilled. The radial shifts of the n_e profiles were determined from the radial shifts of the Thomson scattering and the He I beam data⁵⁸, which measure T_e and n_e at the same location simultaneously. The impurity temperature (T_{imp}) and the toroidal and poloidal velocity ($v_{\phi,\text{imp}}$ and $v_{\theta,\text{imp}}$) profiles, which were determined with CXRS^{59,60}, were not shifted radially. Furthermore, in this study it is assumed that the main ion temperature T_i equals the temperature of the

impurity ions T_{imp} , which is a valid assumption in AUG H-modes⁶¹, but has been found to be incorrect at other machines like DIII-D²⁴. For the uncertainty estimation of the main ion pressure gradient profiles $((\nabla_r p_i)/(en_i))$, a relative shift of the T_i profiles of ± 5 mm with respect to the validated n_e profiles was applied.

E. E_r Profile Measurements and Alignment

The edge E_r profiles at the OMP were determined using Doppler V- and W-band reflectometry in X-mode (DR)^{62,63} and HeII spectroscopy (HES)³⁶. The latter relies on the Doppler spectroscopy of singly ionized helium⁶⁴. Thermal He is periodically injected by a piezoelectric gas valve with on-off times of about 50 ms. The neutral He particles get ionized and excited by plasma interactions (mainly electron impact ionization and excitation) and the emitted light is detected by a spectroscopic system. From the width of the characteristic spectral line the local He¹⁺ temperature, from its Doppler shift the He¹⁺ flow speed and from its intensity the local He¹⁺ density can be determined³⁶. In this way this technique allows for a local measurement of E_r employing the radial force balance equation (see Equation 3) for the singly ionized He particles instead of for the main ions³⁶. It turns out that this E_r measurement technique is restricted to a region of ρ_{pol} 0.98 to approximately 1.02, i.e. the region of the outer E_r gradient, whereas the inner E_r gradient can not be resolved by HES. Furthermore, the spectroscopic system has an acquisition time of $\Delta t_{\text{acquisition}} = 2.45$ ms, which makes this E_r measurement technique not suitable to detect transient phenomena or events which are faster than this time scale, e.g. a resolved measurement of the I-phase oscillations.

For the localisation of the DR- E_r data, the validated n_e profiles (see Section III D) were used. A detailed comparison between the DR and HES diagnostics and a forward model developed for the HES method showed excellent agreement between the two E_r measurements in all four investigated drift configurations³⁶. The determined E_r profiles across the separatrix agree in both size and shape of the outer E_r gradient and its radial position. From these comparisons it was also concluded that the turbulence phase velocity, which would be detected by DR, but not by HES, must be small (no larger than a few hundreds of m/s) in the plasma edge in L-mode.

An example measurement of the three different edge E_r diagnostics is shown for the ref-

This is the author's peer reviewed, accepted manuscript. However, the online version of record will be different from this version once it has been copyedited and typeset.

PLEASE CITE THIS ARTICLE AS DOI: 10.1063/1.50102763

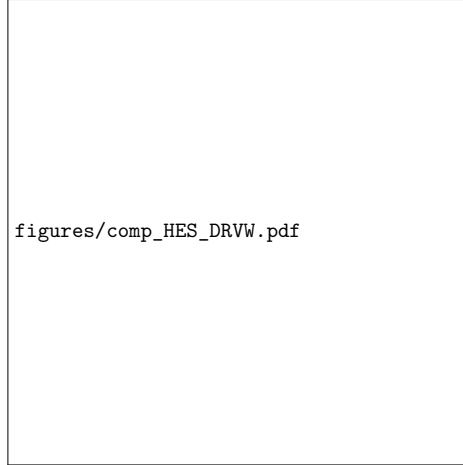


FIG. 2. *Comparison of measured edge E_r profiles.* E_r profiles detected with V- and W-band Doppler reflectometry (DR, stars and squares) and HeII spectroscopy (HES, circles) in a stable L-mode phase of the reference discharge (see Figure 1). The profiles are plotted against the normalized poloidal flux coordinate ρ_{pol} , where $\rho_{\text{pol}} = 1$ denotes the separatrix. The negative E_r gradient located entirely in the confined plasma is termed 'inner' E_r gradient, whereas the positive E_r gradient connecting $E_{r,\text{min}}$ and $E_{r,\text{max}}$ is termed 'outer' E_r gradient.

reference discharge # 35842 in Figure 2. Here and in the following radial profiles are plotted against ρ_{pol} . Since the agreement between the different E_r diagnostics is excellent (below 1 kV/m deviation), normally only one E_r profile is shown in the course of this article. However, a comparison between the different diagnostics has always been performed, if measurements from them were available. In the following these symbols are used (see also Figure 2): stars denote E_r measurements from the V-band DR, squares from the W-band DR and circles from HES.

The $E_{r,\text{min}}$ and $E_{r,\text{max}}$ values were determined as the minimal and maximal measured values of E_r in the radial region $\rho_{\text{pol}} \approx 0.98 - 1$ and $\rho_{\text{pol}} \approx 0.995 - 1.02$, respectively.

F. Neoclassical Calculations

For the deduction of the poloidal and toroidal main ion flows, and with equation 3 also of the edge radial electric field, local neoclassical (NC) theory was employed. The NC calculations were performed with the code NEOART⁶⁵, which was bench-marked against the NEO code⁶⁶ for a subset of discharges in the different drift configurations. For a given impurity, NEOART solves the set of linear coupled equations of the parallel velocity in all collision regimes for each charge state⁶⁷. NEOART includes the collisions of the considered impurity ion with the main plasma ions i and all other impurities. The experimentally determined radial profiles of the electron density and temperature (n_e and T_e), the main ion temperature (T_i) and the density and toroidal rotation of the impurity (n_{imp} and $v_{\phi,\text{imp}}$) are given as input to the code, which calculates the NC poloidal main ion and impurity velocity profiles ($v_{\theta,i}$ and $v_{\theta,\text{imp}}$) and the differential of the toroidal main ion rotation ($v_{\phi,i}$) to a given $v_{\phi,\text{imp}}$.

In all the NEOART calculations it was assumed that besides the main ion species (D) only one impurity species is present in the plasma edge (B or N). If possible, the corresponding impurity density n_{imp} was deduced from the radiance of the CXRS measurements³⁴. To calculate the main ion density, n_i , the charge state distribution of the investigated impurity has to be known. This was determined assuming the coronal ionisation equilibrium. Since the actual impurity density at the plasma edge could not always be determined experimentally, two different assumptions were made and the resulting n_i profiles compared. For the first one it was assumed that the impurity density is the one of the fully ionized impurity, e.g. $n_N = n_{N^{7+}}$. For the second approach a constant impurity concentration of 1% was assumed over the investigated radial range, i.e. $n_{\text{imp}} = 0.01 n_e$. It was found that the resulting n_i profile does not differ strongly, using the two different assumptions on n_{imp} . Therefore, if no n_{imp} measurements were available, a constant impurity concentration of 1% was assumed, which is in good agreement with the experimentally determined Z_{eff} values from Bremsstrahlung measurements³⁵.

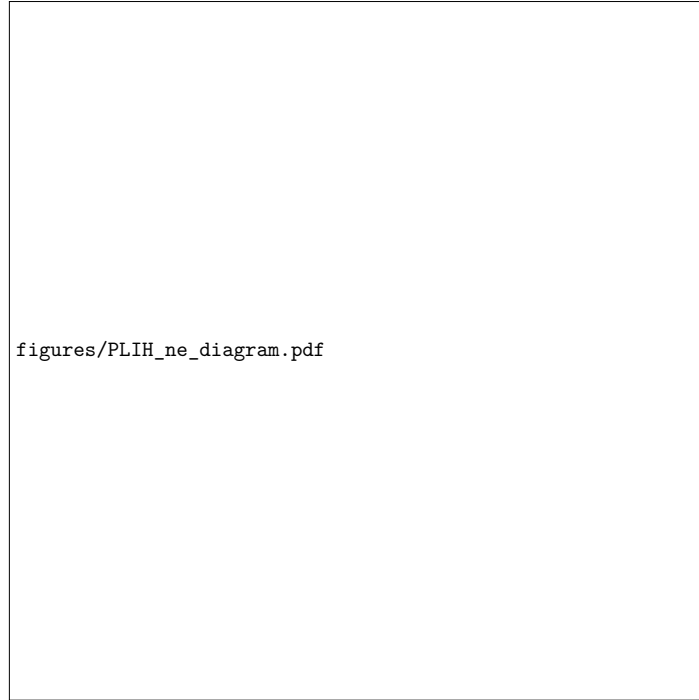


FIG. 3. *Density dependence of the H-mode power threshold in favourable and unfavourable drift configuration.* Net input power at the L-H transition (P_{LH} , blue and purple) and I-H transition (P_{IH} , red and orange) versus line-averaged core electron density, \bar{n}_e . Circles denote dominant ECRH heating, whereas squares denote a mixture of NBI and ECRH heating. The arrow at the data point in unfavourable drift configuration at low density indicates that this is a lower boundary for P_{IH} . Also, for the favourable drift configuration plasmas, the region of the density minimum and the low and high density branches of P_{LH} are denoted.

IV. H-MODE POWER THRESHOLD IN DIFFERENT DRIFT CONFIGURATIONS

Figure 3 shows the net input power P_{net} at the L-H transition (P_{LH} , blue and purple) in favourable drift configuration (LSN and USN) and at the I-H transition (P_{IH} , red and orange) in unfavourable drift configuration (LSN and USN), plotted against the line-averaged

This is the author's peer reviewed, accepted manuscript. However, the online version of record will be different from this version once it has been copyedited and typeset.

PLEASE CITE THIS ARTICLE AS DOI: 10.1063/1.50102763

electron density $\bar{n}_e = \bar{n}_{e,\text{core}}$. In all plotted discharges $|B_\phi| = 2.5\text{ T}$ at the geometric axis, whereas $|I_p| = 0.8\text{ MA}$ for the LSN and $|I_p| = 1\text{ MA}$ for the USN discharges. The values of the power threshold agree within one drift configuration, regardless whether LSN or USN plasmas are investigated, which indicates that the exact divertor configuration (open vs. closed divertor, see also Appendix A for the divertor geometry) has minor impact on the power threshold in these discharges. Furthermore, there is no difference seen in the H-mode power threshold between the 0.8 MA and the 1 MA data-sets, which is in agreement with previous observations at AUG of favourable drift configuration plasmas, where for plasmas located in the high-density branch no dependence of P_{LH} on I_p is found⁶⁸.

As observed at several tokamaks, P_{IH} in unfavourable drift configuration is 2 – 3 times higher than P_{LH} in favourable drift configuration^{9,69,70}. For P_{LH} the typical parabolic dependency on \bar{n}_e is found, with $\bar{n}_{e,\text{min}} \approx 4.0 \times 10^{19}\text{ m}^{-3}$, the commonly observed value of the density minimum at AUG in favourable drift configuration^{48,68}. However, P_{IH} does not show such a parabolic dependence on \bar{n}_e , instead it exhibits a large scatter for a fixed \bar{n}_e . This behaviour of P_{IH} has already been mentioned in previous work from AUG⁶⁹, where it was pointed out that it might be connected to the exact development of the preceding I-mode. Another reason for the larger scatter in P_{IH} could be connected to the fact that the unfavourable drift configuration data are from pure ECRH and mixed NBI+ECRH heated plasmas. From L-H transition studies in favourable drift configuration it is known that P_{LH} depends on the employed heating method in the low-density branch. This observation is connected to a critical $Q_{i,\text{edge}}$ needed to enter H-mode and the different efficiency of ECRH and NBI to heat the ions^{31,48} as well as the impact of external torque input on P_{LH} ^{48,71}, which occurs with NBI, but not with ECRH.

Since power balance calculations could not be performed for all of the discharges under study, mostly, due to a lack of full-radius T_i profiles, it cannot be confirmed whether $Q_{i,\text{edge}}$ is the same at the I-H confinement transition for discharges with either heating mix. It appears, however, that the discharges with NBI have a lower P_{IH} than their counterparts with ECRH only, which indicates that $Q_{i,\text{edge}}$ could also be an important quantity at the I-H confinement transition. Furthermore, there is one data point at low density in Figure 3, marked with an upwards facing arrow, which would confirm the critical role of $Q_{i,\text{edge}}$ for the H-mode transition physics also in unfavourable drift configuration. The given value of P_{IH} for this discharge (AUG # 37375) is only a lower boundary, since the plasma neither transited

into I- nor H-mode. Power balance calculations for this data point give $Q_{i,\text{edge}} \approx 0.59\text{MW}$, which is below the critical $Q_{i,\text{edge}}$ of about 0.71 MW needed to transit from L- into I-mode in these plasma conditions at AUG⁶⁹.

Another interesting observation is that some of the discharges in *unfavourable* drift configuration did not enter I-mode before transiting into H-mode, but a direct transition from L- into H-mode occurred, with the typical signatures of an I-phase during the transition. As stated in Section III B, the I-phase is always observed in *favourable* drift configuration at the L- to H-mode transition. In Figure 3, the unfavourable drift configuration cases with a direct L-H transition are highlighted in grey. As of yet it is not clear which conditions or parameters determine whether an I-mode or an I-phase occurs in the transition from L- to H-mode in unfavourable drift configuration, however, the two regimes have not yet been observed to appear simultaneously. Figure 3 suggests that I-phases in unfavourable drift configuration plasmas tend to appear at higher densities.

V. EVOLUTION OF E_r IN THE TRANSITION FROM L- TO H-MODE

A. Favourable Drift Configuration

Figure 4 shows the time evolution of global and edge plasma quantities in a LSN discharge in favourable drift configuration (AUG # 36983), transiting from L-mode (light blue) to H-mode (dark blue) via I-phase (blue). The presented discharge was density feed-back controlled to $\bar{n}_e \approx 3 \times 10^{19}\text{m}^{-3}$. Except for this lower density, the design of the discharge was as for the reference discharge # 35842, introduced in Section III. For such discharges, namely ECRH discharges located on the low-density branch of P_{LH} (see Figure 3), it is regularly observed that the confinement improvement at or directly after the L-H transition is not as pronounced as for the same type of L-H discharges at higher density, at least for the same plasma current (compare also Figures 4b and 1b). For example, in this low density discharge no pure type-I ELMy H-mode was observed, although the auxiliary heating power was increased to 3.5 MW. However, the development of $(\nabla_r p_i)/(en_i)$ and E_r during the L-H transition, as shown in Figure 4d, are found to be the same for all investigated discharges in favourable drift configuration (in both LSN and USN plasmas), independent of the plasma density and type of applied auxiliary heating.

This is the author's peer reviewed, accepted manuscript. However, the online version of record will be different from this version once it has been copyedited and typeset.
PLEASE CITE THIS ARTICLE AS DOI: 10.1063/1.50102763

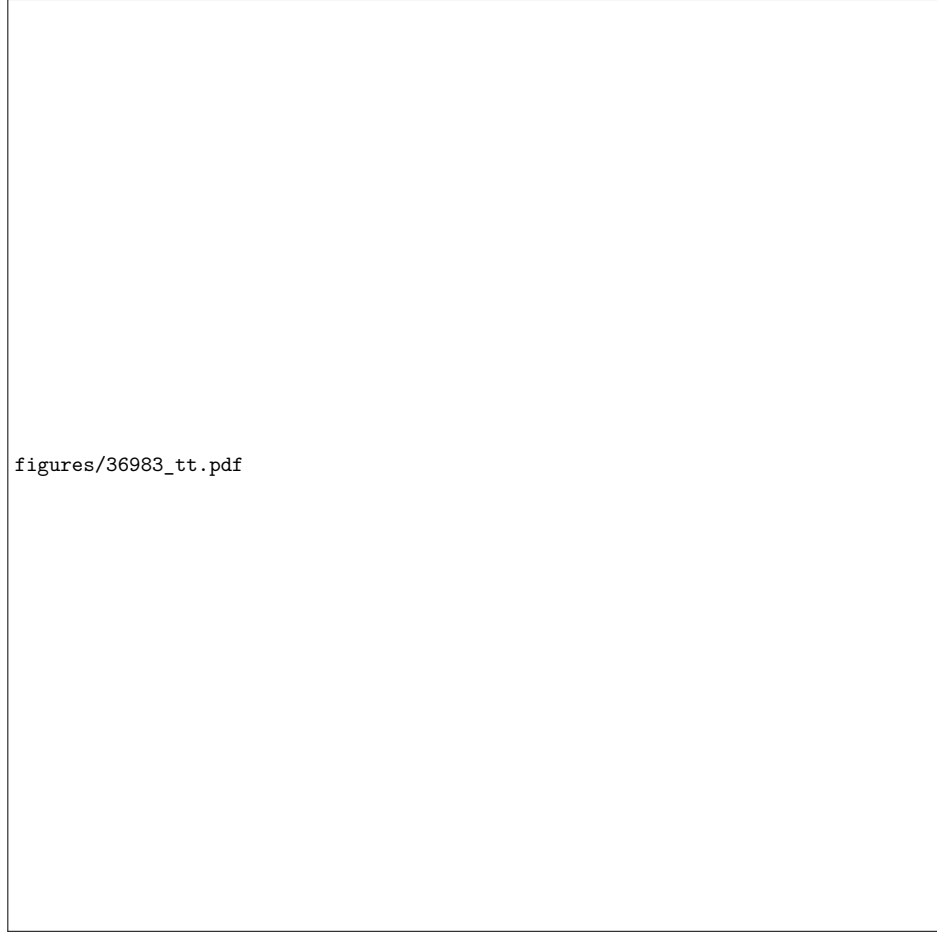


FIG. 4. *Evolution of the L-H transition in favourable drift configuration.* Time traces of (a) NBI and ECRH power (red, green), net input power (blue) and main chamber radiation (purple) during an L-H transition. Corresponding evolution of (b) line-averaged electron density in the plasma core and edge (dark blue, blue), stored plasma energy (green), edge electron and ion temperature (cyan and orange) and (c) magnetic field fluctuations (black), inner and outer shunt current signals (silver and grey) and the minimum of the edge radial electric field (blue). (d) Evolution of the outer E_r gradient and $(\nabla_r p_i)/(en_i)$ at the plasma edge during the L-H transition.

The E_r profiles across the separatrix (Figure 4d) as well as the time evolution of the E_r minimum (Figure 4c) were measured with the HES diagnostic (see Section III E). Each E_r profile is averaged over the acquisition time of 2.45 ms, thus, these are measurements of the mean-field E_r structure. It should be noted that the HES measurements are such that during each He gas puff of about 50 ms length several profiles are acquired (see also the time trace of $E_{r,\min}$ in Figure 4c). Therefore, the development of the E_r profile during the L-H transition does not look continuous in Figure 4d, which can, however, be attributed to the timing of the He gas modulation with respect to the L-H transition. The analysis of several L-H transitions has shown that the development of E_r , i.e. the steepening of the E_r gradients, is rather continuous during the L-H transition. Figure 4d also depicts $(\nabla_r p_i)/(en_i)$ at the plasma edge for the different confinement regimes, which was reconstructed from the experimental edge T_i and n_e profiles, assuming $n_i = n_e$.

The L-H transition is triggered by the NBI blip, at 2.78 s, at a power of about $P_{LH} = 1.1$ MW. As can be seen in Figure 4b in the time traces of plasma density and stored energy (blue and green) the confinement improvement at the L-H transition is weak. Although $T_{e,\text{edge}}$, measured at $\rho_{\text{pol}} = 0.98$, exhibits some variation, the overall trend is that $T_{e,\text{edge}}$ (cyan) and $T_{i,\text{edge}}$ (orange) increase from L- to I-phase to H-mode, which is also confirmed by the steepening of $(\nabla_r p_i)/(en_i)$ (see Figure 4d). The analysis of several L-H transition discharges has shown that $(\nabla_r p_i)/(en_i)$ steepens mainly due to a steepening of the T_i gradient, whereas the logarithmic edge density gradient is rather constant in the different confinement regimes^{36,72}.

The evolution of the edge E_r from L- to H-mode follows to first order the evolution of $(\nabla_r p_i)/(en_i)$. However, in L-mode systematic deviations between $(\nabla_r p_i)/(en_i)$ and E_r are observed, which indicates that the contribution from the plasma flows ($v_i \times B$) to E_r is non-negligible in L-mode. This is discussed in more detail in Section VI. Furthermore, the measurements show that during the entire L-mode phase the outer E_r gradient exhibits only little variation. During the I-phase the outer E_r gradient steepens gradually and $E_{r,\min}$ reaches values of approximately -15 kV/m. These $E_{r,\min}$ values have been observed previously at the H-mode onset at AUG^{73,74}. In H-mode $E_{r,\min}$ values of -20 to -28 kV/m are reached, which are typical values for AUG H-modes⁶¹. At the same time as $E_{r,\min}$ deepens, $E_{r,\max}$ in the SOL increases slightly from L-mode to H-mode, where the radial positions of the two extremes are relatively constant.

B. Unfavourable Drift Configuration

Figure 5 shows a typical L-I-H transition in a LSN unfavourable drift configuration discharge (AUG #37298). This discharge is the equivalent to the previously presented favourable drift L-H transition discharge shown in Figure 4. In #37298 the I-mode (red in Figure 5) starts at around 2.68 s and is soon after followed by the H-mode (dark red) at around 2.77 s. At both confinement transitions (L-I and I-H) $P_{\text{net}} \approx 3 \text{ MW}$, which is more than a factor of 2 higher than the corresponding P_{LH} in favourable drift configuration (see Figure 3). Please note, P_{net} at the I-H transition often tends to be lower compared to P_{net} at the L-I transition, which was already reported in earlier I-mode studies at AUG⁶⁹. This can be attributed to a lower Ohmic power in the I-mode, due to a higher plasma temperature, and to a stronger change of W_{MHD} at the L-I transition. Both terms contribute to P_{net} via Equation 9.

In the following we report on general features of the development of the edge profiles during the L-I-H transition, which have been observed to be the same regardless of the exact plasma configuration (LSN or USN unfavourable drift), the plasma density and the type of applied heating power. As can be seen in Figure 5b $T_{e,\text{edge}}$, $T_{i,\text{edge}}$ and W_{MHD} (cyan, orange and green) start to increase at the L-I transition, whereas the plasma density (blue) stays rather constant and only starts to rise at the I-H transition. Correspondingly, $(\nabla_r p_i)/(en_i)$ steepens gradually from L- to I- to H-mode. Also E_r follows this trend, but in L-mode (light red) discrepancies between $(\nabla_r p_i)/(en_i)$ and E_r are observed, as has been also found in favourable drift configuration. The measurements show that the edge E_r profiles can be entirely positive in unfavourable drift L-modes and, thus, $v_{E \times B}$ points then in the ion diamagnetic drift direction. This observation will be discussed in more detail in Section VIA. In I-mode $E_{r,\text{min}}$ deepens gradually and at values of approximately -15 kV/m the transition into H-mode occurs, consistent with previous I-mode studies⁷⁵. Interestingly, this $E_{r,\text{min}}$ value is about the same as the $E_{r,\text{min}}$ values reached during I-phase at the transition into H-mode in favourable drift configuration plasmas⁴. However, this very similar $E_{r,\text{min}}$ value does not imply that the same outer E_r gradients are reached at the H-mode onset, since the E_r values in the SOL and their radial position can also be different. This is at least the case for the here presented discharge pair in favourable and unfavourable drift configuration (compare Figures 5 and 4).

This is the author's peer reviewed, accepted manuscript. However, the online version of record will be different from this version once it has been copyedited and typeset.

PLEASE CITE THIS ARTICLE AS DOI: 10.1063/1.50102763

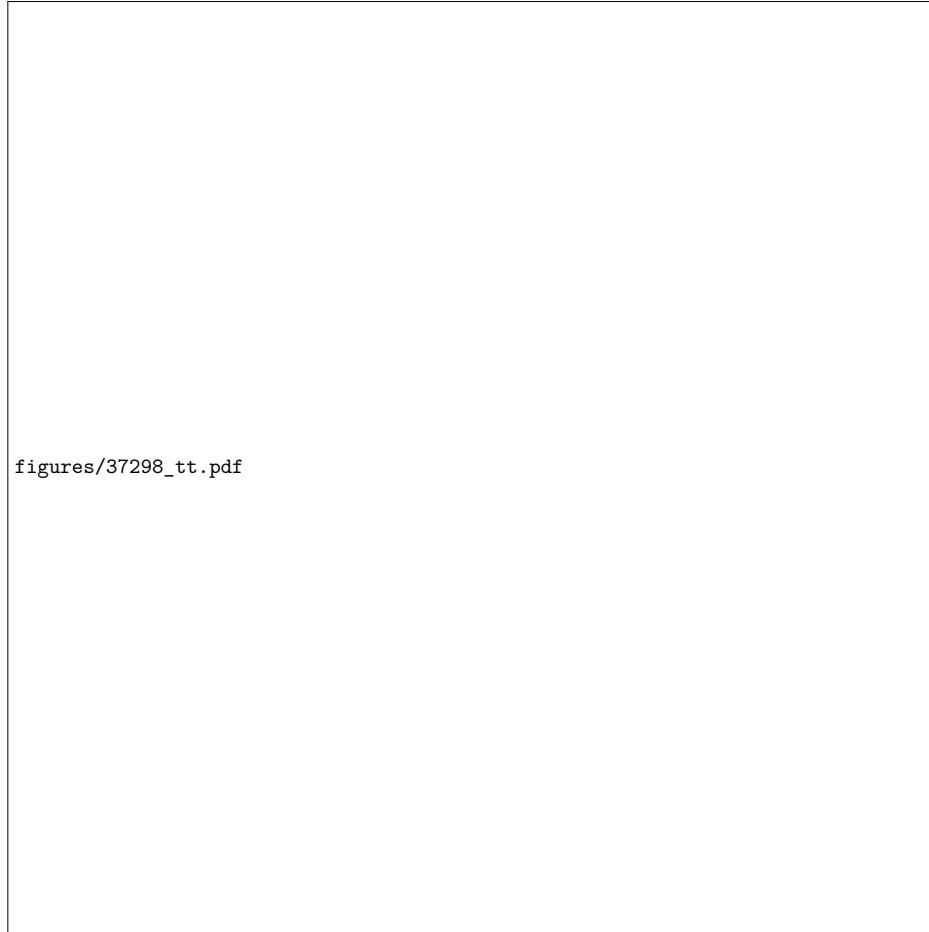


FIG. 5. *Evolution of the L-I-H transition in unfavourable drift configuration.* Time traces of (a) NBI and ECRH power (red, green), net input power (blue) and main chamber radiation (purple) during an L-I-H transition. Corresponding evolution of (b) line-averaged electron density in the plasma core and edge (dark blue, blue), stored plasma energy (green), edge electron and ion temperature (cyan and orange) and (c) magnetic field fluctuations (black), inner and outer shunt current signals (silver and grey) and the minimum of the edge radial electric field (red). (d) Evolution of the outer E_r gradient and $(\nabla_r p_i)/(en_i)$ at the plasma edge during the L-I-H transition.

VI. COMPARISON OF L-MODES IN DIFFERENT DRIFT CONFIGURATIONS AT SAME HEATING POWER AND SAME PLASMA DENSITY

In order to understand the differences and similarities of edge kinetic and E_r profiles as well as the SOL conditions of L-mode plasmas in the two different drift configurations and to study their impact on the transition into an improved confinement regime, pairs of fav./unfav. L-modes with matched parameters, i.e. same heating power and same plasma density, are compared in this section. First we investigate LSN plasmas at low density and then USN plasmas at medium density. Based on the observed differences, conclusions are drawn on which mechanisms could be possible candidates to influence E_r in L-mode.

A. Lower Single-Null and Low Density

In the two investigated L-mode phases a gas puff rate $\Gamma_D \approx 0.7 \times 10^{21}$ el/s was used, which results in a plasma density of about 2.8×10^{19} m⁻³. However, as can be seen in Figure 6b, the edge density is slightly lower in the unfavourable drift case (#37375, light red) compared to the favourable drift case (#36983, blue). Furthermore, in both L-mode phases $P_{\text{ECRH}} = 600$ kW, which is for the favourable drift configuration directly before the L-H transition.

1. Edge Kinetic and E_r Profiles

Figure 6 shows the measured edge electron and ion kinetic profiles and the toroidal rotation and E_r profiles for the two L-mode phases. The edge T_e profiles are the same in favourable and unfavourable drift configuration, whereas n_e is slightly lower in unfavourable drift configuration between $\rho_{\text{pol}} = 0.95$ and 0.98. The logarithmic edge density gradient, $1/L_{n_e} := -(\nabla_r n_e)/n_e$, is found to be the same within the measurement uncertainties in the confined plasma region. Also the T_i profiles agree within the measurement uncertainties, which leads to very similar $(\nabla_r p_i)/(en_i)$ profiles in favourable and unfavourable drift configuration (see Fig. 6f).

In both drift configurations the edge T_i profiles are flatter than the edge T_e profiles, which is regularly observed. The ratio of $T_{i,\text{sep}}/T_{e,\text{sep}}$ is the same for either drift configuration and

This is the author's peer reviewed, accepted manuscript. However, the online version of record will be different from this version once it has been copyedited and typeset.

PLEASE CITE THIS ARTICLE AS DOI: 10.1063/5.0102763

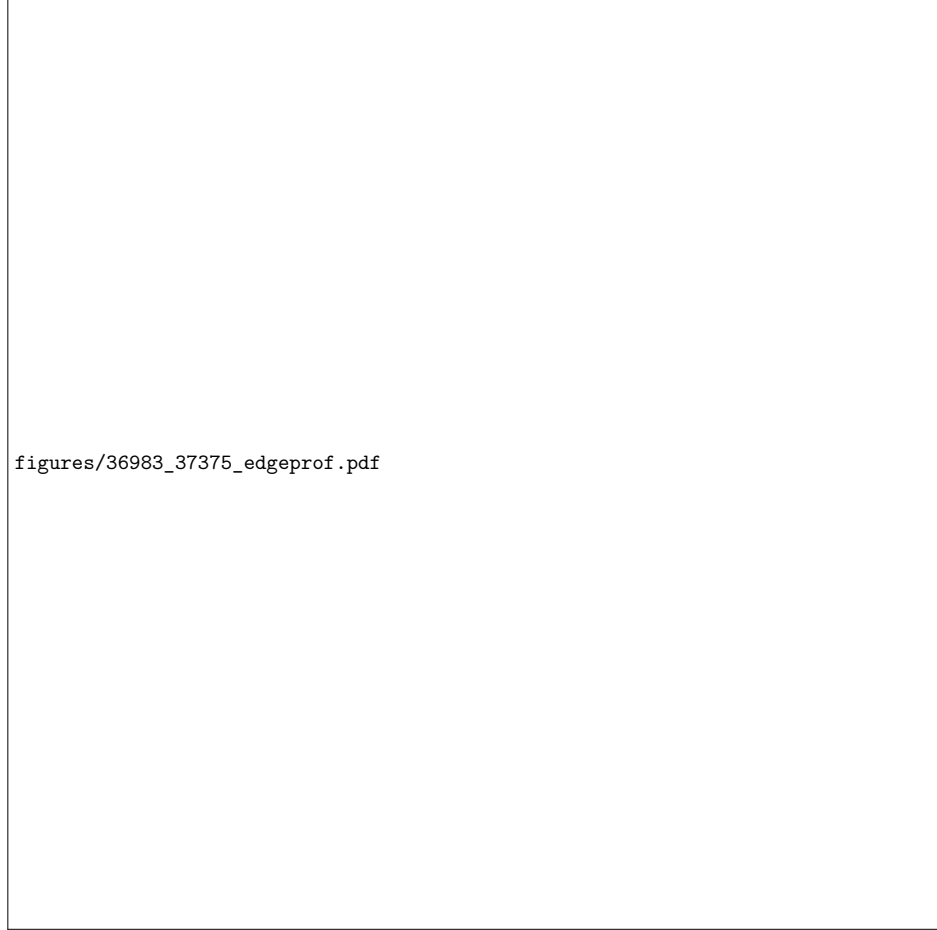


FIG. 6. *Edge kinetic profiles of L-modes in favourable and unfavourable drift configuration at matched parameters.* Radial profiles of measured (a) electron temperature T_e , (b) electron density n_e , (c) logarithmic electron density gradient $1/L_{n_e}$, (d) ion temperature T_i , (e) intrinsic toroidal rotation of impurities $v_{\phi, \text{imp}}$ and (f) radial electric field E_r as well as main ion pressure gradient $(\nabla_r p_i)/(en_i)$ (assuming $n_i = n_e$) for favourable (blue) and unfavourable (light red) drift configuration.

$T_{i, \text{sep}} \approx 100 \text{ eV} = 1.3 T_{e, \text{sep}}$ in both cases. According to Manz *et al.*¹⁵ a transition from ITG-dominated to Drift-Alfvén turbulence can take place if a sufficiently high $T_{i, \text{sep}}/T_{e, \text{sep}}$ or

a rather low ∇T_i is reached at the separatrix, which then would lead to the existence of the I-mode. The observation here that $T_{i,sep}/T_{e,sep}$ and ∇T_i are very similar in both drift configurations, whereas the I-mode is absent in favourable drift configuration, is in variance to the theory proposed by Manz *et al.*¹⁵.

The impurity intrinsic toroidal rotation $v_{\phi,imp}$, which is the toroidal rotation without external torque input, is found to be almost the same and co-current in both drift configurations. This observation is in contrast to intrinsic edge rotation measurements in L-modes of favourable and unfavourable drift configuration in Alcator C-Mod¹, which is observed to change with drift configuration. A more detailed discussion on this can be found in Sec. VII C. Qualitative differences in the profiles shown in Fig. 6e might originate from the fact that the impurity rotation was measured on different impurities (B and N, respectively). Furthermore, although the external torque input by NBI is minimized by the short duration of the NBI blip, a small effect on v_{ϕ} cannot be excluded, even more since in LSN favourable drift configuration the NBI injection is co-current at AUG, whereas it is counter-current in LSN unfavourable drift configuration (see Figure 24).

The biggest difference between the two drift configurations is found in the measured edge E_r profiles. Although the slopes of the inner and outer E_r gradients can vary somewhat e.g. due to heating method, a robust observation is that the E_r well in the confined region is shallower in unfavourable compared to favourable drift configuration. Thus, these new measurements confirm earlier studies at AUG and DIII-D^{10,76} and recent results from the WEST tokamak¹². As shown in Fig. 6f the $E_{r,min}$ value for the unfavourable drift configuration case is less negative than the one in favourable drift configuration, leading to a weaker inner E_r gradient in unfavourable drift configuration. The $E_{r,max}$ values are generally not very different between the two drift configurations, however, it is regularly observed that $E_{r,max}$ is located just inside the separatrix for the unfavourable drift configuration, whereas it is located outside the separatrix for the favourable drift configuration. This causes that the outer E_r gradients are of similar strength between the two drift configurations.

2. Scrape-off Layer Profiles

Figures 7a,b show electron temperature and density profiles of the outer divertor target ($T_{e,target}$ and $n_{e,target}$) in favourable (blue) and unfavourable (light red) drift configuration.

This is the author's peer reviewed, accepted manuscript. However, the online version of record will be different from this version once it has been copyedited and typeset.

PLEASE CITE THIS ARTICLE AS DOI: 10.1063/1.50102763



FIG. 7. SOL profiles in favourable and unfavourable drift configuration L-modes at matched parameters. Radial profiles of measured (a) electron temperature T_e , (b) electron density n_e at the outer target (circles) and at the outer mid-plane (OMP, lines) for favourable (blue) and unfavourable (light red) drift configuration. (c) Plasma potential V_{pi} at the OMP (circles), reconstructed from LP measurements at the outer target, and spline fit to the experimental data (dashed line).

Also shown in the plots are $T_{e,OMP}$ and $n_{e,OMP}$, which were already presented in Figure 6. The strong reduction of T_e along the field lines with a concomitant increase of n_e towards the divertor target ($p_{e,OMP} \approx 2p_{e,target}$ within the measurement uncertainties) indicates that the SOL plasma is in the conduction-limited regime. This, in turn, implies that the Spitzer-Härm power balance can be applied for the determination of the separatrix temperature at the OMP, as was done for all discharges in this work (see Section III).

As expected from a reversal of the drift directions in the SOL, the particle transport towards the outer divertor is increased in unfavourable drift configuration compared to favourable drift configuration, leading to a lower $T_{e,target}$ and a higher $n_{e,target}$ in un-

favourable compared to favourable drift configuration^{13,77,78}. In favourable drift configuration, $T_{e,OMP} \approx 3T_{e,target}$, whereas in unfavourable drift configuration $T_{e,OMP} > 3T_{e,target}$. In unfavourable drift configuration, where the target profiles are fully resolved, $T_{e,target}$ peaks at the separatrix, while the maximum value of $n_{e,target}$ is reached a bit further outside in the SOL, at $\rho_{pol} \approx 1.001$. This is observed regularly and also theoretically predicted due to diffusive processes in the private flux region^{26,79}.

The plasma potential at the OMP, reconstructed from the LP data at the outer divertor target, is shown in Figure 7c. The dashed lines are cubic spline fits to the experimental data. Although the absolute values are similar in both drift configurations, with V_{pl} between 0 and 60 eV, the profile shapes differ. In unfavourable drift configuration, the peak of V_{pl} is narrow and occurs close to the separatrix, at around $\rho_{pol} = 1.002$, whereas in favourable drift configuration the peak is broader and exhibits its maximum at $\rho_{pol} \approx 1.007$. This qualitatively different behaviour of V_{pl} for the different drift configurations has been observed also in other plasma discharges of similar plasma parameters, in which fully radially resolved target profiles were available also for the favourable drift configuration. The analysis of those data showed consistently that the maximum in $T_{e,target}$ does not exceed 30 eV and that the maximum value of V_{pl} is indeed reached at around $\rho_{pol} = 1.007$ in the favourable drift configuration.

The upstream E_r profiles reconstructed from the target profiles using Equation 6 are depicted as dashed lines in Figure 8 for the two drift configurations. For comparison also the respective E_r measurements and $-\nabla_r T_{e,OMP}/e$ profiles (see Equation 8) are plotted. The measured SOL E_r profiles agree well with the $-\nabla_r T_{e,OMP}/e$ profiles around $E_{r,max}$, but the decay of the measured E_r profiles in the SOL is faster than that of $-\nabla_r T_{e,OMP}/e$. The full reconstruction of E_r from $-\nabla_r V_{pl}$ agrees less with the experimental E_r profiles, in particular for unfavourable drift configuration. This discrepancy suggests that the simple SOL model lacks important effects, e.g. from cross-field transport, in order to reproduce the upstream SOL E_r profile from the divertor profiles correctly. It could also be that the assumptions on the shape of p_e along the field lines has to be adapted or that $j_{||}/\sigma_{||}$ is in fact not negligible. This will be further investigated in the future. However, considering the large radial uncertainties around the separatrix, which are critical when aligning the target and upstream profiles for the SOL E_r reconstruction, the deduced E_r profiles from the target measurements are in reasonable qualitative and quantitative agreement with the

measured E_r profiles at the OMP, at least in favourable configuration. A more systematic experimental study at AUG in favourable drift configuration L-modes confirms this²⁷.

Despite different outer divertor target profiles, the measured upstream SOL E_r profiles are very similar between the two drift configurations. This makes an explanation of the increased H-mode power threshold in unfavourable drift configuration due to a weaker SOL E_r hill and, thus, due to a significantly weaker outer E_r gradient implausible, as it was suggested previously based on SOL modelling results^{13,14}.

3. Neoclassical Calculations

In this section the experimental E_r profiles shown in Figure 6f are compared to NEOART calculations (see Section III F). This comparison helps to clarify whether the observed differences in E_r between the two drift configurations are due to NC effects. As input for the NC predictions of $v_{\theta,i}$, $v_{\theta,imp}$ and $v_{\phi,i}$ the experimental n_e , T_e , T_i and $v_{\phi,imp}$ profiles presented in Figure 6a-e were used. The resulting velocity profiles are shown in Figure 9. For completeness, also the measured $v_{\theta,imp}$ and $v_{\phi,imp}$ data from CXRS as well as the fits to the $v_{\phi,imp}$ profiles are shown.

In both drift configurations the measured intrinsic $v_{\phi,imp}$ and the predicted $v_{\phi,i}$ are co-current and the predicted NC poloidal impurity and main ion velocities are in the electron diamagnetic drift direction close to the separatrix. The experimental data of $v_{\theta,imp}$ and the NC predictions are in reasonable agreement, which indicates that also the main ion predictions are reliable.

Inserting the toroidal and poloidal main ion velocity and the $(\nabla_r p_i)/(en_i)$ profiles from NEOART into the radial force balance equation (Equation 3) gives an estimate for the size and shape of the edge E_r based on local NC theory. Since it was found that the resulting predicted E_r profiles depend sensitively on the input T_i data, a discussion on this dependence can be found in Appendix B. The conclusions from this sensitivity study is that the shape of the predicted E_r profile depends strongly on the input T_i profile, however, the differences found in E_r between favourable and unfavourable drift configuration is independent of the choice of the T_i profile fit. Therefore, in Figure 10 a comparison of the predicted E_r profile (solid line), of $(\nabla_r p_i)/(en_i)$ only (dashed line) and of the experimental E_r profile (stars) for favourable (blue) and unfavourable (light red) drift configuration is shown for the 'flat T_i

This is the author's peer reviewed, accepted manuscript. However, the online version of record will be different from this version once it has been copyedited and typeset.
 PLEASE CITE THIS ARTICLE AS DOI: 10.1063/1.50102763

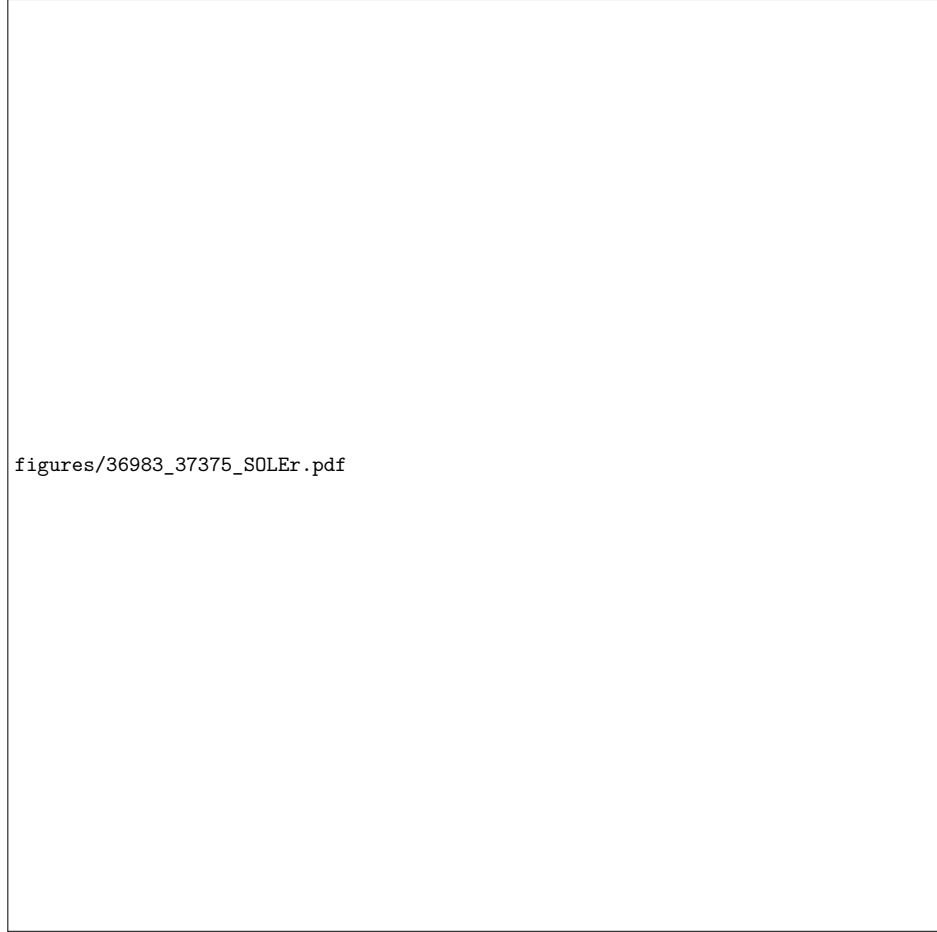


FIG. 8. *SOL E_r profiles in favourable and unfavourable drift configuration L-modes at matched parameters.* Measured E_r profiles at the OMP (stars) in comparison with the reconstructions of E_r from target profiles, using $E_r = -\nabla_r V_{pi}$ (dashed line), and the approximation for the conduction-limited regime $E_r \approx -\nabla_r T_{e,OMP}$ (solid line) for favourable (a) and unfavourable (b) drift configuration.

fit' (see also Appendix B).

In both drift configurations the experimental E_r profiles agree better with the predicted E_r profiles including the main ion velocities, than with solely the $(\nabla_r p_i)/(en_i)$ profile. This

This is the author's peer reviewed, accepted manuscript. However, the online version of record will be different from this version once it has been copyedited and typeset.
 PLEASE CITE THIS ARTICLE AS DOI: 10.1063/1.50102763

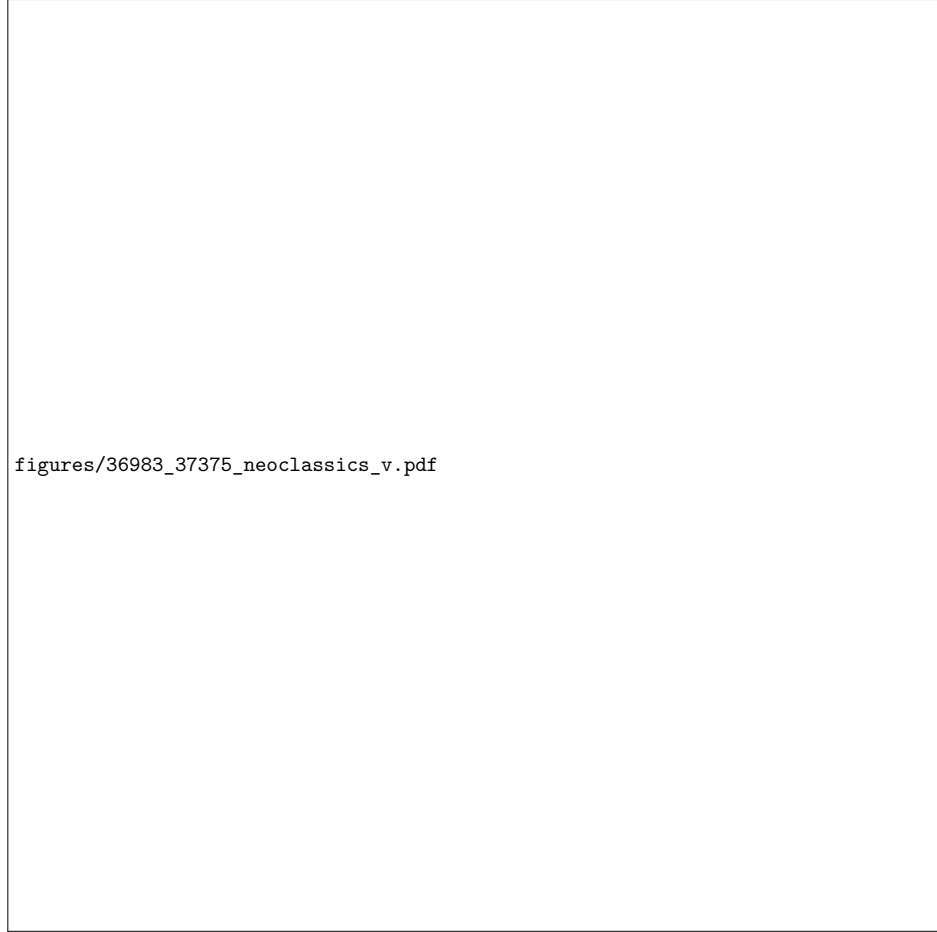


FIG. 9. *Neoclassical and experimental edge velocities in L-mode plasmas of matched parameters in favourable and unfavourable drift configuration.* (a) Measured intrinsic toroidal impurity rotation (triangles) and fit to the experimental data (dashed line), (b) predicted intrinsic toroidal main ion rotation, (c) measured (triangles) and predicted (solid line) poloidal impurity velocity and (d) poloidal main ion velocity profiles of favourable (blue) and unfavourable (light red) drift configuration.

gives evidence that the $v_i \times B$ contribution to E_r is not negligible in L-mode, as has already been shown at DIII-D^{24,80,81}. At AUG in the here investigated L-modes it is actually found

This is the author's peer reviewed, accepted manuscript. However, the online version of record will be different from this version once it has been copyedited and typeset.

PLEASE CITE THIS ARTICLE AS DOI: 10.1063/5.0102763

that the contributions of $(\nabla_r p_i)/(en_i)$, $v_{\phi,i}B_\theta$ and $v_{\theta,i}B_\phi$ are of comparable size, but they can have different signs and, therefore, they can cancel each other out and counteract each other.



FIG. 10. Comparison of exp. E_r profiles with neoclassical predictions in favourable and unfavourable drift configuration L -modes of matched parameters. Predicted E_r profiles from NEOART including main ion velocities (solid lines) and main ion pressure gradient profiles only (dashed lines) and experimental edge E_r profiles (stars, squares) for favourable (blue) and unfavourable (light red) drift configuration. Figure adapted from U. Plank *et al.* Plasma Phys. Control. Fusion **65**, 014001 (2023); licensed under a Creative Commons Attribution (CC BY) license.

As can be seen in Figure 10, for favourable drift configuration the predicted E_r profile agrees with the experimental data quantitatively in the region around $E_{r,\min}$, whereas for the unfavourable drift configuration larger differences between the predicted E_r profiles and the experimental profiles are found. Qualitative agreement of the profile shape between predicted and experimental E_r is only found for the favourable drift configuration using the 'steep T_i fit' (see Appendix B), for which a minimum in the predicted E_r profile can be produced. However, it is not a general result that NC predictions of E_r agree better with experimental data in favourable compared to unfavourable drift configuration. As shown in the next section, counter examples exist.

B. Upper Single-Null and Medium Density

Several pairs of L-H (L-I-H) transition discharges with identical ECRH power ramps and a plasma density of $\bar{n}_e = 4.5 \times 10^{19} \text{ m}^{-3}$ were performed also in USN favourable and unfavourable drift configuration. These discharges were density feedback-controlled and operated with $|B_\phi| = 2.5 \text{ T}$ at the geometric axis, $I_p = 1.0 \text{ MA}$ and $|q_{95}| = 3.8$. Two example L-mode phases are presented in the following which were both heated with $P_{\text{ECRH}} = 200 \text{ kW}$. This phase is, for the favourable drift configuration discharge # 37985, right before the L-H transition, but still long before the L-I transition for the unfavourable drift configuration discharge # 37983 ($P_{\text{ECRH}} \approx 1.4 \text{ MW}$ at L-I). Due to the lower coverage of the upper divertor with LP measurements at AUG, no divertor target profiles are available for these discharges.

1. Edge E_r Profiles

In Figure 11 the measured L-mode E_r profiles for favourable (purple) and unfavourable (orange) drift configuration are plotted together with the experimental $(\nabla_r p_i)/(en_i)$ profiles, assuming $n_i = n_e$ for the latter. Due to the higher density of these discharges the E_r measurements by DR are restricted to the confined region. Therefore, HES measurements of the outer E_r gradient are also shown in the figure. As can be seen, the E_r profiles from both diagnostics are in good agreement, although for the unfavourable drift configuration deviations of up to 2 kV/m are observed between the two diagnostics.

The edge electron and ion kinetic profiles are very similar in both drift configurations, leading to almost identical $(\nabla_r p_i)/(en_i)$ profiles. In contrast to $(\nabla_r p_i)/(en_i)$, the E_r profiles are different between the two drift configurations, where the E_r well in the confined region is again shallower in unfavourable drift configuration, which also causes the inner E_r gradient to be significantly weaker in unfavourable compared to favourable drift configuration, whereas the outer one is of comparable strength.

In summary, these observations are the same as for the pair of low density L-modes in LSN favourable and unfavourable drift configuration described in Section VI A. A difference to the LSN L-modes at low density is that in the L-modes presented here the intrinsic $v_{\phi, \text{imp}}$ (measured on B) is slightly higher in favourable compared to unfavourable drift configuration (see Figure 12a), but it is again co-current for both drift configurations.

This is the author's peer reviewed, accepted manuscript. However, the online version of record will be different from this version once it has been copyedited and typeset.

PLEASE CITE THIS ARTICLE AS DOI: 10.1063/1.50102763



FIG. 11. *Comparison of L-modes in favourable and unfavourable drift configuration at matched parameters.* Edge radial electric field profiles from DR (squares) and HES (circles) and main ion pressure gradient profile (solid lines) for USN favourable (purple) and unfavourable (orange) drift configuration.

2. Neoclassical Calculations

In Figure 12 the impurity and main ion velocities are shown for the two drift configurations as predicted by NEOART. The intrinsic toroidal main ion rotation (b) is co-current for both drift configurations, but, as the measured $v_{\phi, \text{imp}}$ (a), $v_{\phi, i}$ is larger in favourable drift configuration. The predicted NC impurity (c) and main ion (d) poloidal velocities are of comparable size between the two drift configurations, and point for either configuration into the electron diamagnetic drift direction. The experimental $v_{\theta, \text{imp}}$ data exhibit a large scatter, but they rather agree with the NC predictions for the unfavourable drift configuration. In favourable drift configuration the experimental $v_{\theta, \text{imp}}$ data point into the ion diamagnetic drift direction. Accordingly, see Figure 13, the predicted E_r profile employing NC main ion velocities (solid line) agrees better with the experimental E_r profile for the unfavourable (orange) than for the favourable drift configuration (purple). For the latter the predicted E_r profile is much less negative than the experimental data and also the steep inner E_r gradient cannot be resolved. A comparable flat inner E_r gradient, as the predicted E_r profiles exhibit,

This is the author's peer reviewed, accepted manuscript. However, the online version of record will be different from this version once it has been copyedited and typeset.

PLEASE CITE THIS ARTICLE AS DOI: 10.1063/1.50102763

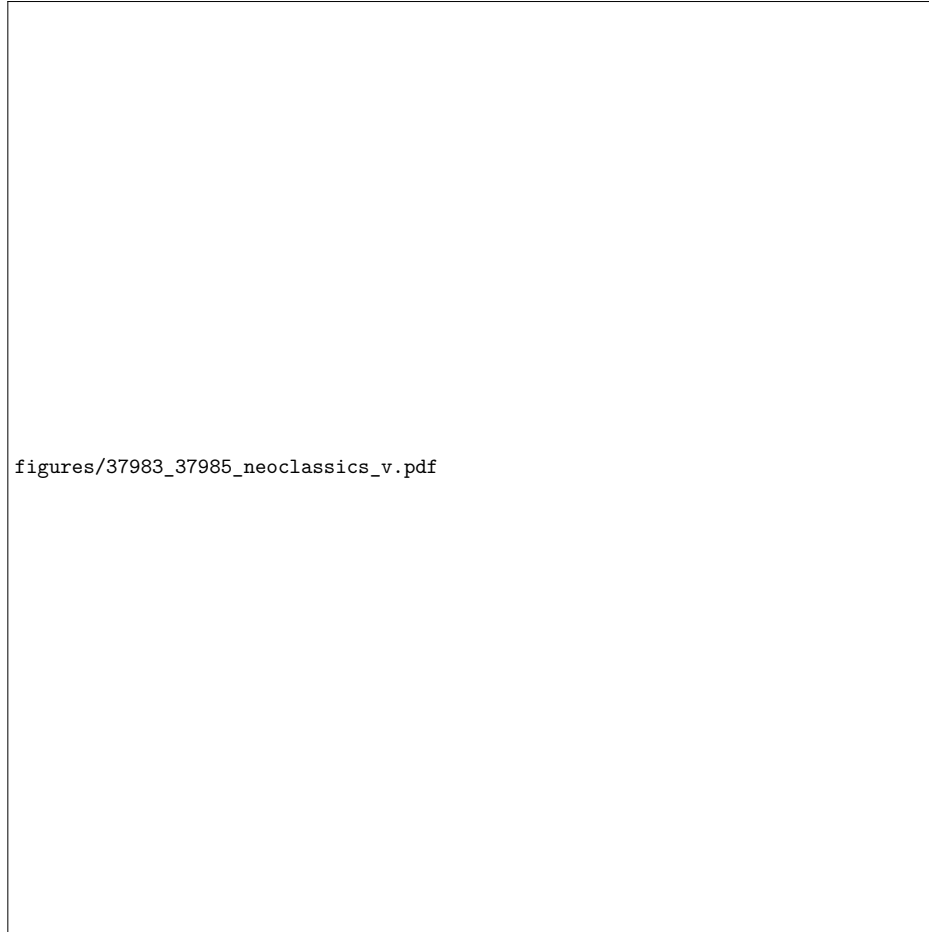


FIG. 12. Neoclassical velocity profiles in favourable and unfavourable drift configuration L -modes of matched parameters. (a) Toroidal intrinsic impurity rotation profile (triangles) and fit of the data (dashed lines), (b) predicted toroidal intrinsic main ion rotation, (c) predicted neoclassical poloidal impurity velocity (solid lines) and experimental data (triangles) and (d) predicted neoclassical poloidal main ion velocity for favourable (purple) and unfavourable (orange) drift configuration.

is only found for the experimental E_r profile in unfavourable drift configuration.

The main reason for the less negative E_r profile prediction by NC theory in favourable compared to unfavourable drift configuration, which is opposite to the experimental obser-

vation, is mainly due to the differences in the measured $v_{\phi,imp}$. The latter has consistently been found to be larger in favourable than in unfavourable drift configuration in several USN discharges. As stated before, this difference in the E_r predictions can also not be resolved by steeper T_i gradient fits to the experimental data (see also Appendix B).



FIG. 13. Comparison of E_r profiles with neoclassical predictions in favourable and unfavourable drift configuration L-modes of matched parameters. Measured E_r profiles (squares) and NC predictions (solid lines) in favourable (purple) and unfavourable (orange) drift configuration.

Please note, the strong deviations between the predicted and the experimental E_r profiles, which are present in the region of the outer E_r gradient between $\rho_{pol} \approx 0.98$ and 1.0 are likely due to other contributions to E_r , which have been assumed to be negligible, or they are not captured by local NC theory. These can be friction forces or non-isotropic pressure contributions (see Equations 1 and 2) as well as ion orbit losses and global NC effects, which are not captured by NEOART. As shown in the Section VII, in the region around the separatrix also a strong interaction between confined plasma and SOL seems to be present.

C. Discussion of Possible Mechanisms Influencing E_r

Comparison of L-mode phases with same heating power and same plasma density, but different drift configuration have shown that, although $(\nabla_r p_i)/(en_i)$ is very similar between

This is the author's peer reviewed, accepted manuscript. However, the online version of record will be different from this version once it has been copyedited and typeset.

PLEASE CITE THIS ARTICLE AS DOI: 10.1063/1.50102763

the two drift configurations, the E_r well in the confined region is shallower in unfavourable compared to favourable drift configuration. This leads to less steep E_r gradients in the unfavourable drift configuration, as has been observed previously^{10–12}. This is found consistently regardless whether pairs of LSN or USN discharges are investigated, which implies that this effect is independent of the exact divertor geometry (closed or open divertor). In both drift configurations it is found that E_r in L-mode deviates from $(\nabla_r p_i)/(en_i)$, showing that $v_i \times B$ is a non-negligible contribution to E_r , as also observed previously at DIII-D^{24,80,81}. Comparisons with local NC theory give better agreement in magnetic configurations in which B_ϕ is negative, i.e. clockwise seen from above (standard B_ϕ direction at AUG). This agreement is, in the discharges presented here, connected to favourable drift configuration in LSN and to unfavourable drift configuration in USN plasmas (see also Appendix A). However, in detail deviations of the measured E_r profiles from NC theory are found in either drift configuration, which is consistent with results from DIII-D in favourable drift configuration plasmas²⁴. In particular the NC predictions can not reproduce the differences observed in E_r between the two drift configurations.

Various mechanisms are discussed in the community that can lead to differences in the edge E_r , depending on the magnetic configuration. Possible candidates, which would be consistent with the experimental data, are a contribution of the magnetic-shear-induced Reynolds stress on the parallel momentum and, thus, E_r ^{16,82,83} or other turbulent stresses which modify the mean-field parallel and toroidal momentum transport^{17,84}. In either case the observed differences in E_r would originate from differences in the momentum stresses due to the up-down asymmetry and/or the different helicity of the magnetic flux surfaces. Further possible effects on the intrinsic edge rotation and E_r in the confined plasma edge could originate from ion orbit losses or from interactions with neutrals^{85–87}. Their impact on the intrinsic edge v_ϕ and on the edge E_r also depend on the exact magnetic configuration^{19,20,86}. First comparisons show that such effects are at least in qualitative agreement with experimental observations from AUG^{88,89}, but further analysis and detailed comparisons are required to draw definitive conclusions. Moreover, it should be noted that the NC calculations in this work were purely local. However, close to the separatrix, in the region where the kinetic profile gradients are steep, also global effects, which are not treated in local calculations, could play an important role, as could be the case for some of the plasmas presented in this study. From theory mainly a change of the poloidal main ion velocity at the plasma

edge is expected, which is confirmed by comparisons of global to local NC simulations⁹⁰. Such effects can as well influence the E_r predictions from NC theory. Comparisons of these different effects to the experimental data are currently undertaken or foreseen in the near future and are not object of this present work. It is important to note that for either of these effects it has to be investigated carefully on how it impacts the edge velocities and edge E_r profiles and whether it changes with the magnetic configuration, i.e. with the B -field direction and/or its helicity.

In conclusion it can be stated that if the paradigm of the suppression of edge turbulence by a large enough $v_{E \times B}$ shear holds (see Section II), the observed differences in the E_r profiles in the confined plasma between the two drift configurations could explain the different H-mode power thresholds for the two drift configurations. In this framework more heating power would be needed in unfavourable drift configuration in order to reach a steep enough E_r gradient, via $\nabla_r T_i$, to suppress the edge turbulence, assuming the latter is unchanged. However, as shown in the following sections, in unfavourable drift configuration it is not always found that the edge E_r gradients steepen as soon as the input power is increased, e.g. for low-density ECRH L-modes (see Section VII A). Furthermore, it is also not observed that similarly steep edge E_r gradients (neither the inner nor the outer E_r gradient) are reached at the respective H-mode transition for plasma pairs in favourable and unfavourable drift configuration. This is discussed in more detail in Section VIII.

VII. HEATING POWER AND PLASMA DENSITY SCANS IN UNFAVOURABLE DRIFT CONFIGURATION L-MODES

In this section constant phases of L-modes in LSN unfavourable drift configuration are compared, to study the evolution of the target profiles, the edge intrinsic toroidal rotation and E_r profiles in L-mode, up to the confinement transition. The unfavourable drift configuration was chosen since, due to the larger L-mode window, also larger variations in heating power and plasma density can be investigated. The dependencies of E_r on plasma density and heating power described in the following are, however, also found in favourable drift configuration L-modes. The investigated L-mode phases of the AUG discharges # 37375, 37298, 35753 and 35758 either had same plasma density of $\bar{n}_e \approx 2.7 \times 10^{19} \text{ m}^{-3}$ and were heated with $P_{\text{ECRH}} = 0.60, 2.9$ and 4.0 MW (see Section VII A) or constant ECRH power

This is the author's peer reviewed, accepted manuscript. However, the online version of record will be different from this version once it has been copyedited and typeset.

PLEASE CITE THIS ARTICLE AS DOI: 10.1063/1.50102763

was applied ($P_{\text{ECRH}} = 2.9\text{MW}$), but the density was increased from $\bar{n}_e = 2.5$ to 4.0 and $6.0 \times 10^{19} \text{m}^{-3}$ (see Section VII B).

A. Different Heating Power at Constant Plasma Density

1. Edge Profiles



FIG. 14. Edge kinetic profiles of L-modes with same plasma density and different ECRH power in unfavourable drift configuration. Experimental radial profiles of the edge (a) electron temperature, (b) ion temperature, (c) electron density and (d) logarithmic electron density gradient.

Figure 14 shows the edge electron and ion kinetic profiles for the L-modes phases heated with different amounts of ECRH power. As expected, T_e increases with increasing P_{ECRH} and for the highest heating power of 4.0 MW $T_{e,\text{sep}} \approx 130\text{eV}$, according to Spitzer-Härm power balancing (see Section III D). Such a high $T_{e,\text{sep}}$ is, in favourable drift configuration plasmas, observed in H-modes only. Also T_i increases with increasing ECRH power, whereas

n_e and $1/L_{n_e}$ vary only slightly. The edge $(\nabla_r p_i)/(en_i)$ profiles, shown in Figure 15b, are the same, within the uncertainties, for all three different L-mode phases. Power balance calculations for these L-modes have shown that $Q_{i,\text{edge}}$ saturates at a value of about 0.6 MW and does not increase further with increasing P_{ECRH} . The reason for this saturation is that in pure electron heated plasmas energy to the ions is only transferred via equipartition. However, the equipartition power density $p_{ei} \propto n_e^2 \frac{T_e - T_i}{T_e^{3/2}}$ is low in these L-modes due to the low plasma density and, for high enough T_e , p_{ei} decreases with increasing T_e . Thus, the critical $Q_{i,\text{edge}}$ needed to enter I-mode in these plasma conditions at AUG is, according to Ryter *et al.*⁶⁹, not reached.

The measured impurity's intrinsic toroidal edge rotation (here N) is shown in Figure 15a. For all three L-mode phases it is co-current and it increases in size with increasing P_{ECRH} . Accordingly the edge E_r becomes less negative (even becomes positive) with increasing P_{ECRH} (see Figure 15b) in the confined plasma, but also shifts upwards by about the same amount in the SOL, leaving the outer E_r gradient almost unchanged. For the two higher heating power phases $v_{E \times B}$ points into the ion diamagnetic drift direction, since $E_r > 0$. Again, the experimental E_r profiles deviate strongly from $(\nabla_r p_i)/(en_i)$ in the confined plasma, which exhibits a minimum value of about -15 kV/m . This indicates that the flow velocity terms are significant and responsible for the shift to positive E_r as shown in the subsequent section.

2. Neoclassical Calculations

A comparison of the experimental E_r profiles with the NEOART predictions is shown in Figure 16. The predicted E_r profiles are more negative than the measured ones, particularly for the lowest heating case (light red), but the relative changes of E_r with increasing heating power are reproduced. They also show that the edge E_r profile becomes positive with higher P_{ECRH} . In conclusion the comparison between experiment and NC predictions confirms that the NC contribution of $v_i \times B$ to E_r is not negligible and $(\nabla_r p_i)/(en_i)$ cannot be used as a proxy for E_r in L-mode. The E_r measurements also reveal that the E_r gradients do not steepen with increasing heating power in these plasma conditions, which could explain the high P_{LH} in such types of plasmas (low density plasmas heated with ECRH)^{48,73} and the observation that the here presented discharges did not enter an improved confinement

This is the author's peer reviewed, accepted manuscript. However, the online version of record will be different from this version once it has been copyedited and typeset.
 PLEASE CITE THIS ARTICLE AS DOI: 10.1063/1.50102763

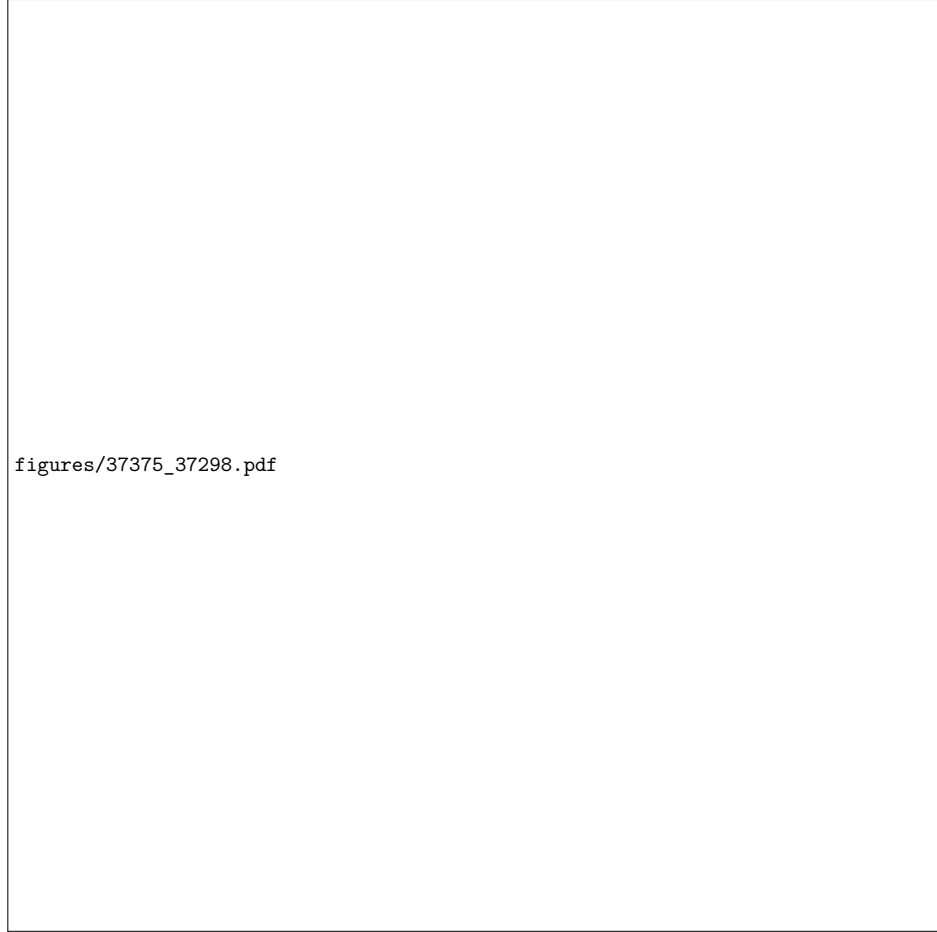


FIG. 15. *Edge rotation and E_r profiles of L-modes with same plasma density and different heating power in unfavourable drift configuration.* Profiles of the measured (a) intrinsic impurity edge rotation and (b) edge radial electric field (stars and squares), together with the approximation ($n_i = n_e$) of the main ion pressure gradient (solid lines).

regime. As stated before, the deviations between the predictions of local NC theory and experimental data, which is an approximately constant offset of 2 – 4kV/m in the ion diamagnetic drift direction, indicates that other effects also contribute to E_r , which are not included in the NEOART calculations. However, it is not clear as of yet which are



FIG. 16. Comparison of E_r profiles with neoclassical predictions in unfavourable drift configuration L -modes of same plasma density at different ECRH powers. Measured E_r profiles (squares and stars) and NC predictions (solid lines).

the (additional) mechanisms influencing the poloidal and/or toroidal velocity and, thus, E_r . This will be addressed in future work. Several candidates can be considered which were already presented in Section VIC.

3. SOL E_r Profiles

Figure 17 shows again the measured upstream E_r profiles, now in comparison with the two different SOL models. As stated before, $E_{r,\max}$ increases with increasing ECRH power and the same trend is found for the two estimates of the upstream E_r , $-\nabla_r T_{e,\text{OMP}}/e$ and $-\nabla_r V_{\text{pl}}$ (see Eqs. 8 and 7). As has been mentioned before (see Section VIA 2), the experimental data agree quantitatively better with $-\nabla_r T_{e,\text{OMP}}/e$, whereas $-\nabla_r V_{\text{pl}}$ overestimates E_r in the SOL.

This is the author's peer reviewed, accepted manuscript. However, the online version of record will be different from this version once it has been copyedited and typeset.

PLEASE CITE THIS ARTICLE AS DOI: 10.1063/1.50102763

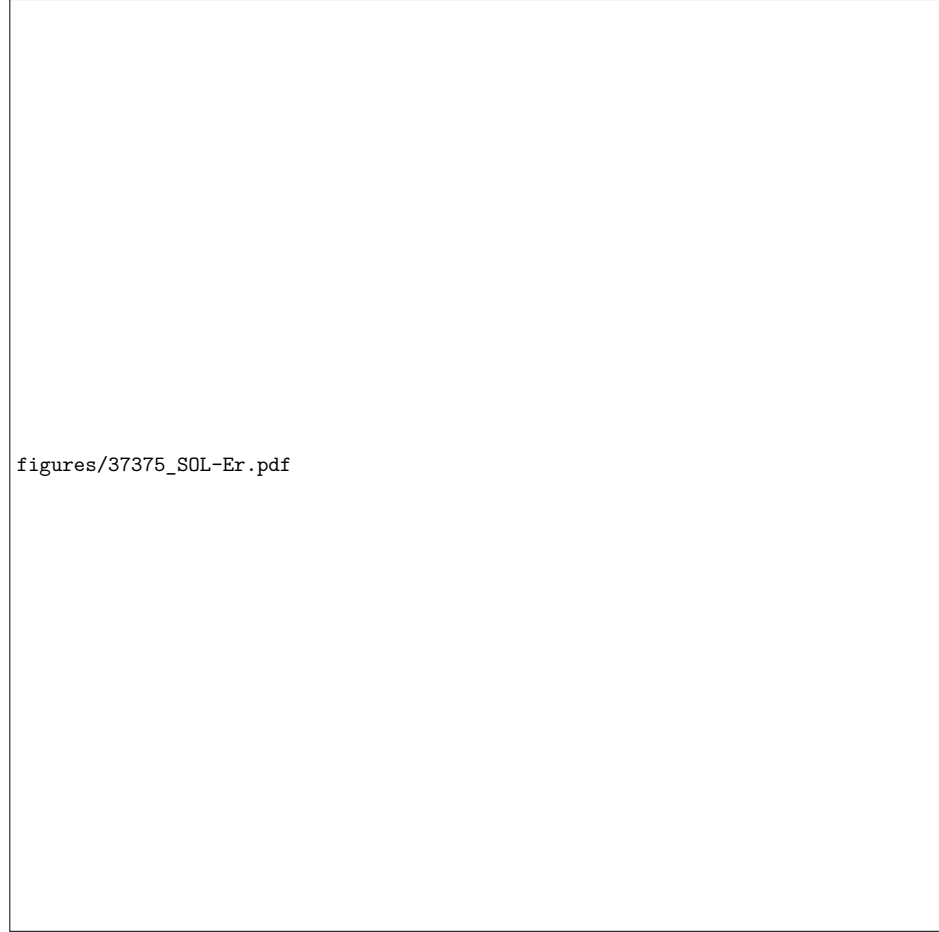


FIG. 17. SOL E_r profiles in unfavourable drift configuration L-modes of same plasma density at different ECRH powers. (a-c) Measured E_r profiles in the SOL (DR, stars) and different estimates of the upstream E_r in the SOL deduced from target profiles ($-\nabla_r V_{pl}$, dashed lines) and from the outer mid-plane profiles ($-\nabla_r T_{e,OMP}/e$, solid lines).



FIG. 18. *Edge kinetic profiles in unfavourable drift configuration L-modes of different plasma densities at same heating power.* Experimental radial profiles of the edge (a) electron temperature, (b) ion temperature, (c) electron density and (d) logarithmic electron density gradient.

B. Same Heating Power and Different Plasma Density

1. Edge Profiles

Figure 18 shows the edge electron and ion kinetic profiles of the L-mode density scan at constant ECRH power. According to Spitzer-Härm power balancing $T_{e,sep}$ is constant, independent of the edge density, which is consistent with a conduction-limited SOL^{26,56}. Also T_i stays rather constant and shows only a very weak decrease with increasing n_e , as well as $1/L_{n_e}$, which does not change with increasing n_e . Bigger changes with varying L-mode density are found for the experimental intrinsic toroidal edge rotation profiles of nitrogen (see Figure 19a). With increasing plasma density $v_{\phi,imp}$ decreases and even becomes counter-current. This behaviour is also consistently reflected in the edge E_r profiles (Figure

This is the author's peer reviewed, accepted manuscript. However, the online version of record will be different from this version once it has been copyedited and typeset.

PLEASE CITE THIS ARTICLE AS DOI: 10.1063/1.50102763

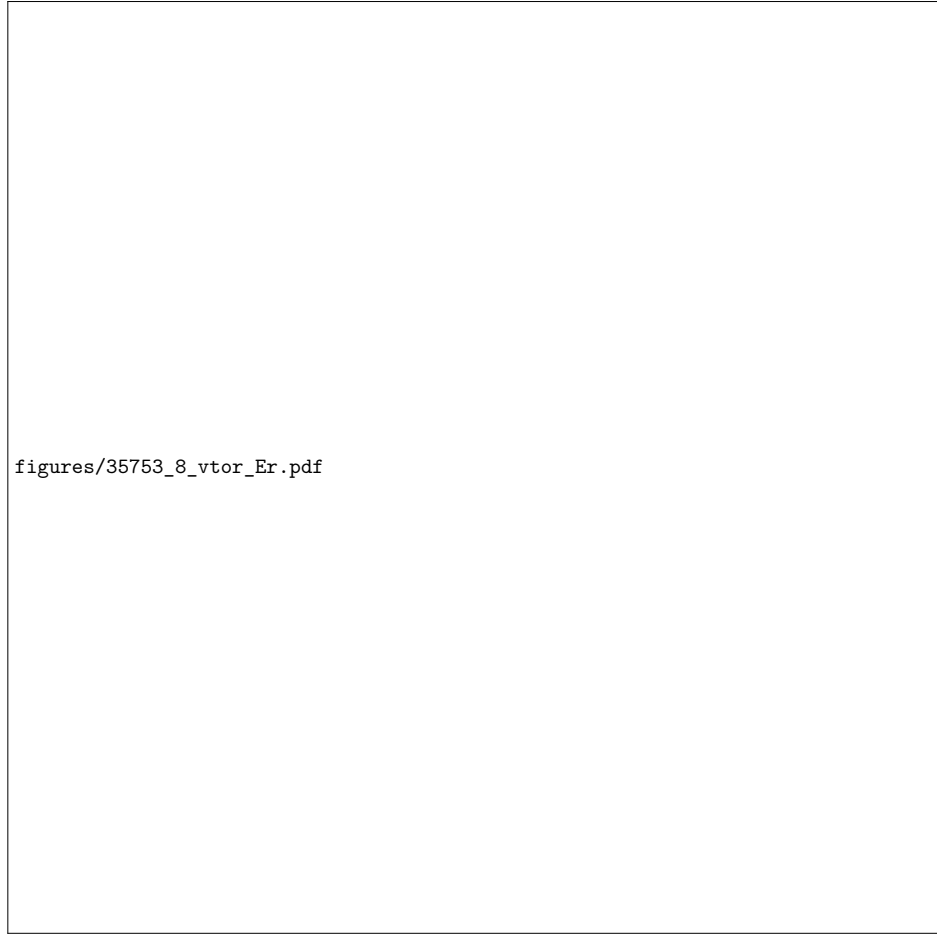


FIG. 19. *Edge rotation and radial electric field profiles in unfavourable drift configuration L-modes of different plasma densities at same heating power.* Profiles of the measured (a) intrinsic impurity edge rotation and (b) edge radial electric field (stars and squares), together with the approximation ($n_i = n_e$) of the main ion pressure gradient (solid lines).

19b). $E_{r,\min}$ decreases with increasing n_e and $v_{E \times B}$ changes from the ion into the electron diamagnetic drift direction, in accordance to observations at DIII-D investigating the impact of edge rotation on the edge E_r and P_{LH} in L-mode^{71,81}.

It is interesting to observe that the radial electric field decreases both in the confined

region and in the SOL, keeping the outer E_r gradient nearly constant. Also the inner E_r gradient does not steepen coherently with decreasing $E_{r,\min}$. This observation implies that $E_{r,\min}$ is not always a good proxy for its edge gradients in L-mode conditions, as often assumed. $(\nabla_r p_i)/(en_i)$, which is always negative, is the same for all three different L-mode phases and its minimum is about -12 kV/m. For the highest density L-mode a quantitative agreement between E_r and $(\nabla_r p_i)/(en_i)$ is found, indicating that for this case $v_i \times B \approx 0$, which is confirmed by NC calculations (see Section VII B 3). Furthermore for this case the E_r hill in the SOL disappears and E_r remains negative or close to 0 in the SOL. As can be seen in Figure 20, in such conditions the SOL E_r can not be approximated by $-\nabla_r T_{e,\text{OMP}}/e$, since the latter is always positive (see Section VII B 2).

2. SOL E_r Profiles

LP measurements at the outer divertor indicate that the target T_e decreases, whereas the target n_e increases with increasing plasma density. This trend is in line with the observation that the SOL E_r decreases at the OMP, however, the divertor measurements are not good enough in order to quantitatively reconstruct E_r in these three L-mode phases from target profiles. Recent studies at AUG in favourable drift configuration L-modes show that a reconstruction of $E_r = -\nabla_r V_{\text{pl}}$ from outer target measurements can reproduce the negative upstream E_r profiles, as they are observed for the highest density L-mode here²⁷. In Figure 20 a comparison of the measured upstream SOL E_r profiles with $-\nabla_r T_{e,\text{OMP}}/e$ is shown. While for the lowest density, the two profiles are in good agreement, $-\nabla_r T_{e,\text{OMP}}/e$ fails to reproduce the decrease of the SOL hill with increasing plasmas density. These deviations suggest that in unfavourable drift configuration plasmas the simple SOL model introduced in Section II to deduce the upstream E_r in the SOL from outer mid-plane measurements is not sufficient and it neglects important mechanisms which could lead to a qualitative and quantitative agreement. Possible modifications could come from parallel currents in the SOL, which are assumed to be small in our analytical model, but could become more important at higher densities²⁶. Also, cross-field transport is not included in the simple SOL model. To capture these effects correctly, more sophisticated SOL modelling would be required as it is included in the SOLPS code package⁹¹.

This is the author's peer reviewed, accepted manuscript. However, the online version of record will be different from this version once it has been copyedited and typeset.

PLEASE CITE THIS ARTICLE AS DOI: 10.1063/1.50102763

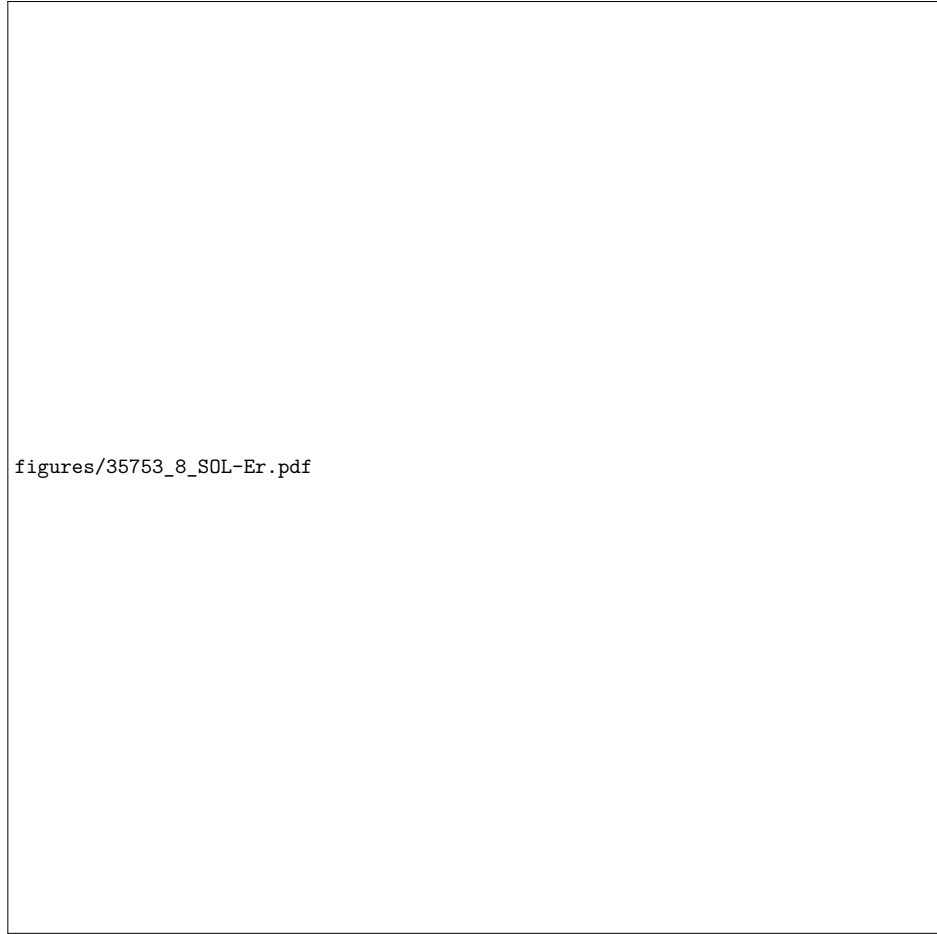


FIG. 20. SOL E_r profiles in unfavourable drift configuration L -modes of different plasma densities at same heating power. (a-c) Measured E_r profiles in the SOL (DR, stars) and an estimate of the upstream E_r in the SOL based on electron temperature profiles at the outer mid-plane ($-\nabla_r T_{e,OMP}/e$, solid lines).

3. Neoclassical Calculations

Figure 21 shows the E_r profiles which were calculated with the main ion velocities as predicted by NEOART (solid lines) and the experimental E_r profiles (squares and stars) for



FIG. 21. Comparison of E_r profiles with neoclassical predictions in unfavourable drift configuration L-modes of different plasma densities at same heating power. Measured E_r profiles (squares and stars) and NC predictions (solid lines).

the three different phases. The predicted E_r profiles reproduce qualitatively the changes in the experimental data with increasing plasma density, but a decent quantitative agreement between the experimental and the predicted E_r profile is only found for the L-mode phase with highest density, for which $v_{i,NEO} \times B \approx 0$.

C. Collisionality-Dependence of Intrinsic Toroidal Edge Rotation and E_r and Connection to SOL Flows

Taking together the results from Section VII A and Section VII B, the intrinsic toroidal edge rotation and E_r increase with increasing P_{ECRH} and decrease with increasing n_e in AUG L-modes. This suggests a correlation between the intrinsic edge v_ϕ and the edge E_r with the electron or ion edge collisionality, ν_e^* or ν_i^* , since the latter two quantities are proportional to n_e/T_e^2 and n_i/T_i^2 , respectively. Indeed it has been already found at TCV that the intrinsic toroidal edge rotation changes with density and temperature in L-modes, particularly in unfavourable drift configuration⁹². The correlations between ion collisionality, the intrinsic toroidal edge rotation (multiplied by the local poloidal magnetic field, which is constant

This is the author's peer reviewed, accepted manuscript. However, the online version of record will be different from this version once it has been copyedited and typeset.

PLEASE CITE THIS ARTICLE AS DOI: 10.1063/1.50102763

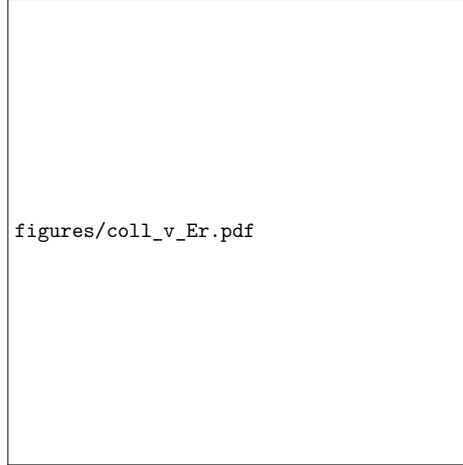


FIG. 22. (a) Measured intrinsic toroidal edge rotation of impurities (triangles) and predicted values for the main ions (stars) multiplied with the local poloidal magnetic field strength and plotted against the main ion collisionality. (b) $E_{r,\max}$ (squares) and $E_{r,\min}$ (circles), determined by DR and HES plotted against the main ion collisionality. The different collisionality regimes are indicated in the data (banana, plateau, Pfirsch-Schlüter). (c) $E_{r,\max}$ (squares) and $E_{r,\min}$ (circles) plotted against the toroidal main ion rotation, which was predicted using NEOART. The dotted lines are linear fits to the experimental data, their respective slopes and offsets are written in the plots.

at $|B_\theta| \approx 0.33\text{T}$ for this data set) and the E_r profile across the separatrix are summarized in Figure 22. Please note, these data originate from LSN unfavourable drift configuration plasmas only, but the same trends have been found in the other magnetic configurations as well.

For this figure the collisionality of deuterium (main ion species) was calculated at $\rho_{\text{pol}} = 0.98$. The different collisional regimes (banana, plateau, Pfirsch-Schlüter (PS)) are indicated at the top of the figure. The impurity intrinsic toroidal edge rotation $v_{\phi,\text{imp}}$, evaluated at $\rho_{\text{pol}} = 0.98$, was experimentally determined via CXRS and the main ion rotation was inferred with NEOART. The minimum value of E_r in the confined plasma region ($E_{r,\min}$) and the maximum value of E_r in the SOL ($E_{r,\max}$) were taken from measurements (HES and DR).

As can be seen in Figure 22a the intrinsic edge v_ϕ decreases linearly with increasing

ν_i^* , where it is co-current in the banana-plateau regime, but starts to become counter-current in the PS-regime. This dependency of the intrinsic edge v_ϕ on n_e and T_e (T_i) is also found in favourable drift configuration L-modes, although, due to the smaller L-mode window, the variations in the edge parameters is much more limited in this configuration. Therefore, the AUG results would also be consistent with DIII-D intrinsic edge rotation measurements in favourable drift configuration L-modes, for which only a weak dependence on n_e is observed⁹³.

The dependence of v_ϕ on ν_i^* is interesting, because the currently most well-established theories on the generation of intrinsic edge rotation rather predict a dependence on T_i or ∇T_i only^{94–96} and also measurements of intrinsic edge v_ϕ and $v_{\phi,\text{imp}}$ in DIII-D show a similar dependence on the local T_i (or its gradient), for constant I_p , at least in H-mode⁹⁷. There it is also found that the intrinsic toroidal edge rotation is mostly co-current, which is in line with the present observations from AUG, because DIII-D usually operates at lower edge collisionalities than AUG. In the L-mode data-set presented here (with $|I_p| = 0.8\text{MA}$) a pure dependence of v_ϕ on T_i (or its gradient) is not found, whereas the observed density dependence could be attributed to damping mechanisms of the parallel momentum due to atomic processes (charge exchange or ionization) with neutrals penetrating into the confined plasma. The importance of neutrals on the formation of the intrinsic edge rotation has been investigated experimentally together with simulations before, where in JET H-modes²⁰ and in AUG L-modes⁸⁹ they have been found to play an important role, whereas at DIII-D their impact on the intrinsic edge rotation was insignificant in H-mode pedestals⁹⁸. The data set presented here, which concentrates on L-mode plasmas, could serve as a good basis for further investigations on the importance of the various mechanisms which can influence the parallel momentum (residual stress, ion orbit losses, neutrals, SOL currents)⁸⁵ and, ultimately, E_r at the plasma edge.

Due to the linear dependence of E_r on v_ϕ (see also Equation 3), a correlation between $E_{r,\text{min}}$ and the edge v_ϕ is observed (see Figure 22c). This causes that E_r in the confined region (represented by $E_{r,\text{min}}$) decreases with increasing ν_i^* , as is shown in Figure 22b. However, also $E_{r,\text{max}}$, the maximum of the SOL hill, decreases by about the same amount as $E_{r,\text{min}}$. Although the positions of $E_{r,\text{min}}$ and $E_{r,\text{max}}$ can vary, which implies that the outer E_r gradient does not have to be constant over the entire observed collisionality range, the coherent change of edge and SOL E_r suggests a certain level of interaction between these

two plasma regions. Recently a similar behaviour of the edge E_r with plasma density, as it is found at AUG, has been observed at JET in ion wave heated L-modes in favourable drift configuration⁹⁹.

Also at Alcator C-Mod a correlation between the intrinsic edge v_ϕ and parallel SOL flows was observed¹ and it was suggested that the parallel SOL flows set the boundary condition for the intrinsic toroidal edge rotation. There it was also found that the intrinsic edge v_ϕ at the OMP follows the direction of transport-driven SOL flows of the HFS. This leads to a co-current intrinsic edge v_ϕ in favourable and to a counter-current intrinsic edge v_ϕ in unfavourable drift configuration, which was confirmed experimentally. Thus, $v_{\phi,i}B_\theta$ could, dependent on the exact v_ϕ profile, potentially decrease $E_{r,\min}$ and lead to stronger edge E_r gradients in favourable and to an increase of $E_{r,\min}$ and weaker E_r gradients in unfavourable drift configuration, although no direct E_r measurements were available for these plasmas. It was concluded, that this different behaviour of the intrinsic toroidal edge rotation could explain the increased P_{LH} in unfavourable compared to favourable drift configuration¹.

At AUG the behaviour of the intrinsic toroidal edge rotation is different and v_ϕ is found to be co-current in all observed drift configurations for a wide range of ν_i^* (banana-plateau regime), in agreement with observations at DIII-D, although there differences in the intrinsic $|v_\phi|$ are found between favourable and unfavourable drift configuration¹⁰⁰. A co-current v_ϕ adds always positively to E_r in either drift configuration and, therefore, at AUG it cannot explain the altered P_{LH} in the same way as suggested for Alcator C-Mod.

The intrinsic edge v_ϕ measurements at AUG show that the direction of v_ϕ changes with the sign and helicity of the magnetic field. This indicates that the corresponding parallel SOL flows are dominated by Pfirsch-Schlüter (PS) flows. This indirect assessment of the nature of the parallel SOL flows is in line with direct measurements of parallel SOL flows at TCV, JET and DIII-D, where it was found that the field-dependent PS flows are the main component to the parallel SOL flows^{101,102}, at least close to the separatrix¹⁰⁰. Direct measurements of the parallel SOL flows in the different drift configurations in L-mode and the investigation of their impact on quantities in the confined plasma are foreseen in the near future at AUG.

This is the author's peer reviewed, accepted manuscript. However, the online version of record will be different from this version once it has been copyedited and typeset.

PLEASE CITE THIS ARTICLE AS DOI: 10.1063/5.0102763

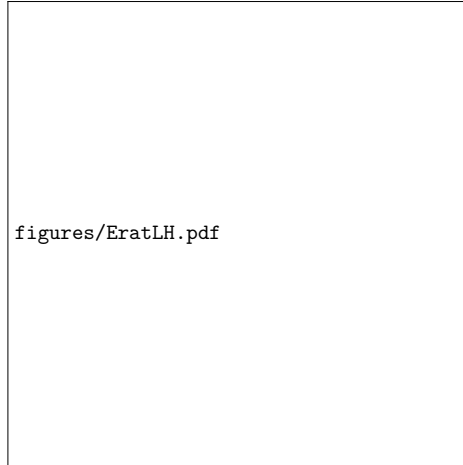


FIG. 23. *Equilibrium E_r profiles at the confinement transition in favourable and unfavourable drift configuration plasmas of same density.* Experimental edge E_r profiles acquired with DR (squares) and HES (circles) in favourable drift configuration at the L-H transition (violet) and in unfavourable drift configuration at the L-I transition (orange) and at the I-H transition (dark red). Figure adapted from U. Plank *et al.* Plasma Phys. Control. Fusion **65**, 014001 (2023); licensed under a Creative Commons Attribution (CC BY) license.

VIII. E_r AT THE CONFINEMENT TRANSITION

Three equilibrium E_r profiles, acquired in stable L-mode and I-mode phases 15 ms before the respective confinement transition (into I- or into H-mode), are shown in Figure 23. The L-H transition in favourable drift configuration (violet) occurred with $P_{\text{net}} = 1.0\text{MW}$. In unfavourable drift configuration the L-I transition (orange) was triggered with $P_{\text{net}} = 1.8\text{MW}$ and the I-H transition (dark red) with $P_{\text{net}} = 3.3\text{MW}$. In order to have comparable plasma conditions, the presented E_r profiles are from three consecutive USN discharges (# 37980, 37983 and 37985) in which the density was feedback-controlled to $4.5 \times 10^{19} \text{m}^{-3}$ and only the drift configuration as well as the amount of ECRH power was changed.

For each of the three E_r profiles (i.e. within one drift configuration) it is found that their inner and outer E_r gradients are, within the uncertainties, of comparable strength. This is connected to the fact that ECRH is used as heating system in these plasmas, for which it is

This is the author's peer reviewed, accepted manuscript. However, the online version of record will be different from this version once it has been copyedited and typeset.

PLEASE CITE THIS ARTICLE AS DOI: 10.1063/1.50102763

regularly observed that the outer E_r gradient is at least as steep as the inner E_r gradient. In NBI plasmas the inner E_r gradient can be significantly stronger than the outer E_r gradient.

A comparison of the E_r profiles amongst each other, i.e. between the different drift configurations, shows that they are all different. In favourable drift configuration $E_{r,\min}$ is at about -8 kV/m at the L-H transition, which is a relatively high value of $E_{r,\min}$ compared to usually observed $E_{r,\min}$ values in favourable drift configuration at the L-H transition at AUG^{4,73}. This $E_{r,\min}$ value of -8 kV/m is in between the $E_{r,\min}$ values of -3 kV/m found at the L-I transition and -12 kV/m at the I-H transition. The latter two are typical $E_{r,\min}$ values observed in unfavourable drift configuration at AUG at the confinement transitions into I- and H-mode, respectively⁷⁵. In the SOL the lowest $E_{r,\max}$ is found for the favourable drift configuration, which is about 5 kV/m . The $E_{r,\max}$ values in unfavourable drift configuration are at about 10 kV/m for both the L-mode and the I-mode phase. Compared to favourable drift configuration the $E_{r,\max}$ values are again located closer to the separatrix in unfavourable drift configuration. Consequently, the weakest E_r gradients (inner and outer) are found at the L-H transition in favourable drift configuration and the steepest gradients at the I-H transition in unfavourable drift configuration. For these specific discharges the E_r gradients at the L-I transition are comparable or slightly steeper than the E_r gradients at the L-H transition, but this is not a general feature. Plasmas of different parameters, e.g. at lower density, can also exhibit E_r gradients which are weaker at the L-I transition than at the L-H transition.

These different E_r gradients observed at the respective confinement transitions show that there is not one a single critical E_r gradient at the confinement transition, which has to be reached in order to trigger the transition into H-mode (or I-mode), independent of the drift configuration. If it is the case that the mean $v_{E\times B}$ shear is responsible for the edge turbulence suppression, then the different E_r gradients may indicate that the strength or type of the characteristic turbulence is different in the different drift configurations. Indeed turbulence in I-mode, preceding an I-H transition, has different spectral features than typical L-mode plasma turbulence and it also gives lower thermal transport^{75,103–106}. For this reason it is foreseen to simulate these plasmas, employing experimental profiles and power fluxes, with gyro-kinetic models in order to address the impact of the drift configuration on the edge turbulence and related quantities.

IX. SUMMARY AND CONCLUSIONS

In this experimental study at AUG, edge and SOL electron and ion kinetic profiles, rotation and E_r profiles were compared in L-modes of favourable and unfavourable drift configuration (in both LSN and USN plasmas with normal and reversed B_ϕ), using new and improved diagnostic capabilities. The improvement of these measurements and the systematic study of the behaviour of these different quantities in L-mode helps to elucidate the mechanisms leading to the increased H-mode power threshold in unfavourable drift configuration. Special focus was put on the investigation of the equilibrium E_r across the separatrix and its characterisation in L-mode, right before the L-H transition.

It is found that the evolution of the equilibrium E_r during the L-H confinement transition is very similar between the two drift configurations. The E_r gradients steepen only significantly once an improved confinement regime has been entered, in agreement with observations at COMPASS-D and JET^{107?}. It is found that in the transition from L- to H-mode the E_r profile follows the evolution of $(\nabla_r p_i)/(en_i)$, but in L-mode strong deviations of E_r from $(\nabla_r p_i)/(en_i)$ are found in both drift configurations, where $(\nabla_r p_i)/(en_i)$, $v_{\phi,i}B_\theta$ and $v_{\theta,i}B_\phi$ are similar in magnitude.

Comparisons of L-modes in different drift configurations with matched parameters (ECRH power and plasma density) show that the edge ion and electron profiles, including $(\nabla_r p_i)/(en_i)$, are the same, but the E_r well in the confined region is shallower in unfavourable compared to favourable drift configuration. The maximum of E_r in the SOL is of comparable size in both drift configurations, which shows that the measured upstream SOL E_r is little influenced by the changed divertor conditions. However, the maximum of the SOL E_r is consistently found to be located closer to the separatrix in unfavourable compared to favourable drift configuration. Comparisons of the measured upstream E_r profiles to a simple 1D SOL model give good agreement in favourable drift configuration, but in unfavourable drift configuration the E_r profiles are overestimated.

The experimental edge E_r profiles in the confined plasma are only in reasonable agreement with local NC theory. For the investigated L-mode plasmas the strength of the measured inner E_r gradient is regularly underestimated by the NC predictions, particularly in favourable drift configuration. Also the differences found in the experimental E_r profiles between the two drift configurations cannot be reproduced by the local NC predictions. This indicates

that other, non-neoclassical, effects are important to set E_r in L-mode, which could produce a different edge E_r for the two drift configurations.

Comparisons of E_r profiles in favourable and unfavourable drift configuration and matched plasma density show that at the respective confinement transition (L-H, L-I and I-H) the E_r gradients have a different strength. In the framework of a critical mean $E \times B$ shear needed to suppress turbulence, this could imply that the type or strength of the underlying edge turbulence is different for the different drift configurations. These differences will be assessed in the near future with the help of edge turbulence measurements and gyro-kinetic simulations⁸⁷. With the latter also the role of additional fluctuating shear flows, like zonal flows¹⁰⁸, which are also often considered to be the responsible trigger for the L-H transition, but have not been scope of this work, can be addressed.

ECRH power and plasma density scans in L-mode have shown that the intrinsic toroidal edge rotation and, with this, $E_{r,\min}$ in the confined plasma, order with edge collisionality, whereas the outer E_r gradient remains roughly constant in L-mode, independent of the edge collisionality. Furthermore, the intrinsic toroidal edge rotation is found to be co-current in the banana-plateau regime and it becomes counter-current when the PS-regime is reached. It is observed that in all investigated drift configurations, for a given collisionality, the intrinsic edge rotation is in the same direction (either co- or counter-current), thus following the PS flows in the SOL. For this reason, the hypothesis of the increase of P_{LH} in unfavourable drift configuration due to counter-current edge rotation impeding the L-H transition, as suggested by LaBombard *et al.* based on Alcator C-mod data¹, can not be confirmed in AUG.

In summary, it is found that the edge E_r is composed by a complex interaction between the main ion pressure gradient and the main ion flows, where the latter are found to be non-neoclassical. In specific circumstances, e.g. in low-density ECRH L-modes in unfavourable drift configuration, $(\nabla_r p_i)/(en_i)$ and $v_i \times B$ even have competing roles and, therefore, in these conditions an increase of the heating power does not necessarily lead to a steepening of the E_r gradients, but just to an upward shift of the entire edge E_r profile. The lack of dependence of the E_r gradients on heating power could also explain the increased H-mode threshold in such plasma conditions. Furthermore, these observations show that at least in L-mode it is not always valid to use the minimum of the edge E_r as a proxy for its gradients.

ACKNOWLEDGMENTS

The main author would like to thank Gregor Birkenmeier, Raul Gerr -Miguelan ez, Ondrej Grover, Rachael McDermott, Ulrich Stroth and Elisabeth Wolfrum for fruitful discussions and valuable input.

This work has been carried out within the framework of the EUROfusion Consortium, funded by the European Union via the Euratom Research and Training Programme (Grant Agreement No 101052200 — EUROfusion). Views and opinions expressed are however those of the author(s) only and do not necessarily reflect those of the European Union or the European Commission. Neither the European Union nor the European Commission can be held responsible for them.

Work of A. Hubbard was supported by US Department of Energy Awards DE-FC02-99ER54512 and DE-SC0014264.

DATA AVAILABILITY

The data that support the findings of this study are available from the corresponding author upon reasonable request.

Appendix A: Coordinate System and Magnetic Configurations of AUG

Figure 24 shows a bird's-eye view image and Figure 25 the poloidal cross-sections of the different magnetic configurations (drift configurations) of AUG employed in this experimental study. AUG uses a right-handed, orthogonal (R, Θ, Φ) coordinate system (COCOS 17¹⁰⁹), with Φ being counter-clockwise if viewed from above and Θ pointing downwards at the outer mid-plane (OMP). In the standard magnetic configuration, the lower-single null (LSN) favourable drift configuration (blue), B_ϕ is negative and directed clockwise if seen from above. In this configuration I_p is counter-clockwise and positive, which leads to a left-handed helicity of the magnetic field lines. The NBI injection is co-current.

Due to technical constraints, the helicity of the B -field has to be preserved in the lower divertor at AUG. Thus, the unfavourable drift configuration in LSN (red) can only be obtained if both B_ϕ and I_p are reversed, which leads to a counter-current NBI injection. In the upper single-null (USN) unfavourable drift configuration (orange) the drift directions

This is the author's peer reviewed, accepted manuscript. However, the online version of record will be different from this version once it has been copyedited and typeset.

PLEASE CITE THIS ARTICLE AS DOI: 10.1063/1.50102763

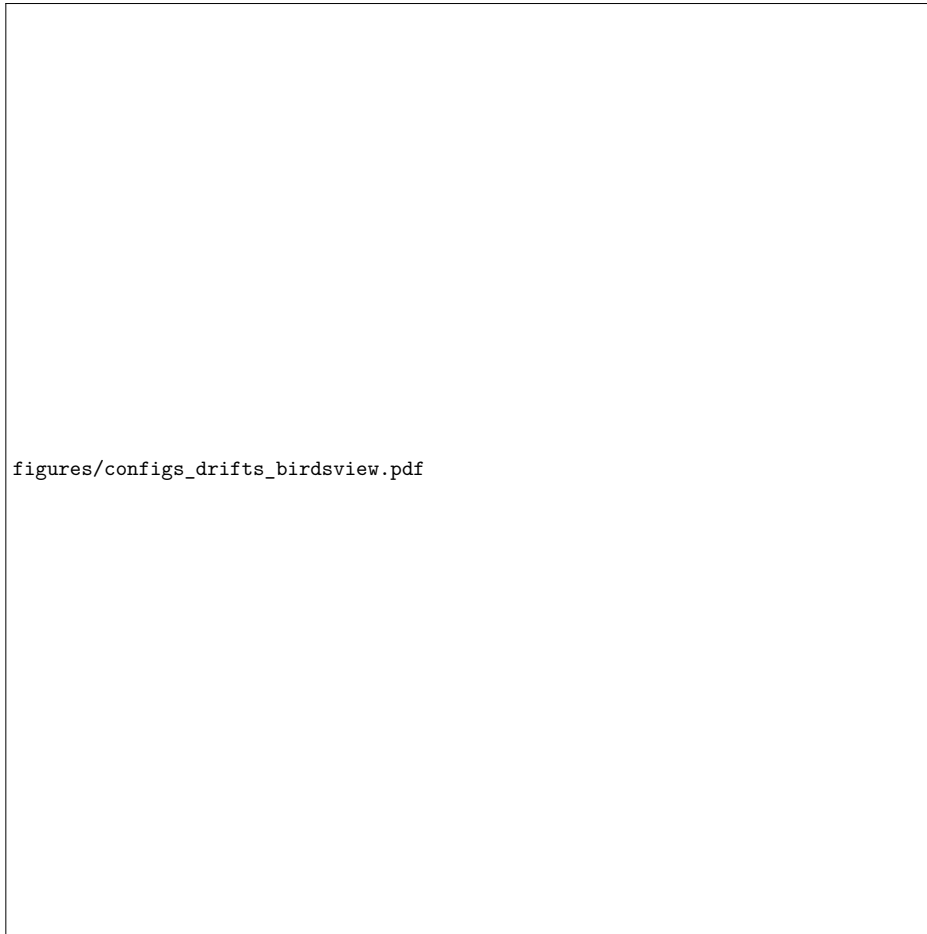


FIG. 24. Sign convention of AUG and the corresponding drift directions in the four investigated magnetic configurations at AUG.

are the same as in the LSN favourable drift configuration, except that in this case $v_{\nabla B, i}$ points away from the primary X-point. The USN favourable drift configuration can then simply be achieved by reversing B_ϕ only, which, at the same time, changes the helicity of the B -field to right-handed. The NBI injection is co-current in this case.

In Figure 25, besides the directions of the ion ∇B -drift (blue), also the directions of the electron and ion diamagnetic drifts are indicated (black) at the high field side (HFS) and

This is the author's peer reviewed, accepted manuscript. However, the online version of record will be different from this version once it has been copyedited and typeset.

PLEASE CITE THIS ARTICLE AS DOI: 10.1063/1.50102763



FIG. 25. Poloidal cross sections of the four investigated magnetic configurations at AUG. The directions of the different drifts are also indicated in the plots.

low field side (LFS). For the directions of the poloidal component of the $E \times B$ drift (shown in magenta) the following assumptions on E_r at the OMP were made: In the core plasma E_r is dominated by the toroidal rotation and, thus, by the injection direction of the NBI and it is dominated by $(\nabla_r p_i)/(en_i)$ at the plasma edge. In the SOL it was assumed to be positive.

This is the author's peer reviewed, accepted manuscript. However, the online version of record will be different from this version once it has been copyedited and typeset.
 PLEASE CITE THIS ARTICLE AS DOI: 10.1063/5.0102763

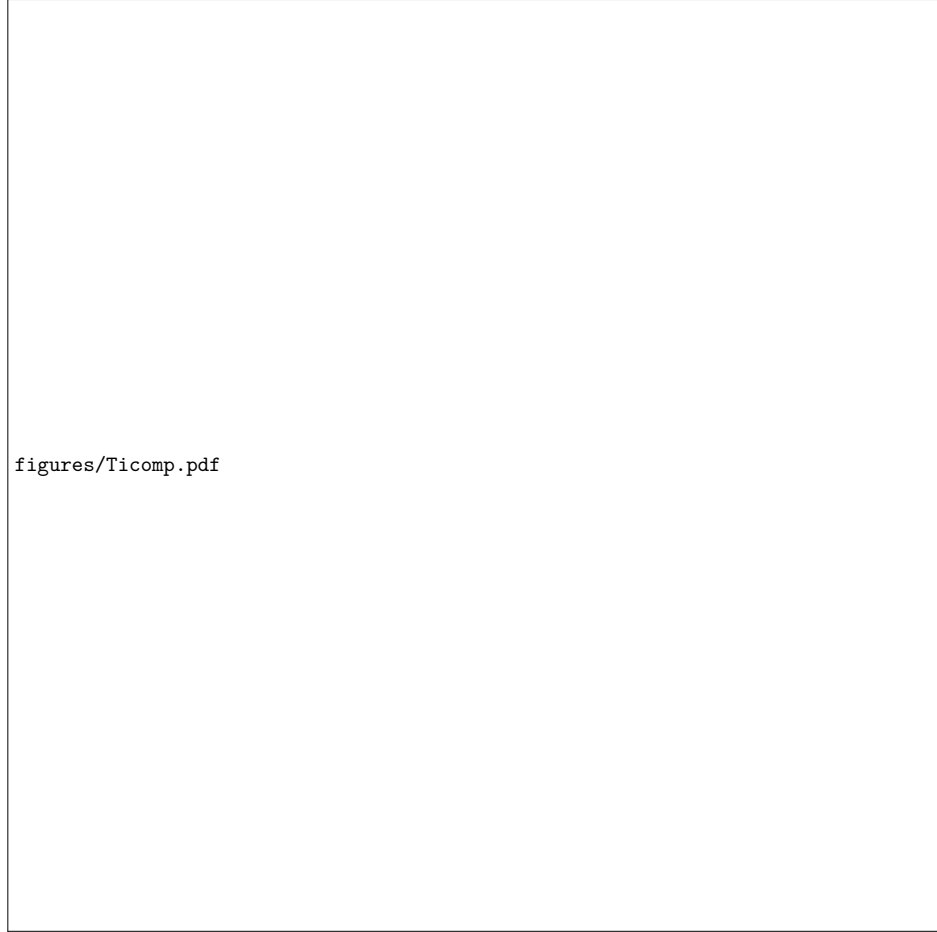


FIG. 26. T_i fits of different stiffness to the experimental edge T_i data of the L-mode phases presented in Section VI A. (a) Favourable and (b) unfavourable drift configuration.

Appendix B: Sensitivity Study of the NC Prediction of E_r on the Choice of the T_i Profile

A sensitivity study has shown that the NC calculations of the main ion velocities and the resulting E_r profiles are most sensitive to the T_i input profiles. Therefore, in Figure 26 a comparison of cubic-spline fits of different stiffness is shown, which were used to fit the edge

T_i data in favourable (a, blue) and unfavourable (b, light red) drift configuration L-modes. These L-mode phases are also presented in Section VI A. The solid lines result from stiffer and the dashed lines from less stiff fits to the experimental T_i data. These different T_i fits were given as input to NEOART and the resulting E_r profiles are shown, together with the experimental data, in Figure 27.

For producing the E_r profiles of both drift configurations, shown in Figure 27a, the stiffer fits were used (flat T_i gradient). For Figure 27b less stiff fits were used, which allow for steeper gradients in the edge T_i profiles, but are at the same time more sensitive to outliers in the experimental T_i data. The figure shows that for the less stiff T_i fits the predicted E_r profiles agree qualitatively better with the measured E_r profiles in the region around $E_{r,\min}$ for favourable drift configuration, whereas for the unfavourable drift configuration larger differences are found. Also the minimum in the E_r profile can only be produced using the less stiff T_i fit, however, also with these fits the slope of the inner E_r gradient can not be fully reproduced. Furthermore, the differences observed in the experimental E_r between favourable and unfavourable drift configuration are not captured by the predicted E_r profiles, neither with the stiff nor the less stiff T_i profiles.

From this it can be seen that conclusions on the different drift configurations can be drawn when comparing the experimental data with the NC predictions, independently of the exact shape of the input profiles, as long as fits of the same stiffness are used for the NC calculations.

REFERENCES

- ¹B. LaBombard, J. E. Rice, A. E. Hubbard, J. W. Hughes, M. Greenwald, R. S. Granetz, J. H. Irby, Y. Lin, B. Lipschultz, E. S. Marmor, K. Marr, D. Mossessian, R. Parker, W. Rowan, N. Smick, J. A. Snipes, J. L. Terry, S. M. Wolfe, and S. J. Wukitch, *Phys. Plasmas* **12**, 1 (2005).
- ²ASDEX Team, *Nucl. Fusion* **29**, 1959 (1989).
- ³H. Biglari, P. H. Diamond, and P. W. Terry, *Phys. Fluids B* **2**, 1 (1990).
- ⁴M. Cavedon, G. Birkenmeier, T. Pütterich, F. Ryter, E. Viezzer, E. Wolfrum, R. Dux, T. Happel, P. Hennequin, U. Plank, U. Stroth, and M. Willensdorfer, *Nucl. Fusion* **60**, 066026 (2020).

This is the author's peer reviewed, accepted manuscript. However, the online version of record will be different from this version once it has been copyedited and typeset.

PLEASE CITE THIS ARTICLE AS DOI: 10.1063/1.50102763

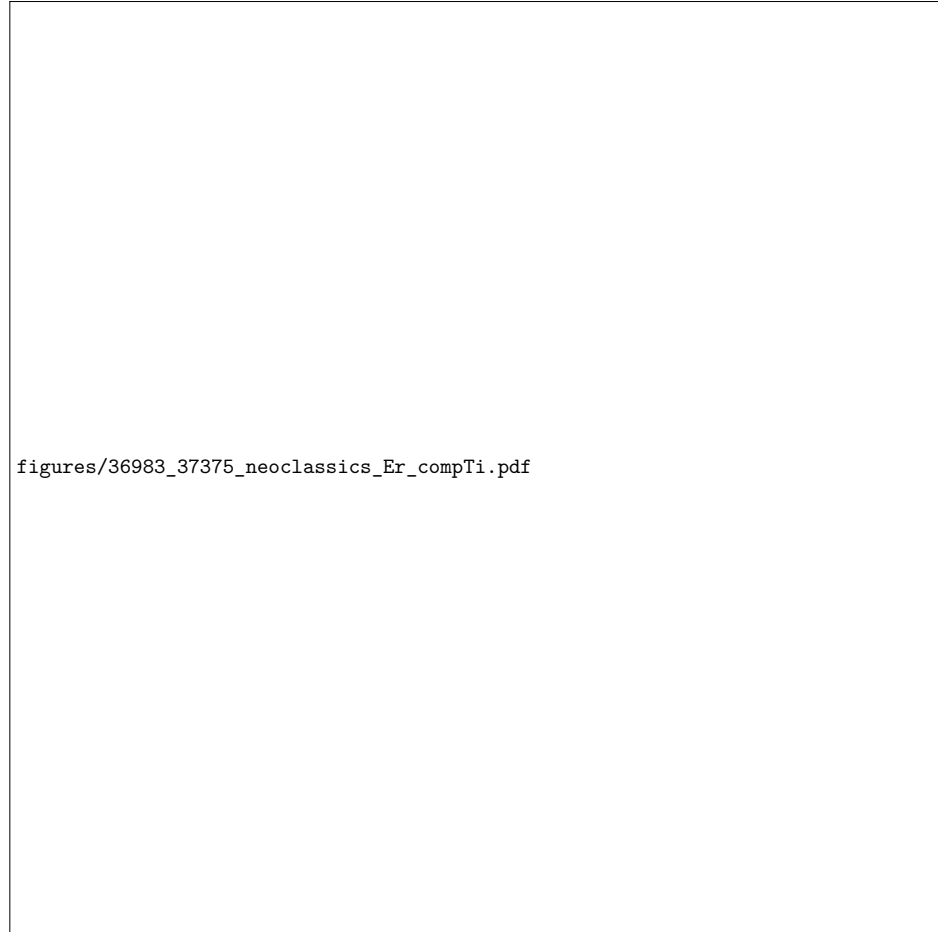


FIG. 27. Predicted E_r profiles from NEOART velocities (solid), main ion pressure gradient (dashed) and experimental edge E_r profiles (stars), using a stiff fit for the edge T_i data, allowing for less steep edge gradients (a) and using a less stiff fit for the edge T_i data, allowing for steeper edge gradients (b).

⁵Y. R. Martin and T. Takizuka, J. Phys. Conf. Ser. **123**, 012033 (2008).

⁶F. Ryter, W. Suttrop, B. Brüsehaber, M. Kaufmann, V. Mertens, H. Murmann, A. G. Peeters, J. Stober, J. Schweinzer, and H. Zohm, Plasma Phys. Control. Fusion **40**, 725 (1998).

This is the author's peer reviewed, accepted manuscript. However, the online version of record will be different from this version once it has been copyedited and typeset.

PLEASE CITE THIS ARTICLE AS DOI: 10.1063/5.0102763

- ⁷T. N. Carlstrom, K. H. Burrell, R. J. Groebner, and S. G. M., 24th Eur. Phys. Soc. Conf. Control. Fusion Plasma Phys. **21a**, 1089 (1997).
- ⁸M. Greenwald, R. L. Boivin, F. Bombarda, P. T. Bonoli, C. L. Fiore, D. Garnier, J. A. Goetz, S. N. Golovato, M. A. Graf, R. S. Granetz, S. Horne, A. Hubbard, I. H. Hutchinson, J. H. Irby, B. LaBombard, B. Lipschultz, E. S. Marmor, M. J. May, G. M. McCracken, P. OShea, J. E. Rice, J. Schachter, J. A. Snipes, P. C. Stek, Y. Takase, J. L. Terry, Y. Wang, R. Watterson, B. Welch, and S. M. Wolfe, Nucl. Fusion **37**, 793 (1997).
- ⁹D. G. Whyte, A. E. Hubbard, J. W. Hughes, B. Lipschultz, J. E. Rice, E. S. Marmor, M. Greenwald, I. Cziegler, A. Dominguez, T. Golfopoulos, N. Howard, L. Lin, R. M. McDermottb, M. Porkolab, M. L. Reinke, J. Terry, N. Tsujii, S. Wolfe, S. Wukitch, and Y. Lin, Nucl. Fusion **50**, 105005 (2010).
- ¹⁰T. N. Carlstrom, R. J. Groebner, C. Fenzi, G. R. McKee, R. A. Moyer, and T. L. Rhodes, Plasma Phys. Control. Fusion **44** (2002), 10.1088/0741-3335/44/5A/335.
- ¹¹J. Schirmer, G. D. Conway, H. Zohm, W. Suttrop, and ASDEX Upgrade Team, Nucl. Fusion **46**, S780 (2006).
- ¹²L. Vermare, P. Hennequin, C. Honoré, M. Peret, G. Dif-Pradalier, X. Garbet, J. Gunn, C. Bourdelle, F. Clairet, J. Morales, R. Dumont, M. Goniche, P. Maget, and R. Varennes, Nucl. Fusion **62** (2022), 10.1088/1741-4326/ac3c85.
- ¹³L. Aho-Mantila, M. Wischmeier, H. W. Müller, S. Potzel, D. P. Coster, X. Bonnin, and G. D. Conway, Nucl. Fusion **52**, 103006 (2012).
- ¹⁴A. V. Chankin, E. Delabie, G. Corrigan, D. Harting, C. F. Maggi, and H. Meyer, Plasma Phys. Control. Fusion **59**, 045012 (2017).
- ¹⁵P. Manz, T. Happel, U. Stroth, T. Eich, and D. Silvagni, Nucl. Fusion **60**, 096011 (2020).
- ¹⁶N. Fedorczak, P. H. Diamond, G. Tynan, and P. Manz, Nucl. Fusion **52** (2012), 10.1088/0029-5515/52/10/103013.
- ¹⁷G. M. Staebler and R. J. Groebner, Plasma Phys. Control. Fusion **57** (2015), 10.1088/0741-3335/57/1/014025.
- ¹⁸K. C. Shaing and E. C. Crume, Phys. Rev. Lett. **63**, 2369 (1989).
- ¹⁹R. W. Brzozowski, F. Jenko, R. Bilato, and M. Cavedon, Phys. Plasmas **26**, 042511 (2019).
- ²⁰T. W. Versloot, P. C. De Vries, C. Giroud, M. Brix, M. G. Von Hellermann, P. J. Lomas, D. Moulton, M. O. Mullane, I. M. Nunes, A. Salmi, T. Tala, I. Voitsekhovitch, and K. D.

This is the author's peer reviewed, accepted manuscript. However, the online version of record will be different from this version once it has been copyedited and typeset.

PLEASE CITE THIS ARTICLE AS DOI: 10.1063/1.50102763

- Zastrow, *Plasma Phys. Control. Fusion* **53** (2011), 10.1088/0741-3335/53/6/065017.
- ²¹D. Moulton, G. Corrigan, J. R. Harrison, B. Lipschultz, and JET Contributors, *Nucl. Fusion* **58**, 096029 (2018).
- ²²S. I. Braginskii, *Rev. Plasma Phys.* **1**, 205 (1965).
- ²³E. Viezzer, T. Pütterich, C. Angioni, A. Bergmann, R. Dux, E. Fable, R. M. McDermott, U. Stroth, and E. Wolfrum, *Nucl. Fusion* **54**, 012003 (2014).
- ²⁴S. R. Haskey, B. A. Grierson, C. Chrystal, A. Ashourvan, K. H. Burrell, R. J. Groebner, E. A. Belli, L. Stagner, D. J. Battaglia, T. Stoltzfus-Dueck, and A. Bortolon, *Plasma Physics and Controlled Fusion* **60**, 105001 (2018).
- ²⁵R. J. Goldston and P. H. Rutherford, *Introduction to Plasma Physics* (IOP Publishing, Bristol and Philadelphia, 1995).
- ²⁶P. C. Stangeby, *The Plasma Boundary of Magnetic Fusion Devices* (IOP Publishing Ltd., London, 2000).
- ²⁷D. Brida, G. Conway, J. Adamek, D. Silvagni, P. David, T. Eich, G. Grenfell, M. Komm, and U. Plank, *Nuclear Materials and Energy* **33**, 101262 (2022).
- ²⁸A. V. Chankin, D. P. Coster, G. Corrigan, S. K. Erements, W. Fundamenski, A. Kallenbach, K. Lackner, J. Neuhauser, and R. Pitts, *Plasma Phys. Control. Fusion* **51**, 065022 (2009).
- ²⁹P. C. Stangeby and A. V. Chankin, *Nucl. Fusion* **36**, 839 (1996).
- ³⁰M. Cavedon, R. Dux, T. Happel, P. Hennequin, U. Plank, T. Pütterich, F. Ryter, U. Stroth, E. Viezzer, and E. Wolfrum, in *46th EPS Conf. Plasma Physics, EPS 2019* (Milan, 2019) p. P5.1069.
- ³¹U. Plank, T. Pütterich, C. Angioni, M. Cavedon, G. D. Conway, R. Fischer, T. Happel, A. Kappatou, R. M. McDermott, P. A. Schneider, G. Tardini, and M. Weiland, *Nucl. Fusion* **60**, 074001 (2020).
- ³²R. Fischer, C. J. Fuchs, B. Kurzan, W. Suttrop, and E. Wolfrum, *Fusion Sci. Technol.* **58**, 675 (2010).
- ³³F. Ryter, M. Cavedon, T. Happel, R. M. McDermott, E. Viezzer, G. D. Conway, R. Fischer, B. Kurzan, T. Pütterich, G. Tardini, M. Willensdorfer, and the ASDEX Upgrade Team, *Plasma Phys. Control. Fusion* **58**, 014007 (2016).
- ³⁴R. M. McDermott, R. Dux, T. Pütterich, B. Geiger, A. Kappatou, A. Lebschy, C. Bruhn, M. Cavedon, A. Frank, N. D. Harder, E. Viezzer, and the ASDEX Upgrade Team, *Plasma Phys. Control. Fusion* **60**, 095007 (2018).

This is the author's peer reviewed, accepted manuscript. However, the online version of record will be different from this version once it has been copyedited and typeset.

PLEASE CITE THIS ARTICLE AS DOI: 10.1063/5.0102763

- ³⁵R. Fischer, S. K. Rathgeber, S. Fietz, J. Hobirk, A. Kallenbach, H. Meister, T. Pütterich, F. Ryter, G. Tardini, E. Wolfrum, and H. Zohm, in *37th EPS Conf. Plasma Phys. 2010, EPS 2010* (2010) p. P5.107.
- ³⁶U. Plank, *The Effect of the Radial Electric Field around the Separatrix on the Access to the High Confinement Mode at ASDEX Upgrade*, PhD thesis, Ludwig Maximilian University Munich (2021).
- ³⁷G. D. Conway, C. Angioni, F. Ryter, P. Sauter, and J. Vicente, *Phys. Rev. Lett.* **106**, 065001 (2011).
- ³⁸H. Zohm and the ASDEX Upgrade Team, *Phys. Rev. Lett.* **72**, 222 (1994).
- ³⁹H. Zohm, W. Suttrop, K. Buchl, H. J. De Blank, O. Gruber, A. Kallenbach, V. Mertens, F. Ryter, and M. Schittenhelm, *Plasma Phys. Control. Fusion* **37**, 437 (1995).
- ⁴⁰L. Schmitz, L. Zeng, T. L. Rhodes, J. C. Hillesheim, E. J. Doyle, R. J. Groebner, W. A. Peebles, K. H. Burrell, and G. Wang, *Phys. Rev. Lett.* **108**, 1 (2012).
- ⁴¹O. Grover, J. Seidl, D. Refy, J. Adamek, P. Vondracek, M. Tomes, P. Junek, P. Hacek, J. Krbec, V. Weinzettl, M. Hron, S. Zoletnik, and The COMPASS Team, *Nucl. Fusion* **58**, 112010 (2018).
- ⁴²L. M. Shao, G. S. Xu, R. Chen, L. Chen, G. Birkenmeier, Y. M. Duan, W. Gao, P. Manz, T. H. Shi, H. Q. Wang, L. Wang, M. Xu, N. Yan, L. Zhang, and the EAST Team, *Plasma Phys. Control. Fusion* **60**, 035012 (2018).
- ⁴³G. Birkenmeier, M. Cavedon, G. D. Conway, P. Manz, U. Stroth, R. Fischer, G. Fuchert, T. Happel, F. M. Laggner, M. Maraschek, A. Medvedeva, V. Nikolaeva, D. Prisiazhniuk, T. Pütterich, F. Ryter, L. M. Shao, M. Willensdorfer, E. Wolfrum, and H. Zohm, *Nucl. Fusion* **56**, 086009 (2016).
- ⁴⁴A. E. Hubbard, D. G. Whyte, R. M. Churchill, I. Cziegler, A. Dominguez, T. Golfopoulos, J. W. Hughes, J. E. Rice, I. Bespamyatnov, M. J. Greenwald, N. Howard, B. Lipschultz, E. S. Marmor, M. L. Reinke, W. L. Rowan, and J. L. Terry, *Phys. Plasmas* **18**, 056115 (2011).
- ⁴⁵T. Happel, S. J. Freethy, P. Hennequin, P. Manz, D. Prisiazhniuk, F. Ryter, and the ASDEX Upgrade Team, in *27th IAEA Fusion Energy Conf. (Gandhinagar, 2018)*.
- ⁴⁶T. Happel, M. Griener, D. Silvagni, S. J. Freethy, P. Hennequin, F. Janky, P. Manz, D. Prisiazhniuk, F. Ryter, M. Bernert, D. Brida, T. Eich, M. Faitsch, L. Gil, L. Guimaraes, A. Merle, D. Nille, J. Pinzón, B. Sieglin, U. Stroth, and E. Viezzer, *Nucl. Mater. Energy*

This is the author's peer reviewed, accepted manuscript. However, the online version of record will be different from this version once it has been copyedited and typeset.

PLEASE CITE THIS ARTICLE AS DOI: 10.1063/1.50102763

- 18, 159 (2019).
- ⁴⁷D. Silvagni, T. Eich, T. Happel, G. F. Harrer, M. Griener, M. Dunne, M. Cavedon, M. Faitsch, L. Gil, D. Nille, B. Tal, R. Fischer, U. Stroth, D. Brida, P. David, P. Manz, and E. Viezzer, *Nucl. Fusion* **60**, 126028 (2020), 2006.11452.
- ⁴⁸F. Ryter, L. Barrera Orte, B. Kurzan, R. M. McDermott, G. Tardini, E. Viezzer, M. Bernert, and R. Fischer, *Nucl. Fusion* **54**, 083003 (2014).
- ⁴⁹M. Weiland, R. Bilato, R. Dux, B. Geiger, A. Lebschy, F. Felici, R. Fischer, D. Rittich, and M. Van Zeeland, *Nucl. Fusion* **58**, 082032 (2018).
- ⁵⁰P. David, M. Bernert, T. Pütterich, C. Fuchs, S. Glöggler, and T. Eich, *Nucl. Fusion* **61**, 066025 (2021).
- ⁵¹G. V. Pereverzev and P. N. Yushmanov, “ASTRA—Automated System for Transport Analysis in a Tokamak,” Tech. Rep. IPP 5/98 (Max Planck Institute for Plasma Physics, 2002).
- ⁵²E. Poli, A. G. Peeters, and G. V. Pereverzev, *Comput. Phys. Commun.* **136**, 90 (2001).
- ⁵³R. Fischer, A. Bock, A. Burckhart, M. Dunne, O. Ford, J. C. Fuchs, L. Giannone, A. Gude, V. Igochine, A. Lebschy, M. Maraschek, P. J. McCarthy, A. Mlynek, A. Snicker, J. Stober, G. Tardini, M. Weiland, and M. Willensdorfer, in *43rd Eur. Phys. Soc. Conf. Plasma Physics, EPS 2016* (2016).
- ⁵⁴J. Illerhaus, *Estimation, Validation and Uncertainty of the Position of the Separatrix Contour at ASDEX Upgrade*, Diploma thesis, Technical University, Munich (2018).
- ⁵⁵H. J. Sun, E. Wolfrum, T. Eich, B. Kurzan, S. Potzel, U. Stroth, and the ASDEX Upgrade Team, *Plasma Physics and Controlled Fusion* **57**, 125011 (2015).
- ⁵⁶T. Eich, P. Manz, R. J. Goldston, P. Hennequin, P. David, M. Faitsch, B. Kurzan, B. Sieglin, and E. Wolfrum, *Nucl. Fusion* **60** (2020), 10.1088/1741-4326/ab7a66.
- ⁵⁷D. Silvagni, T. Eich, M. Faitsch, T. Happel, B. Sieglin, P. David, D. Nille, L. Gil, and U. Stroth, *Plasma Phys. Control. Fusion* **62** (2020), 10.1088/1361-6587/ab74e8.
- ⁵⁸M. Griener, J. M. Burgos, M. Cavedon, G. Birkenmeier, R. Dux, B. Kurzan, O. Schmitz, B. Sieglin, U. Stroth, E. Viezzer, and E. Wolfrum, *Plasma Phys. Control. Fusion* **60**, 025008 (2018).
- ⁵⁹R. M. McDermott, A. Lebschy, B. Geiger, C. Bruhn, M. Cavedon, M. Dunne, R. Dux, R. Fischer, A. Kappatou, T. Pütterich, and E. Viezzer, *Rev. Sci. Instrum.* **88**, 73508

This is the author's peer reviewed, accepted manuscript. However, the online version of record will be different from this version once it has been copyedited and typeset.

PLEASE CITE THIS ARTICLE AS DOI: 10.1063/5.0102763

- (2017).
- ⁶⁰E. Viezzer, T. Pütterich, R. Dux, and R. M. McDermott, *Rev. Sci. Instrum.* **83** (2012), 10.1063/1.4755810.
- ⁶¹E. Viezzer, T. Pütterich, G. D. Conway, R. Dux, T. Happel, J. C. Fuchs, R. M. McDermott, F. Ryter, B. Sieglin, W. Suttrop, M. Willensdorfer, and E. Wolfrum, *Nucl. Fusion* **53**, 053005 (2013).
- ⁶²G. D. Conway, J. Schirmer, S. Klenge, W. Suttrop, and E. Holzhauser, *Plasma Phys. Control. Fusion* **46**, 951 (2004).
- ⁶³T. Happel, A. B. Navarro, G. D. Conway, C. Angioni, M. Bernert, M. Dunne, E. Fable, B. Geiger, T. Görler, F. Jenko, R. M. McDermott, F. Ryter, and U. Stroth, *Phys. Plasmas* **22** (2015), 10.1063/1.4914153.
- ⁶⁴H. Meyer, C. Bunting, G. Carolan, J. Conway, R. Dunstan, A. Kirk, R. Scannell, D. Temple, and M. Walsh, *J. Phys. Conf. Ser.* **123**, 012005 (2008).
- ⁶⁵A. G. Peeters, *Phys. Plasmas* **7**, 268 (2000).
- ⁶⁶E. A. Belli and J. Candy, *Plasma Physics and Controlled Fusion* **50**, 095010 (2008).
- ⁶⁷R. Dux, “STRAHL User Manual,” Tech. Rep. (Max Planck Institute for Plasma Physics, 2006).
- ⁶⁸F. Ryter, S. K. Rathgeber, L. Barrera Orte, M. Bernert, G. D. Conway, R. Fischer, T. Happel, B. Kurzan, R. M. McDermott, A. Scarabosio, W. Suttrop, E. Viezzer, M. Willensdorfer, and E. Wolfrum, *Nucl. Fusion* **53**, 113003 (2013).
- ⁶⁹F. Ryter, R. Fischer, J. C. Fuchs, T. Happel, R. M. McDermott, E. Viezzer, E. Wolfrum, L. Barrera Orte, M. Bernert, A. Burckhart, S. Da Graça, B. Kurzan, P. McCarthy, T. Pütterich, W. Suttrop, and M. Willensdorfer, *Nucl. Fusion* **57**, 016004 (2017).
- ⁷⁰T. N. Carlstrom, P. Gohil, J. G. Watkins, K. H. Burrell, S. Coda, E. J. Doyle, R. J. Groebner, J. Kim, R. A. Moyer, and C. L. Rettig, *Plasma Phys. Control. Fusion* **36**, A147 (1994).
- ⁷¹P. Gohil, T. C. Jernigan, T. H. Osborne, J. T. Scoville, and E. J. Strait, *Nucl. Fusion* **50**, 064011 (2010).
- ⁷²N. Bonanomi, C. Angioni, U. Plank, P. A. Schneider, and C. F. Maggi, *Phys. Plasmas* **28**, 052504 (2021).
- ⁷³P. Sauter, T. Pütterich, F. Ryter, E. Viezzer, E. Wolfrum, G. D. Conway, R. Fischer, B. Kurzan, R. M. McDermott, and S. K. Rathgeber, *Nucl. Fusion* **52**, 012001 (2012).

This is the author's peer reviewed, accepted manuscript. However, the online version of record will be different from this version once it has been copyedited and typeset.

PLEASE CITE THIS ARTICLE AS DOI: 10.1063/1.50102763

- ⁷⁴M. Cavedon, T. Pütterich, E. Viezzer, G. Birkenmeier, T. Happel, F. M. Laggner, P. Manz, F. Ryter, and U. Stroth, *Nucl. Fusion* **57**, 014002 (2017).
- ⁷⁵T. Happel, P. Manz, F. Ryter, M. Bernert, M. Dunne, P. Hennequin, A. Hetzenecker, U. Stroth, G. D. Conway, L. Guimaraes, C. Honoré, and E. Viezzer, *Plasma Phys. Control. Fusion* **59**, 014004 (2017).
- ⁷⁶H. Meyer, P. G. Carolan, G. D. Conway, G. Cunningham, L. D. Horton, A. Kirk, R. Maingi, F. Ryter, S. Saarelma, J. Schirmer, W. Suttrop, and H. R. Wilson, *Nucl. Fusion* **46**, 64 (2006).
- ⁷⁷A. V. Chankin, *J. Nucl. Mater.* **241-243**, 199 (1997).
- ⁷⁸I. Paradel Pérez, M. Groth, M. Wischmeier, A. Scarabosio, D. Brida, P. David, D. Silvagni, D. Coster, T. Lunt, M. Faitsch, and the ASDEX Upgrade Team and the EUROfusion MST1 Team, *Nucl. Mater. Energy* **19**, 521 (2019).
- ⁷⁹T. Eich, A. W. Leonard, R. A. Pitts, W. Fundamenski, R. J. Goldston, T. K. Gray, A. Herrmann, A. Kirk, A. Kallenbach, O. Kardaun, A. S. Kukushkin, B. Labombard, R. Maingi, M. A. Makowski, A. Scarabosio, B. Sieglin, J. Terry, and A. Thornton, *Nucl. Fusion* **53**, 093031 (2013).
- ⁸⁰R. A. Moyer, K. H. Burrell, T. N. Carlstrom, S. Coda, R. W. Conn, E. J. Doyle, P. Gohil, R. J. Groebner, J. Kim, R. Lehmer, W. A. Peebles, M. Porkolab, C. L. Rettig, T. L. Rhodes, R. P. Seraydarian, R. Stockdale, D. M. Thomas, G. R. Tynan, and J. G. Watkins, *Physics of Plasmas* **2**, 2397 (1995), <https://doi.org/10.1063/1.871263>.
- ⁸¹G. McKee, P. Gohil, D. Schlossberg, J. Boedo, K. Burrell, J. deGrassie, R. Groebner, R. Moyer, C. Petty, T. Rhodes, L. Schmitz, M. Shafer, W. Solomon, M. Umansky, G. Wang, A. White, and X. Xu, *Nuclear Fusion* **49**, 115016 (2009).
- ⁸²N. Fedorczak, P. Ghendrih, P. Hennequin, G. R. Tynan, P. H. Diamond, and P. Manz, *Plasma Phys. Control. Fusion* **55** (2013), 10.1088/0741-3335/55/12/124024.
- ⁸³P. Manz, A. Stegmeir, B. Schmid, T. T. Ribeiro, G. Birkenmeier, N. Fedorczak, S. Garland, K. Hallatschek, M. Ramisch, and B. D. Scott, *Phys. Plasmas* **25** (2018), 10.1063/1.5037511.
- ⁸⁴G. M. Staebler and R. J. Groebner, *Nucl. Fusion* **55**, 73008 (2015).
- ⁸⁵T. Stoltzfus-Dueck, *Plasma Phys. Control. Fusion* **61** (2019), 10.1088/1361-6587/ab4376.
- ⁸⁶J. Omotani, I. Pusztai, S. Newton, and T. Fülöp, *Nucl. Fusion* **56** (2016), 10.1088/0029-5515/56/12/124002.

This is the author's peer reviewed, accepted manuscript. However, the online version of record will be different from this version once it has been copyedited and typeset.

PLEASE CITE THIS ARTICLE AS DOI: 10.1063/5.0102763

- ⁸⁷W. Zholobenko, A. Stegmeir, M. Griener, G. D. Conway, T. Body, D. Coster, and F. Jenko, *Nucl. Fusion* **61** (2021), 10.1088/1741-4326/ac1e61.
- ⁸⁸P. Cano-Megias, E. Viezzer, R. W. Brzozowski, U. Plank, M. Cavedon, T. Happel, K. Höfler, D. J. Cruz-Zabala, R. Dux, M. Griener, J. Hobirk, A. J. Van Vuuren, T. Pütterich, and R. Chacartegui, 47th EPS Conf. Plasma Physics, EPS 2021 **2021-June**, 181 (2021).
- ⁸⁹J. T. Omotani, S. L. Newton, I. Pusztai, E. Viezzer, and T. Fülöp, *Nucl. Fusion* **57** (2017), 10.1088/1741-4326/aa6ce4.
- ⁹⁰S. Buller, I. Pusztai, S. L. Newton, and J. T. Omotani, *Plasma Phys. Control. Fusion* **59**, 055019 (2017).
- ⁹¹R. Schneider, X. Bonnin, K. Borrass, D. P. Coster, H. Kastelewicz, D. Reiter, V. A. Rozhansky, and B. J. Braams, *Contrib. to Plasma Phys.* **46**, 3 (2006).
- ⁹²B. P. Duval, A. Bortolon, A. Karpushov, R. A. Pitts, A. Pochelon, O. Sauter, A. Scarabosio, and G. Turri, *Phys. Plasmas* **15** (2008), 10.1063/1.2841528.
- ⁹³A. Ashourvan, B. A. Grierson, D. J. Battaglia, S. R. Haskey, and T. Stoltzfus-Dueck, *Physics of Plasmas* **25**, 056114 (2018), <https://doi.org/10.1063/1.5018326>.
- ⁹⁴T. Stoltzfus-Dueck, *Phys. Rev. Lett.* **108**, 1 (2012), arXiv:1109.0171.
- ⁹⁵T. Stoltzfus-Dueck, *Physics of Plasmas* **19**, 055908 (2012), <https://doi.org/10.1063/1.4718335>.
- ⁹⁶Y. Kosuga, P. H. Diamond, and Ö. D. Gürçan, *Phys. Plasmas* **17**, 1 (2010).
- ⁹⁷J. S. deGrassie, R. J. Groebner, K. H. Burrell, and W. M. Solomon, *Nucl. Fusion* **49** (2009), 10.1088/0029-5515/49/8/085020.
- ⁹⁸C. Chrystal, B. A. Grierson, S. R. Haskey, A. C. Sontag, F. M. Poli, M. W. Shafer, and J. S. deGrassie, *Nucl. Fusion* **60** (2020), 10.1088/1741-4326/ab6434.
- ⁹⁹C. Silva, E. R. Solano, J. C. Hillesheim, E. Delabie, S. Aleiferis, G. Birkenmeier, L. Gil, C. Giroud, E. Litherland-Smith, R. B. Morales, D. Nina, and A. Silva, *Nucl. Fusion* **61** (2021), 10.1088/1741-4326/ac2abb.
- ¹⁰⁰J. A. Boedo, J. S. deGrassie, B. Grierson, T. Stoltzfus-Dueck, D. J. Battaglia, D. L. Rudakov, E. A. Belli, R. J. Groebner, E. Hollmann, C. Lasnier, W. M. Solomon, E. A. Unterberg, and J. Watkins, *Physics of Plasmas* **23**, 092506 (2016), <https://doi.org/10.1063/1.4962683>.
- ¹⁰¹R. A. Pitts and J. Horacek, 34th EPS Conf. Plasma Phys. 2007, EPS 2007 - Europhys.

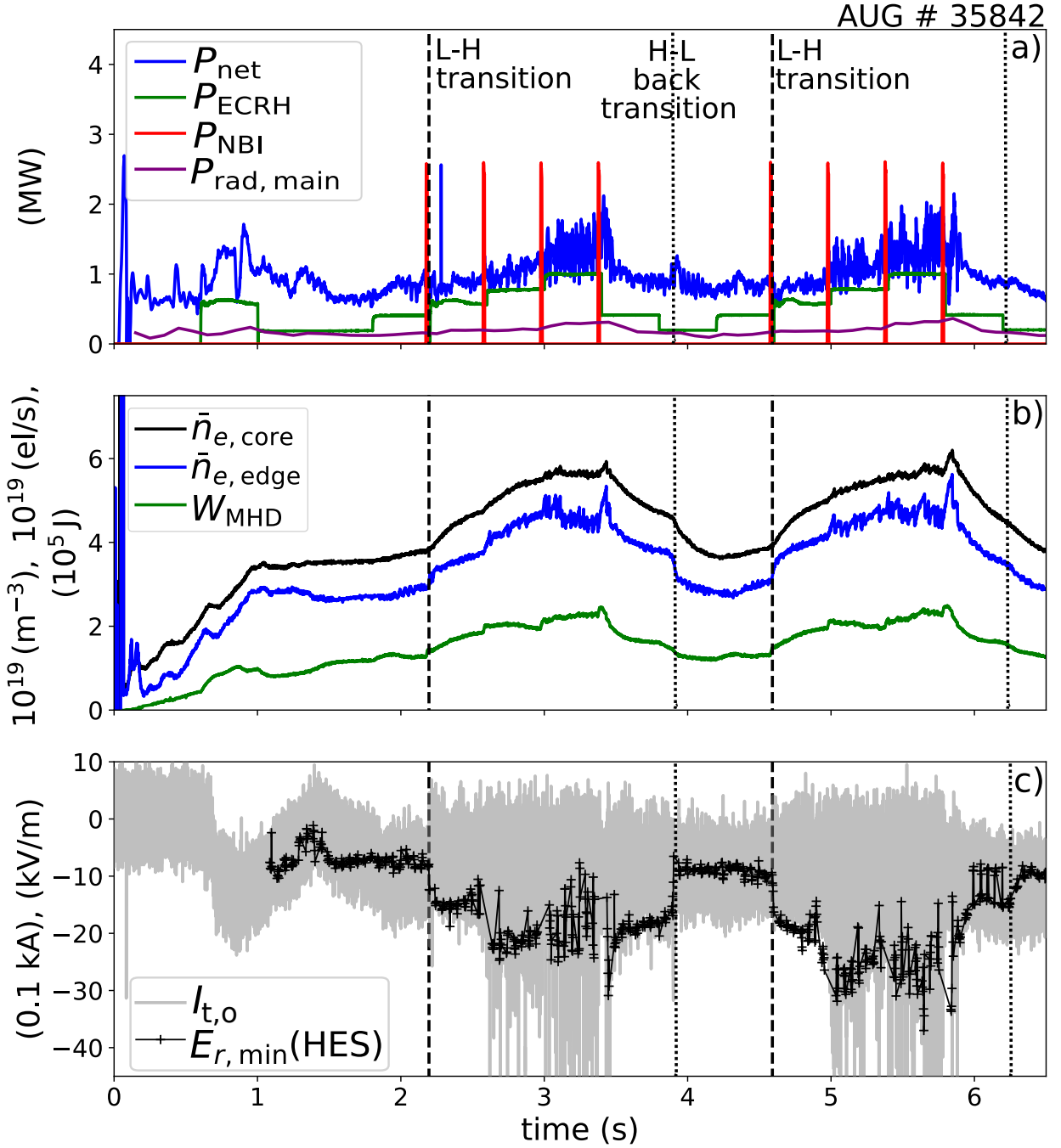
This is the author's peer reviewed, accepted manuscript. However, the online version of record will be different from this version once it has been copyedited and typeset.

PLEASE CITE THIS ARTICLE AS DOI: 10.1063/1.50102763

- Conf. Abstr. **31**, 109 (2007).
- ¹⁰²S. K. Erents, A. V. Chankin, G. F. Matthews, and P. C. Stangeby, *Plasma Phys. Control. Fusion* **42**, 905 (2000).
- ¹⁰³T. Happel, P. Manz, F. Ryter, P. Hennequin, A. Hetzenecker, G. D. Conway, L. Guimarães, C. Honoré, U. Stroth, and E. Viezzer, *Nucl. Fusion* **56**, 064004 (2016).
- ¹⁰⁴P. Manz, T. Happel, F. Ryter, M. Bernert, G. Birkenmeier, G. D. Conway, M. Dunne, L. Guimarães, P. Hennequin, A. Hetzenecker, C. Honoré, P. Lauber, M. Maraschek, V. E. Nikolaeva, D. Prisiazhniuk, U. Stroth, E. Viezzer, and the ASDEX Upgrade Team, *Nucl. Fusion* **57** (2017), 10.1088/1741-4326/aa7476.
- ¹⁰⁵A. E. White, P. Phillips, D. G. Whyte, A. E. Hubbard, C. Sung, J. W. Hughes, A. Dominguez, J. Terry, and I. Cziegler, *Nucl. Fusion* **51** (2011), 10.1088/0029-5515/51/11/113005.
- ¹⁰⁶I. Cziegler, P. H. Diamond, N. Fedorczak, P. Manz, G. R. Tynan, M. Xu, R. M. Churchill, A. E. Hubbard, B. Lipschultz, J. M. Sierchio, J. L. Terry, and C. Theiler, *Phys. Plasmas* **20** (2013), 10.1063/1.4803914.
- ¹⁰⁷H. Meyer, P. G. Carolan, N. J. Conway, A. R. Field, S. J. Fielding, and P. Helander, *Czechoslov. J. Phys.* **50**, 1451 (2000).
- ¹⁰⁸P. H. Diamond, S. I. Itoh, K. Itoh, and T. S. Hahm, *Plasma Phys. Control. Fusion* **47**, R35 (2005).
- ¹⁰⁹O. Sauter and S. Y. Medvedev, *Comput. Phys. Commun.* **184**, 293 (2013).

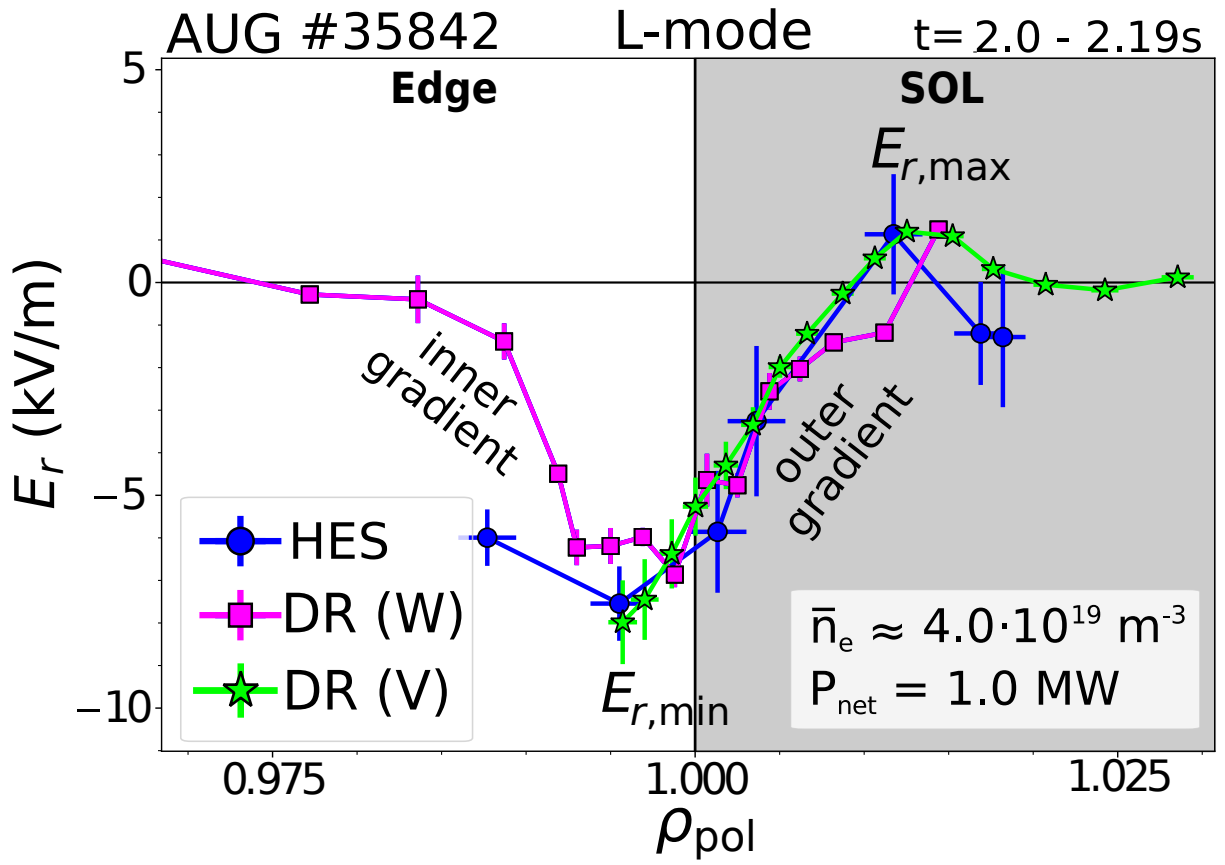
This is the author's peer reviewed, accepted manuscript. However, the online version of record will be different from this version once it has been copyedited and typeset.

PLEASE CITE THIS ARTICLE AS DOI: 10.1063/5.0102763



This is the author's peer reviewed, accepted manuscript. However, the online version of record will be different from this version once it has been copyedited and typeset.

PLEASE CITE THIS ARTICLE AS DOI: 10.1063/5.0102763



This is the author's peer reviewed, accepted manuscript. However, the online version of record will be different from this version once it has been copyedited and typeset.

PLEASE CITE THIS ARTICLE AS DOI: 10.1063/5.0102763



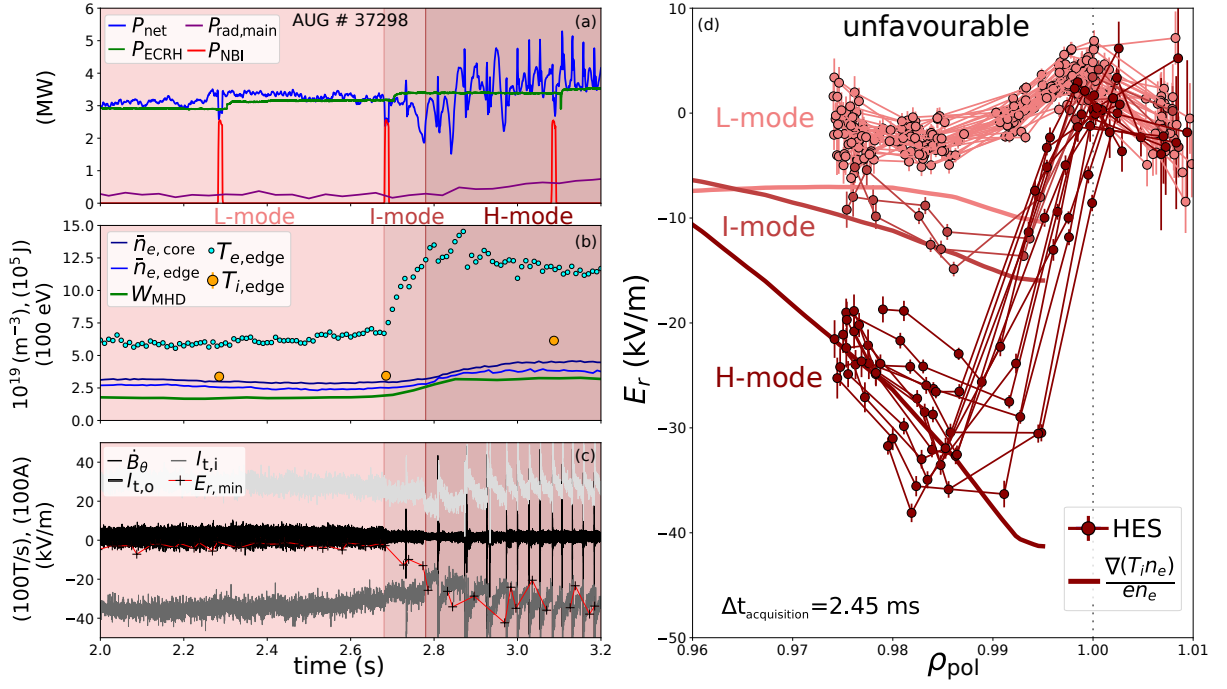
-  unfavourable
-  favourable
-   ECRH
-  NBI+ECRH
-   LSN, 0.8 MA
-   USN, 1.0 MA

This is the author's peer reviewed, accepted manuscript. However, the online version of record will be different from this version once it has been copyedited and typeset.

PLEASE CITE THIS ARTICLE AS DOI: [10.1063/5.0102763](https://doi.org/10.1063/5.0102763)

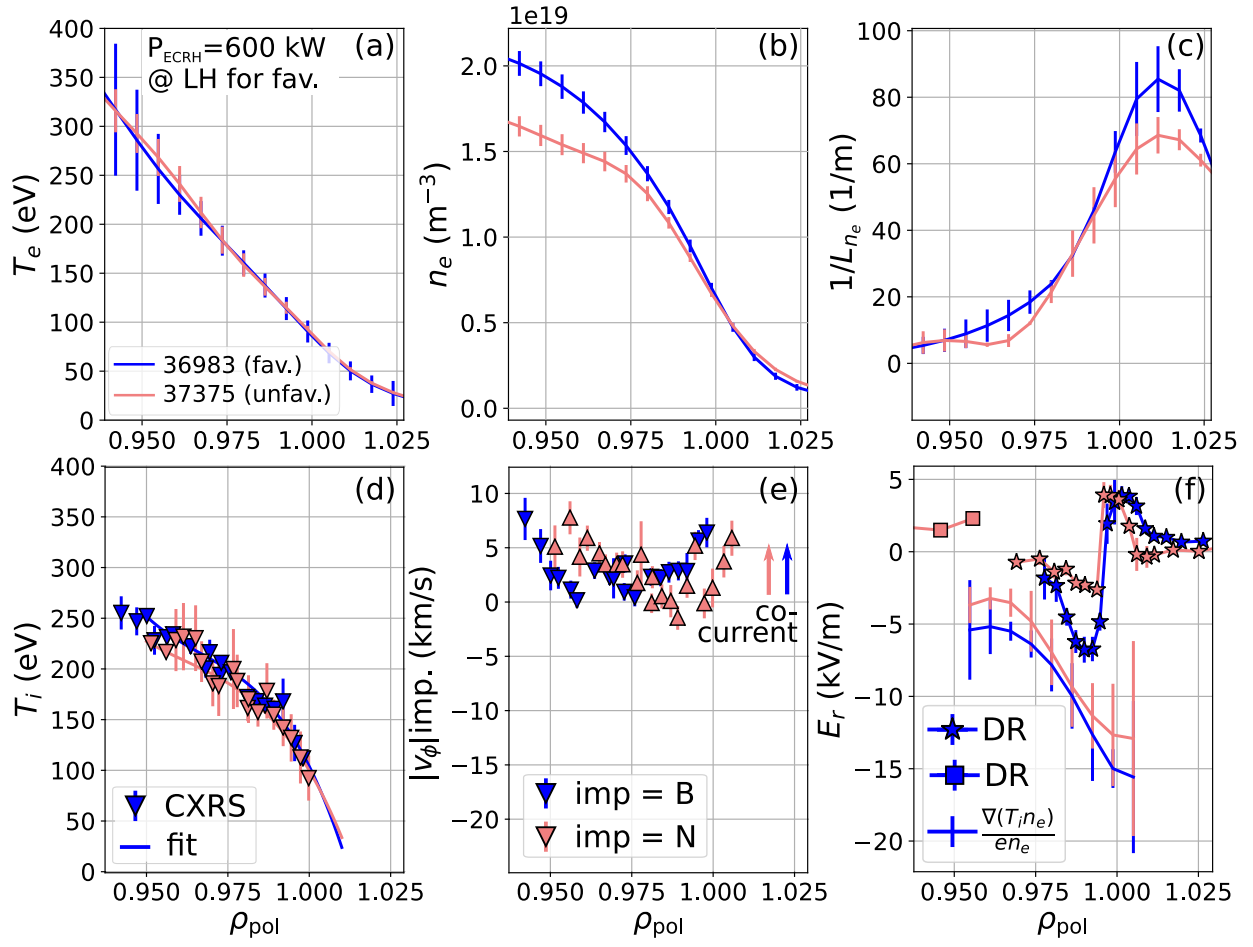
This is the author's peer reviewed, accepted manuscript. However, the online version of record will be different from this version once it has been copyedited and typeset.

PLEASE CITE THIS ARTICLE AS DOI: 10.1063/5.0102763



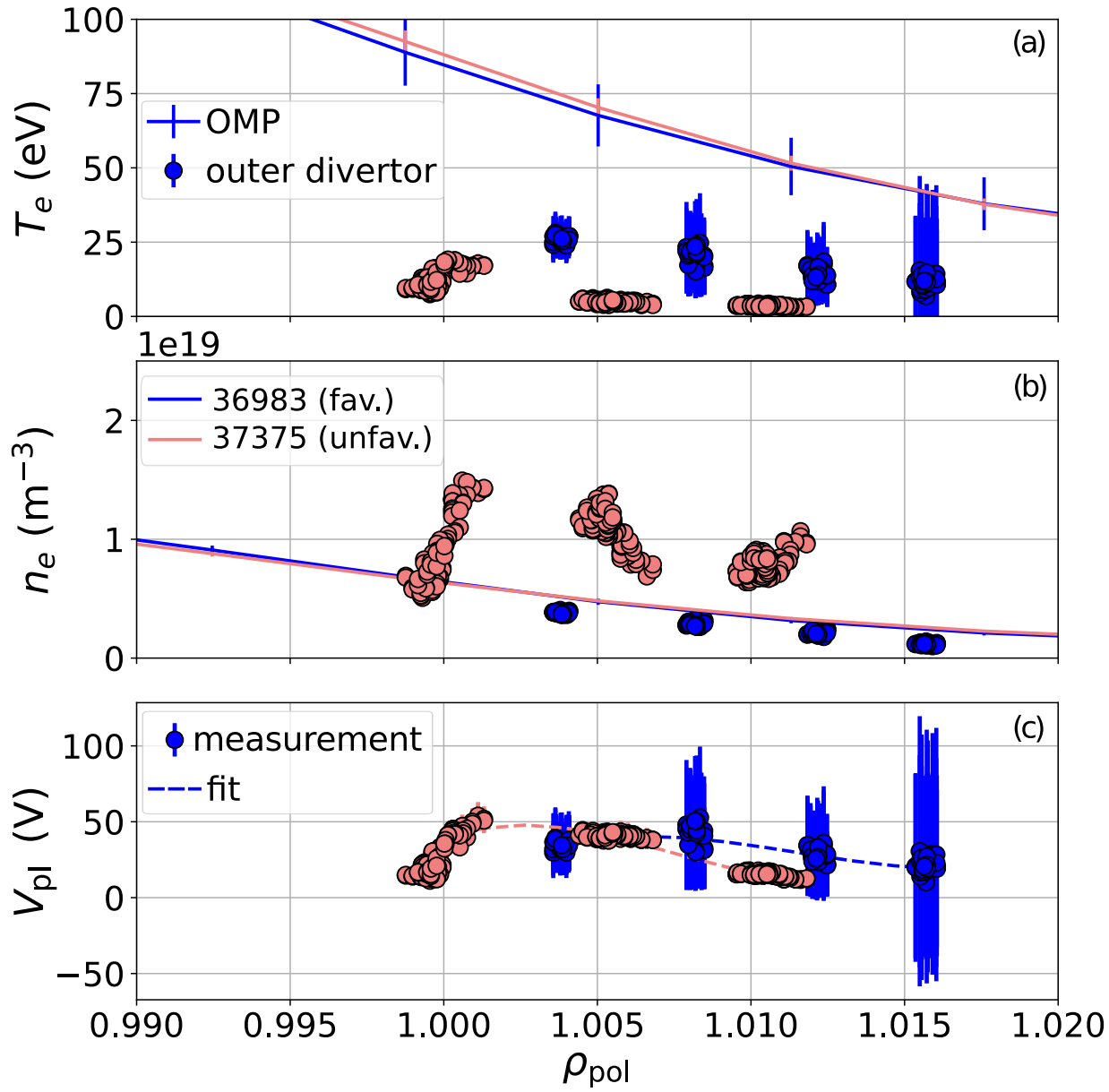
This is the author's peer reviewed, accepted manuscript. However, the online version of record will be different from this version once it has been copyedited and typeset.

PLEASE CITE THIS ARTICLE AS DOI: 10.1063/5.0102763



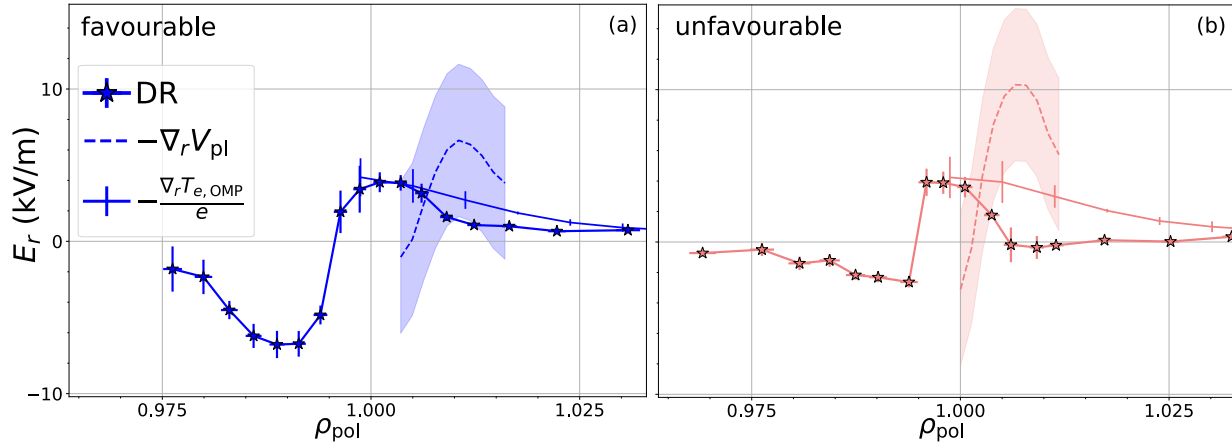
This is the author's peer reviewed, accepted manuscript. However, the online version of record will be different from this version once it has been copyedited and typeset.

PLEASE CITE THIS ARTICLE AS DOI: 10.1063/5.0102763



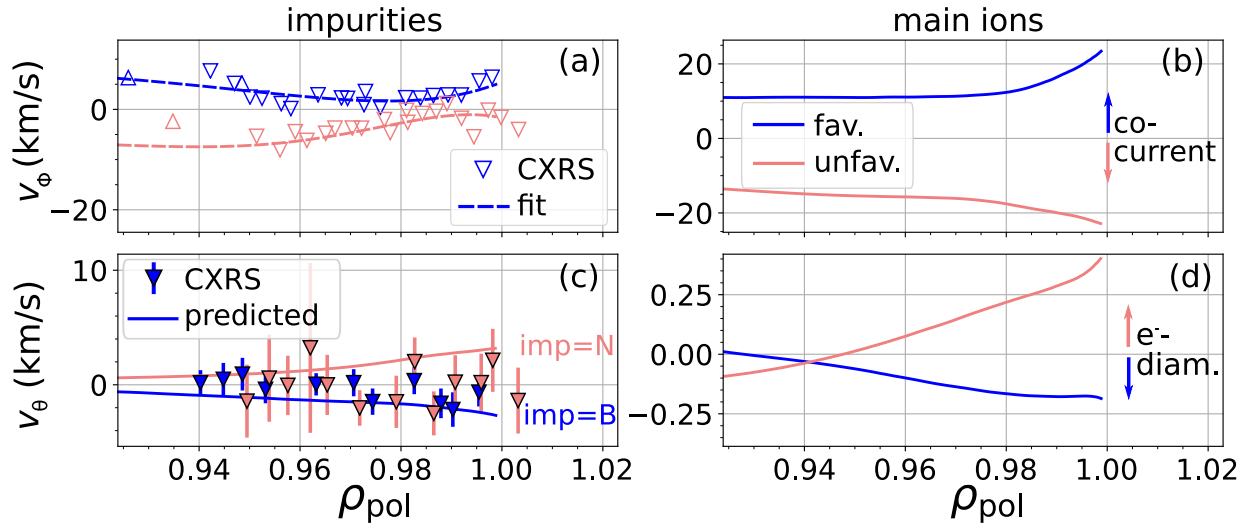
This is the author's peer reviewed, accepted manuscript. However, the online version of record will be different from this version once it has been copyedited and typeset.

PLEASE CITE THIS ARTICLE AS DOI: 10.1063/5.0102763

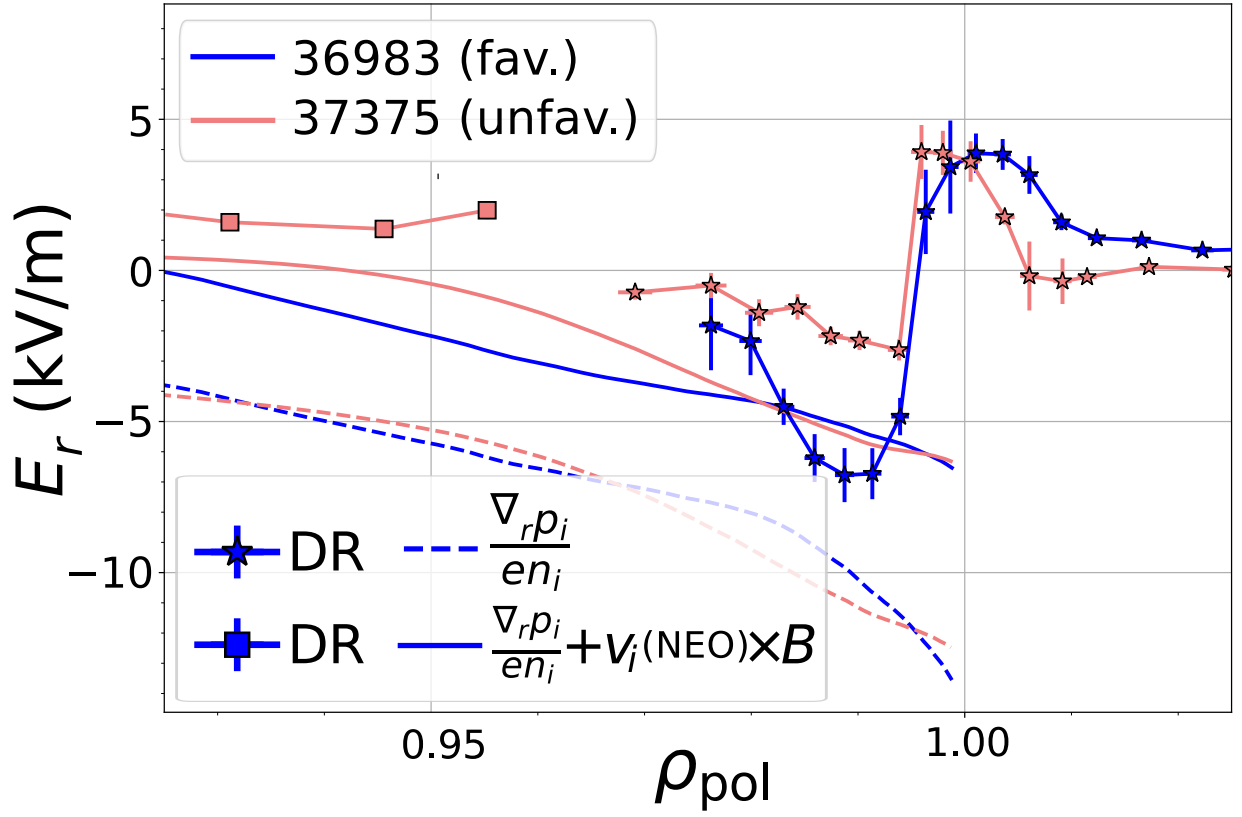


This is the author's peer reviewed, accepted manuscript. However, the online version of record will be different from this version once it has been copyedited and typeset.

PLEASE CITE THIS ARTICLE AS DOI: 10.1063/5.0102763

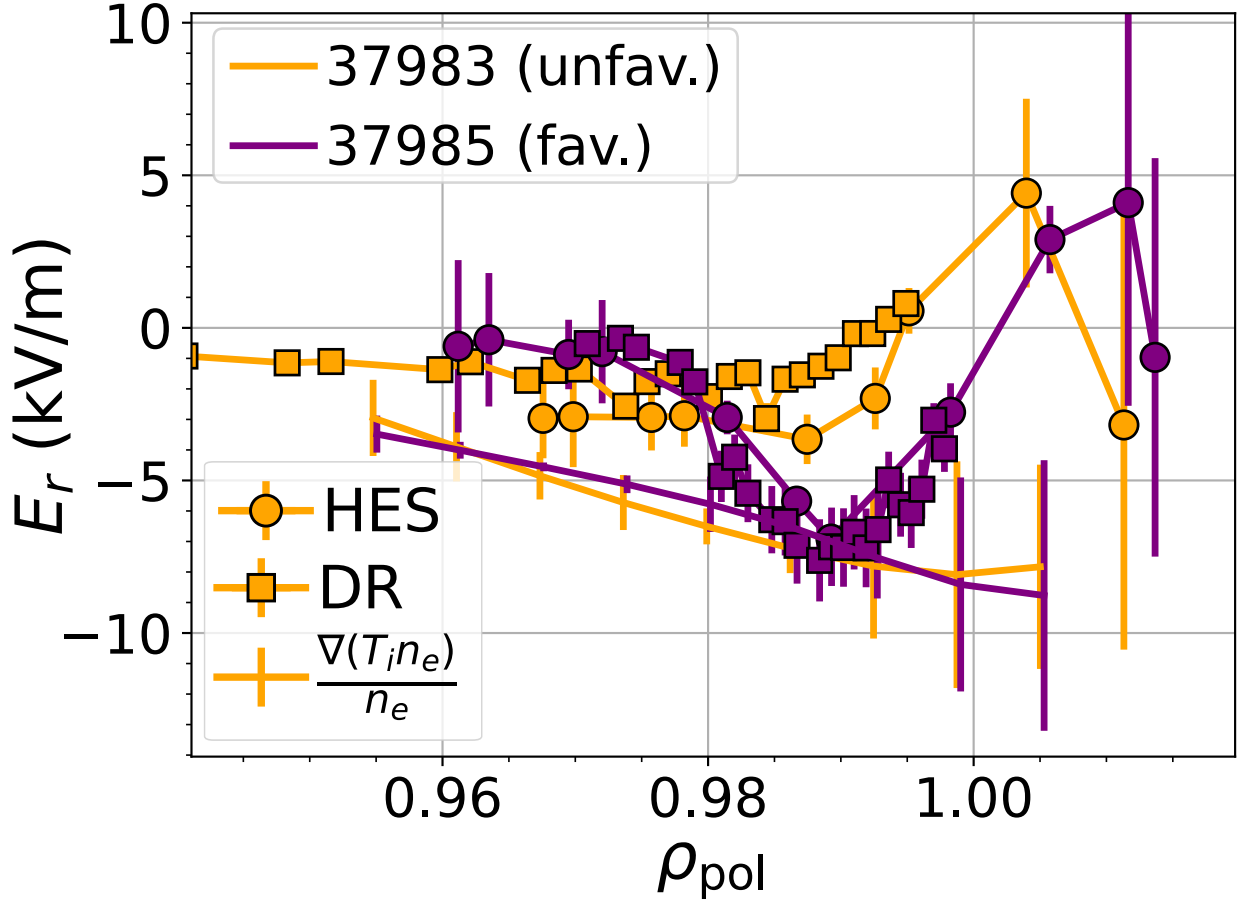


This is the author's peer reviewed, accepted manuscript. However, the online version of record will be different from this version once it has been copyedited and typeset.
 PLEASE CITE THIS ARTICLE AS DOI: 10.1063/5.0102763



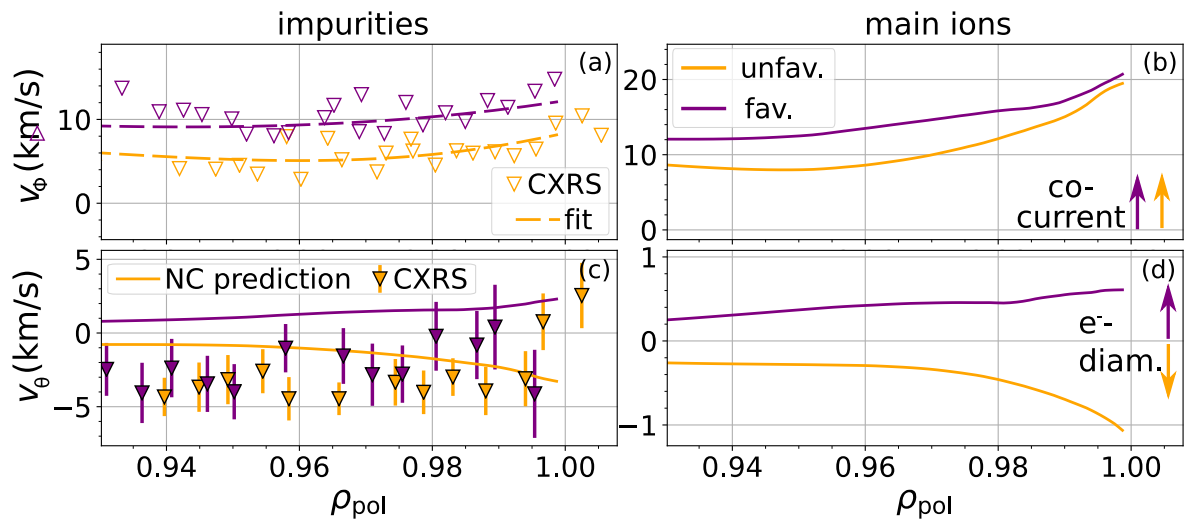
This is the author's peer reviewed, accepted manuscript. However, the online version of record will be different from this version once it has been copyedited and typeset.

PLEASE CITE THIS ARTICLE AS DOI: 10.1063/5.0102763

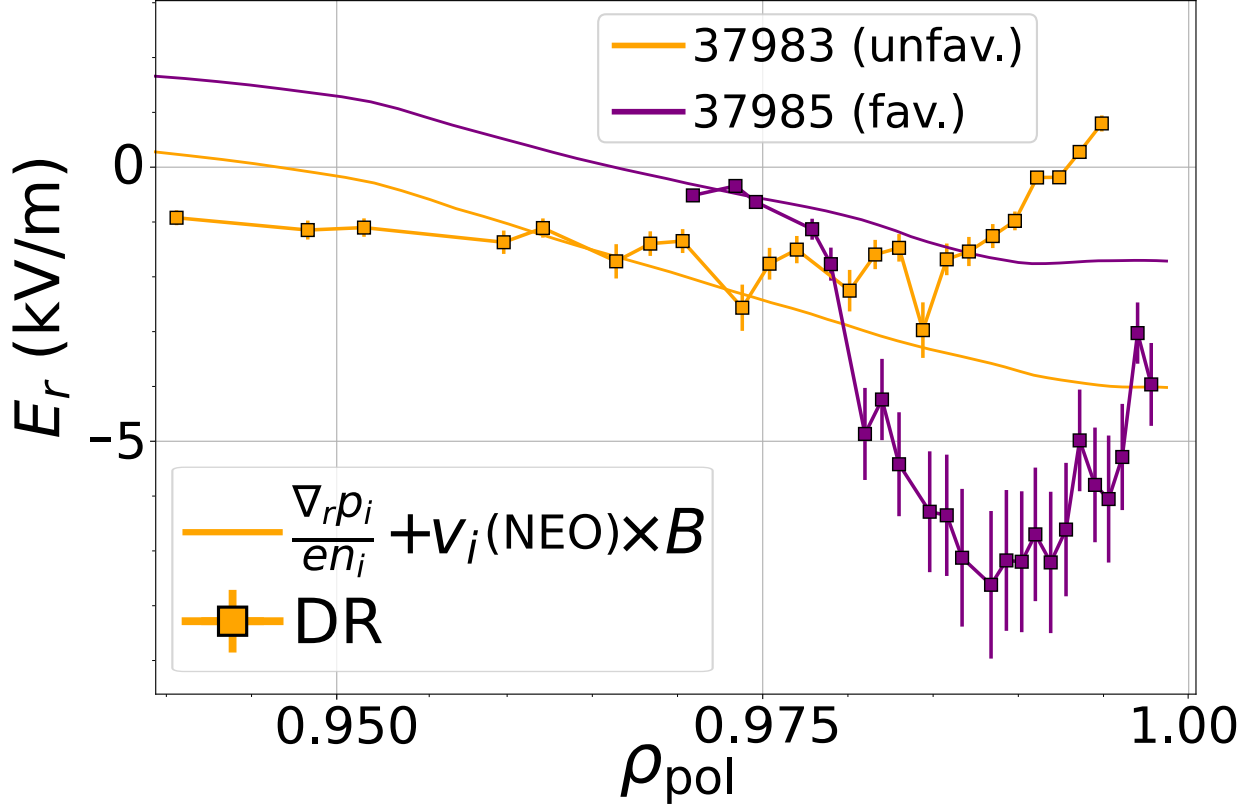


This is the author's peer reviewed, accepted manuscript. However, the online version of record will be different from this version once it has been copyedited and typeset.

PLEASE CITE THIS ARTICLE AS DOI: 10.1063/5.0102763

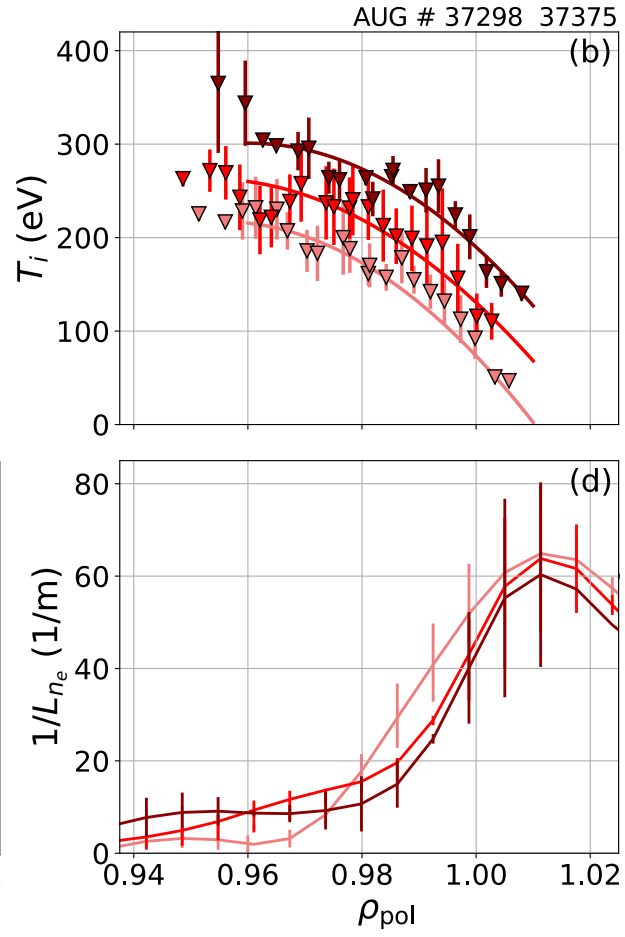
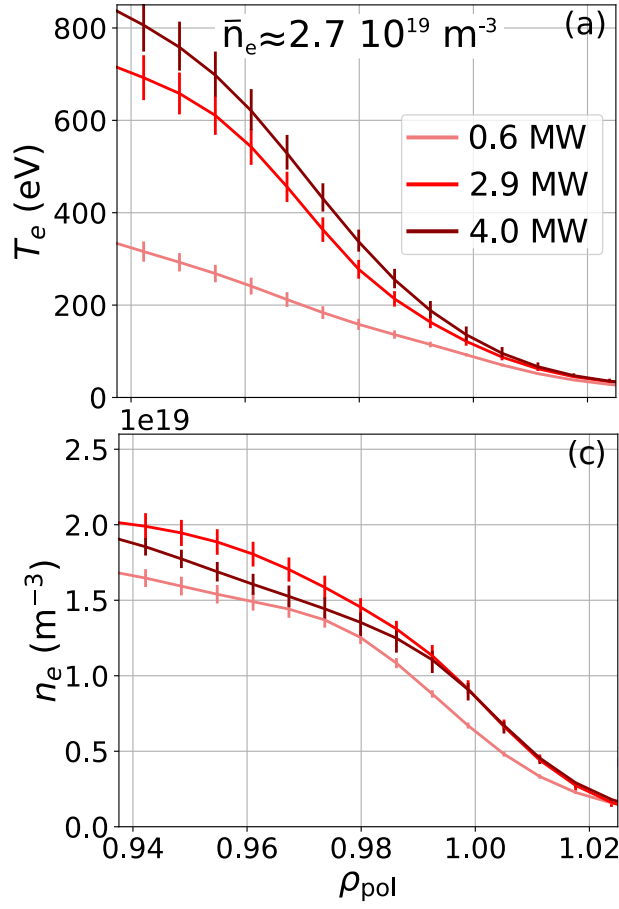


This is the author's peer reviewed, accepted manuscript. However, the online version of record will be different from this version once it has been copyedited and typeset.
 PLEASE CITE THIS ARTICLE AS DOI: 10.1063/5.0102763



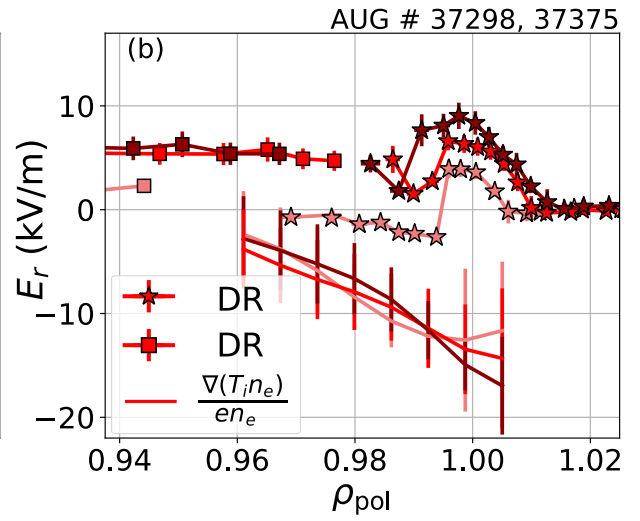
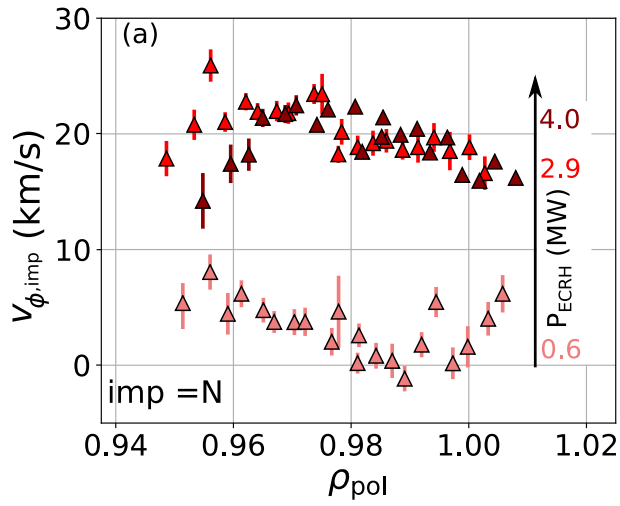
This is the author's peer reviewed, accepted manuscript. However, the online version of record will be different from this version once it has been copyedited and typeset.

PLEASE CITE THIS ARTICLE AS DOI: 10.1063/1.50102763



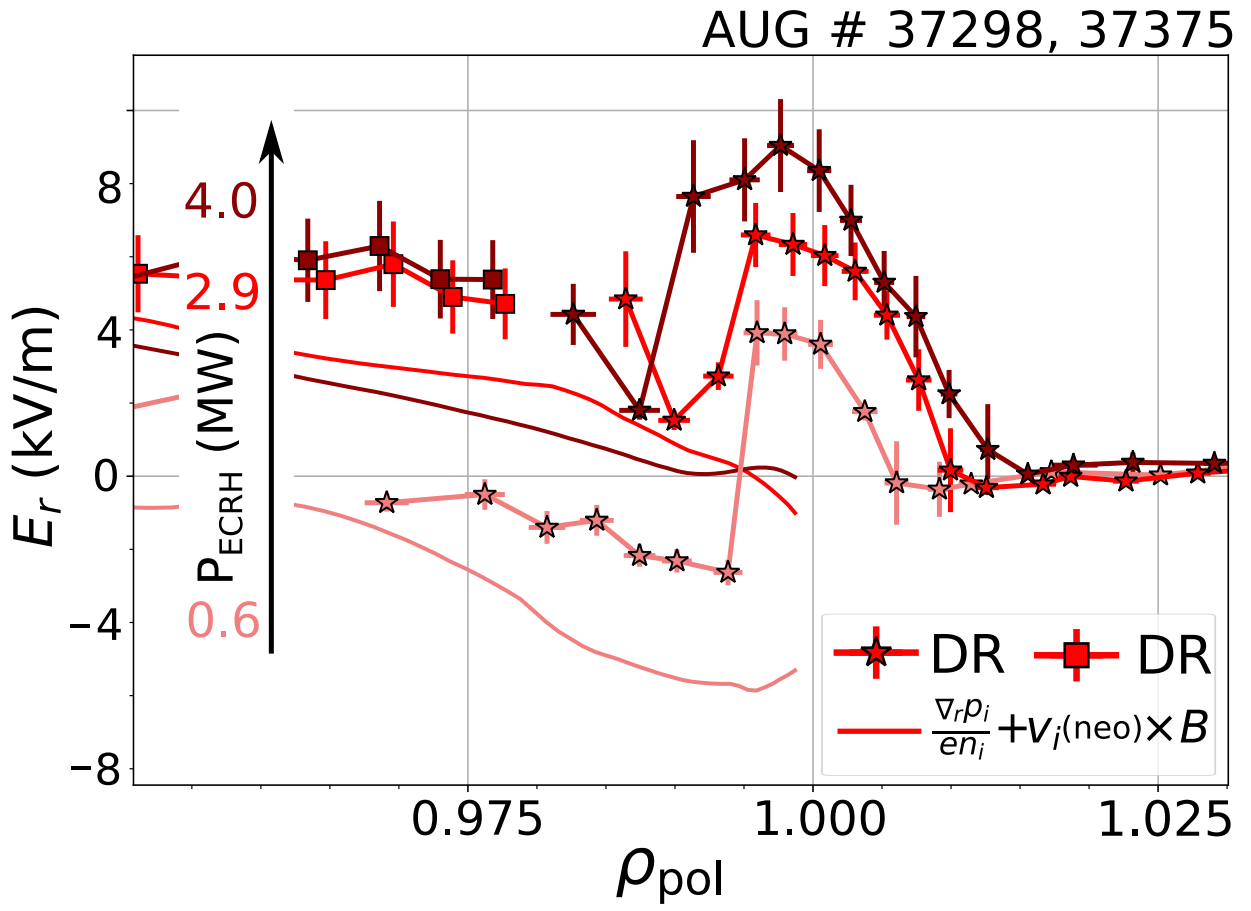
This is the author's peer reviewed, accepted manuscript. However, the online version of record will be different from this version once it has been copyedited and typeset.

PLEASE CITE THIS ARTICLE AS DOI: 10.1063/1.50102763



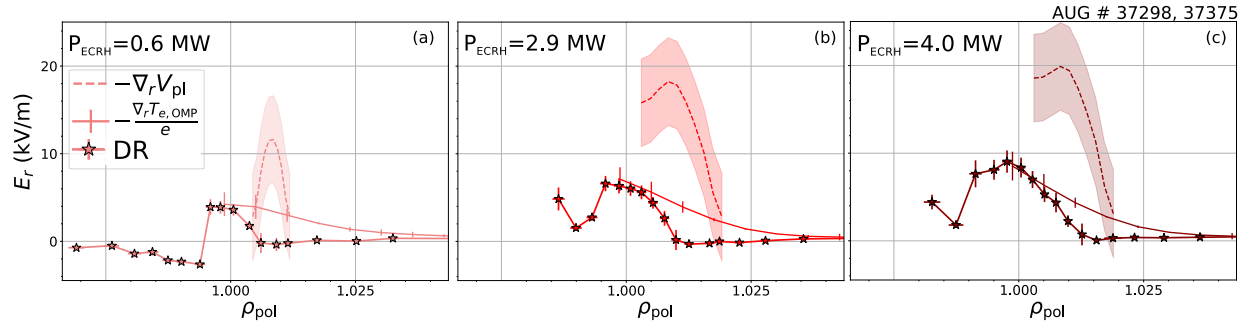
This is the author's peer reviewed, accepted manuscript. However, the online version of record will be different from this version once it has been copyedited and typeset.

PLEASE CITE THIS ARTICLE AS DOI: 10.1063/5.0102763

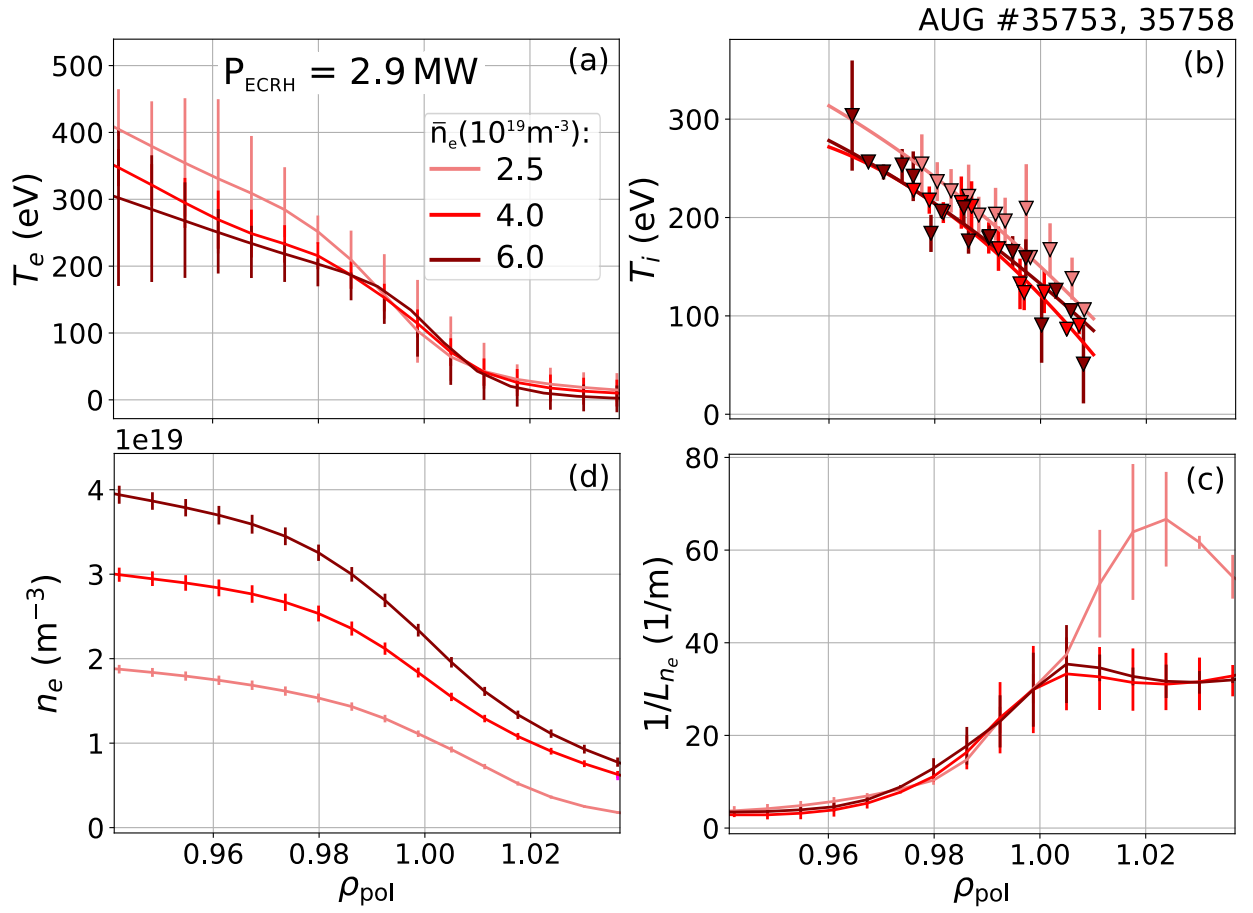


This is the author's peer reviewed, accepted manuscript. However, the online version of record will be different from this version once it has been copyedited and typeset.

PLEASE CITE THIS ARTICLE AS DOI: 10.1063/5.0102763

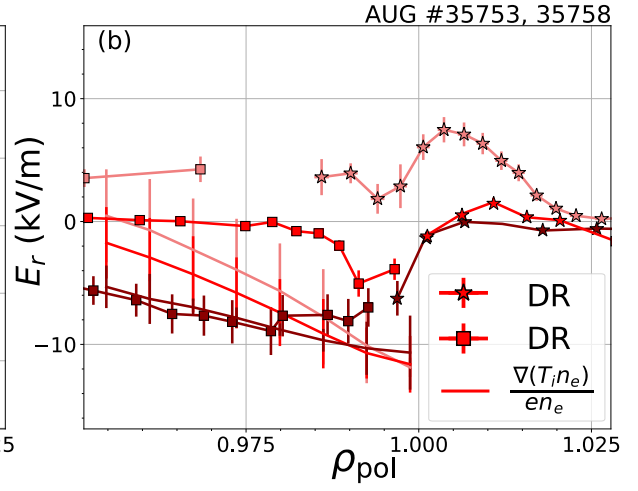
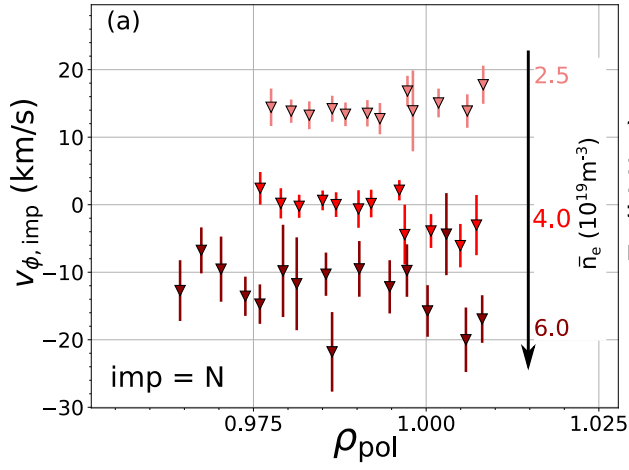


This is the author's peer reviewed, accepted manuscript. However, the online version of record will be different from this version once it has been copyedited and typeset.
 PLEASE CITE THIS ARTICLE AS DOI: 10.1063/1.50102763



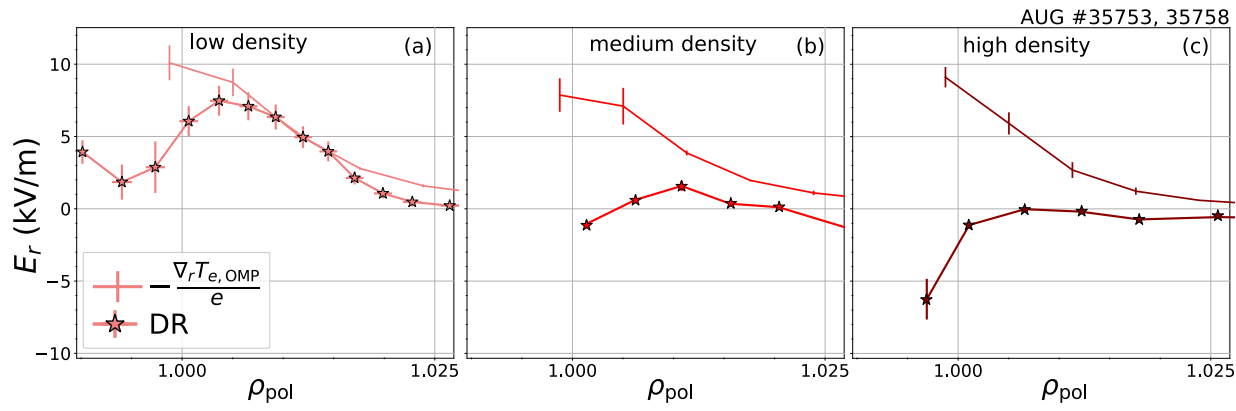
This is the author's peer reviewed, accepted manuscript. However, the online version of record will be different from this version once it has been copyedited and typeset.

PLEASE CITE THIS ARTICLE AS DOI: 10.1063/1.50102763



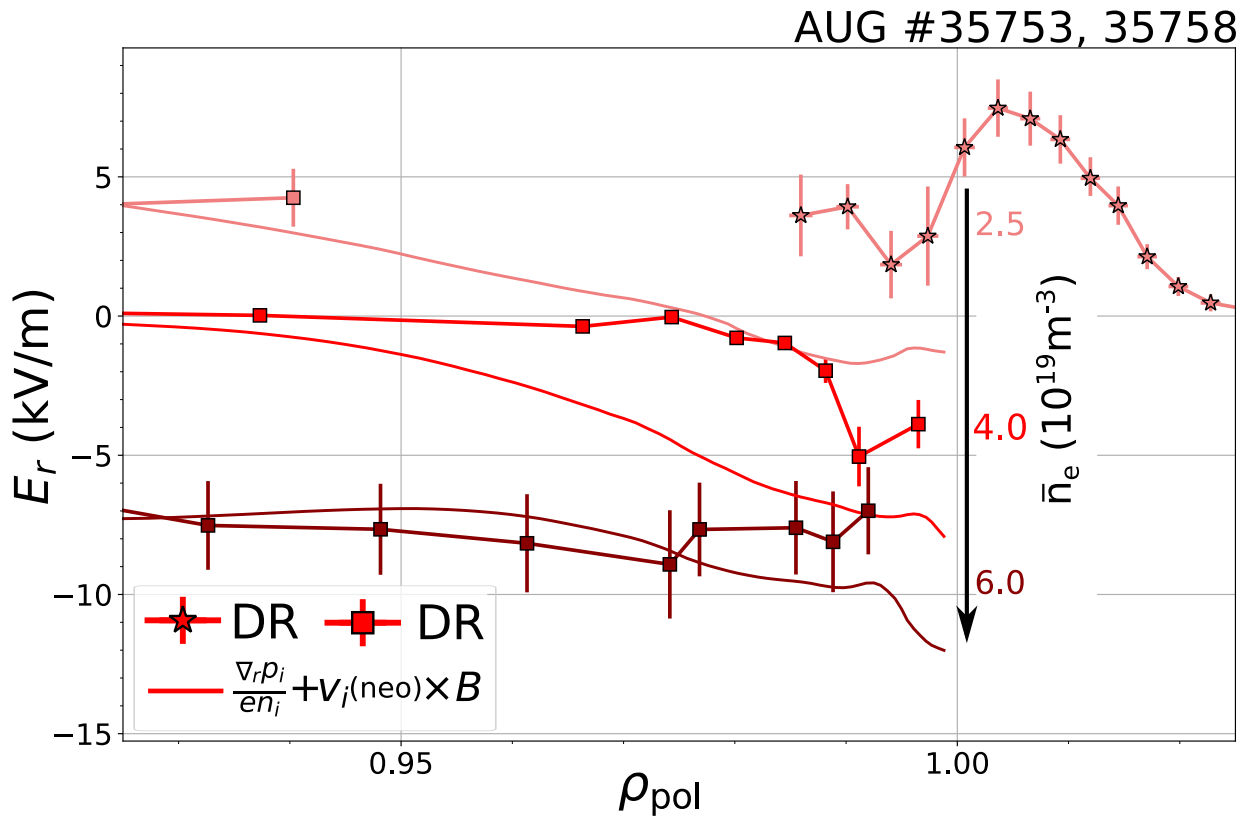
This is the author's peer reviewed, accepted manuscript. However, the online version of record will be different from this version once it has been copyedited and typeset.

PLEASE CITE THIS ARTICLE AS DOI: 10.1063/5.0102763



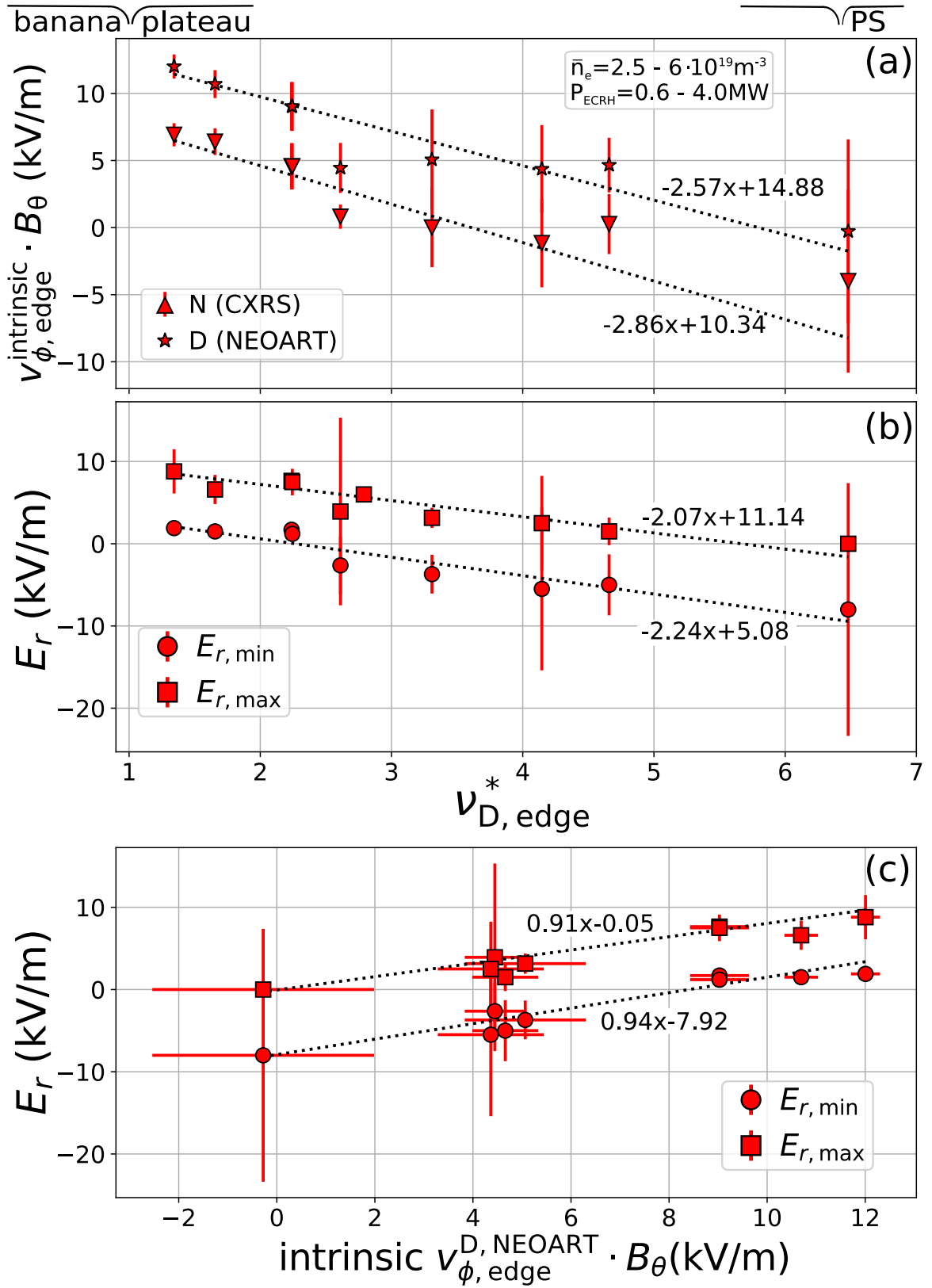
This is the author's peer reviewed, accepted manuscript. However, the online version of record will be different from this version once it has been copyedited and typeset.

PLEASE CITE THIS ARTICLE AS DOI: 10.1063/5.0102763



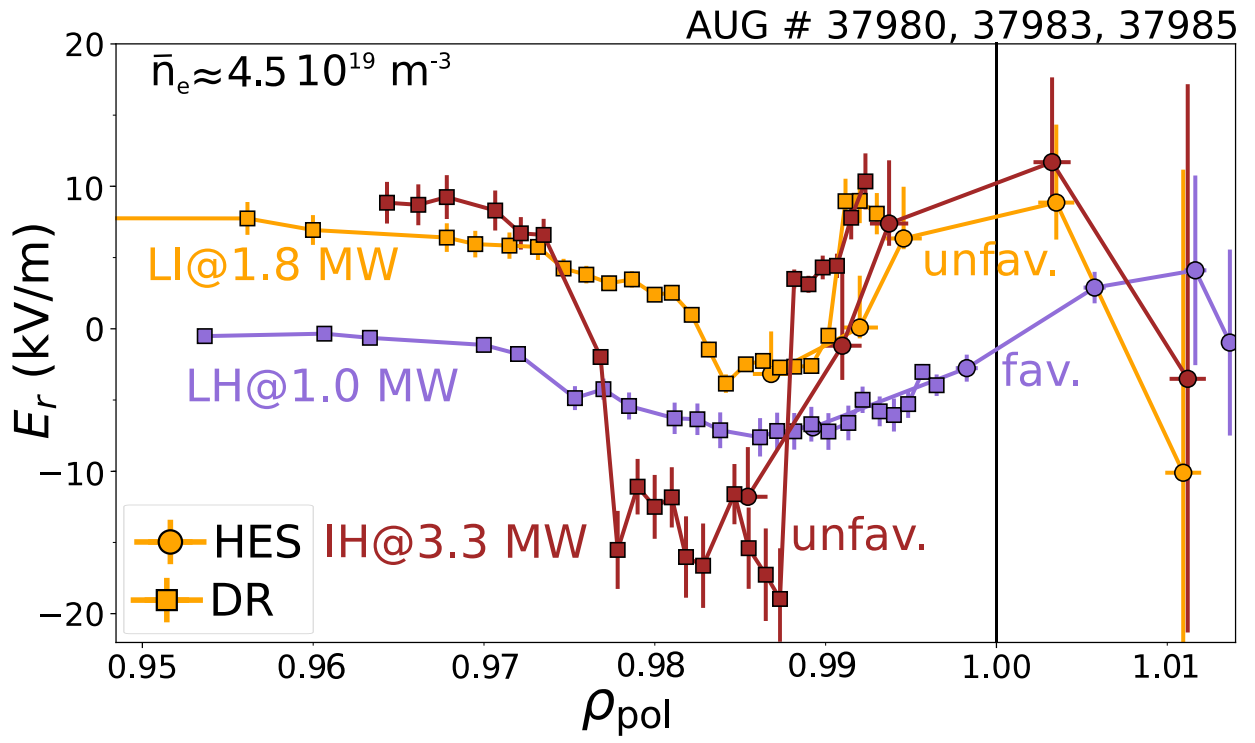
This is the author's peer reviewed, accepted manuscript. However, the online version of record will be different from this version once it has been copyedited and typeset.

PLEASE CITE THIS ARTICLE AS DOI: 10.1063/5.0102763



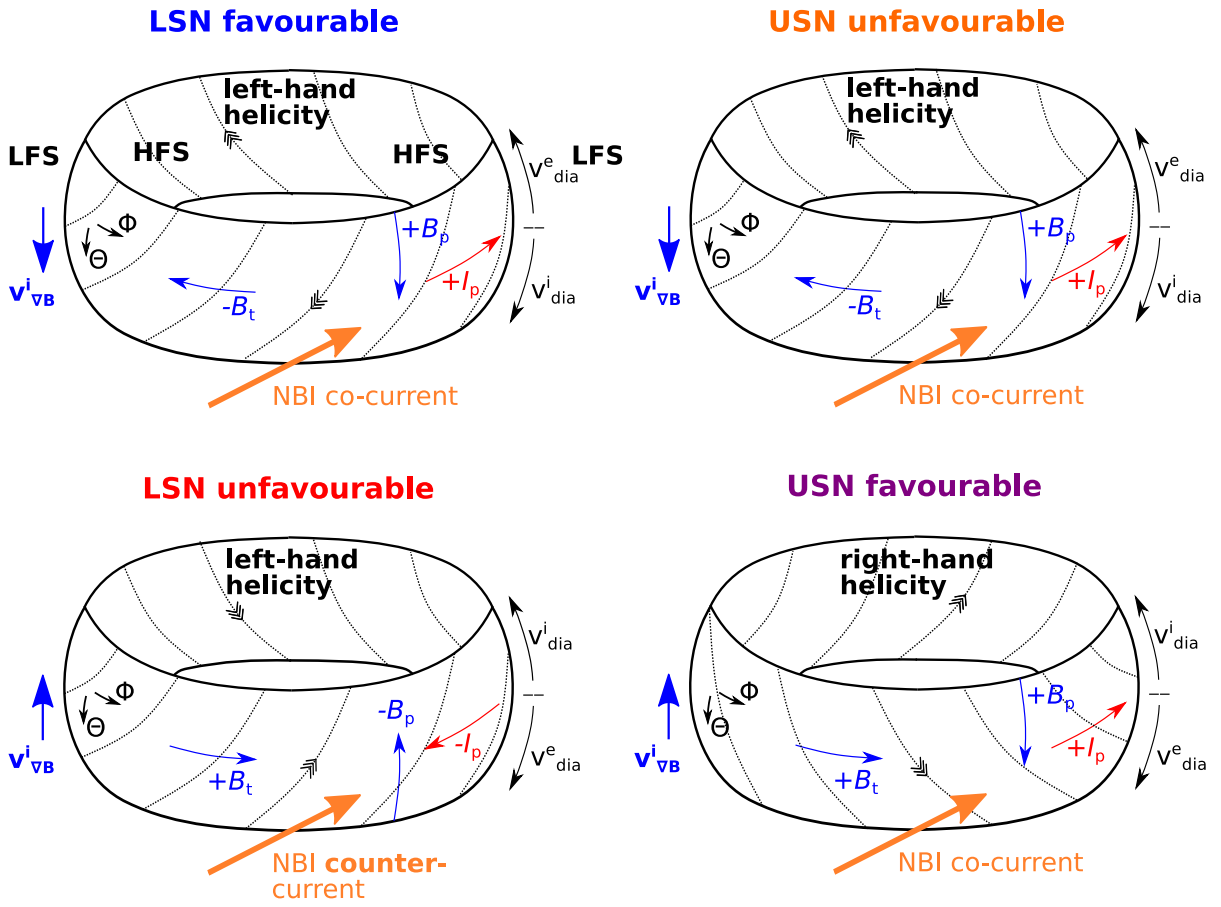
This is the author's peer reviewed, accepted manuscript. However, the online version of record will be different from this version once it has been copyedited and typeset.

PLEASE CITE THIS ARTICLE AS DOI: 10.1063/5.0102763



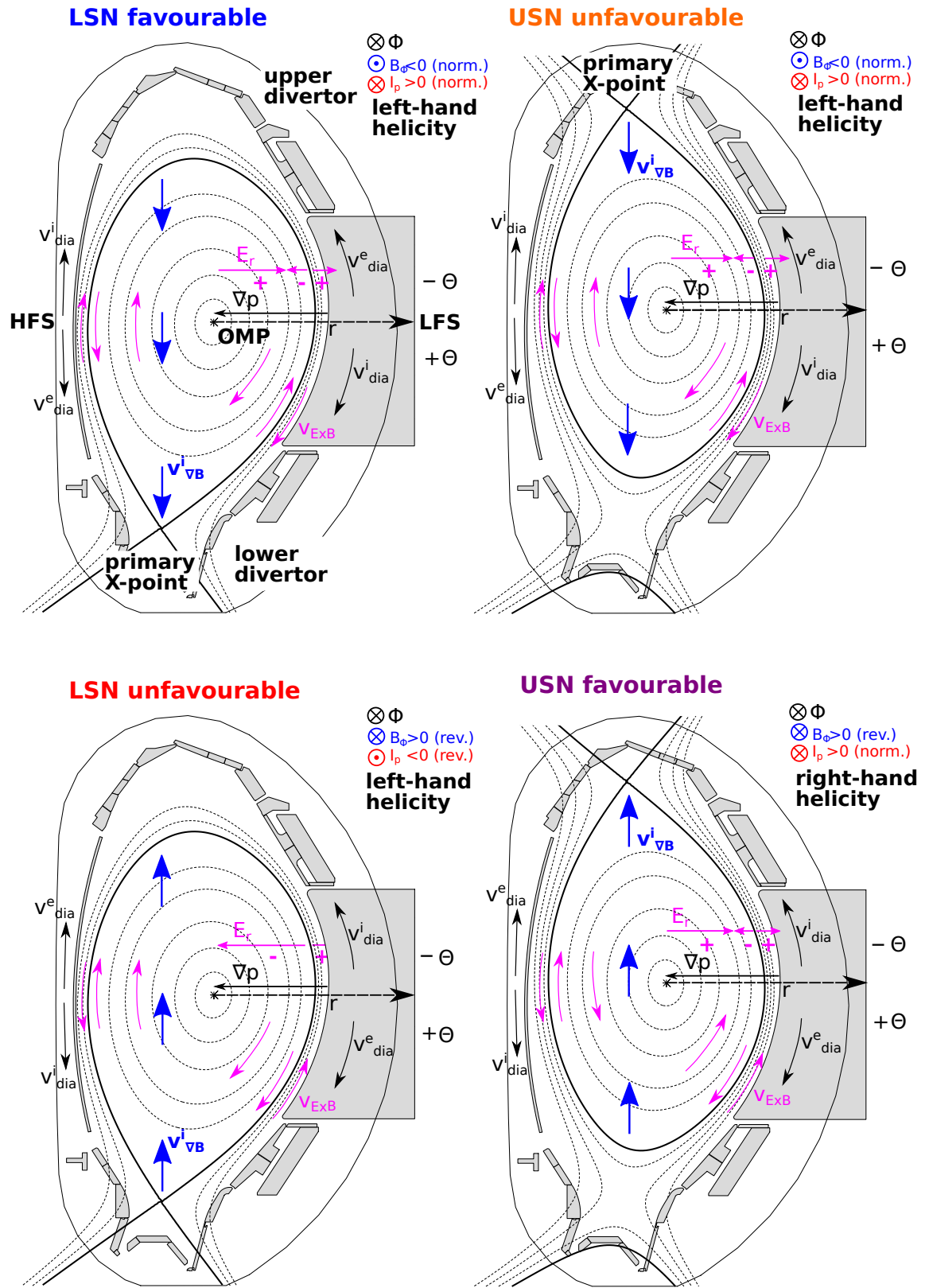
This is the author's peer reviewed, accepted manuscript. However, the online version of record will be different from this version once it has been copyedited and typeset.

PLEASE CITE THIS ARTICLE AS DOI: 10.1063/1.50102763



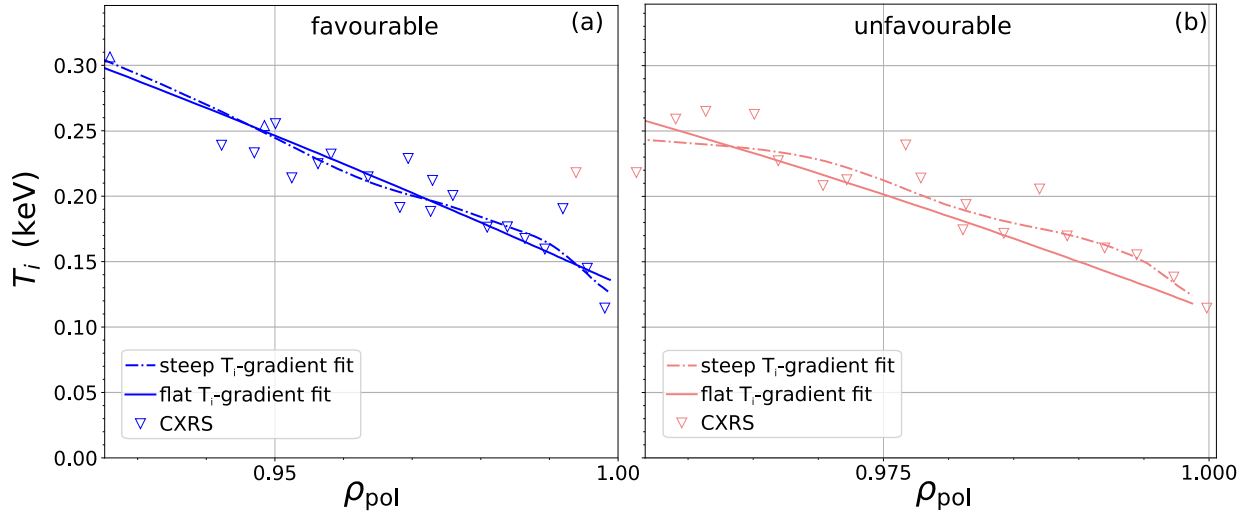
This is the author's peer reviewed, accepted manuscript. However, the online version of record will be different from this version once it has been copyedited and typeset.

PLEASE CITE THIS ARTICLE AS DOI: 10.1063/1.50102763



This is the author's peer reviewed, accepted manuscript. However, the online version of record will be different from this version once it has been copyedited and typeset.

PLEASE CITE THIS ARTICLE AS DOI: 10.1063/5.0102763



This is the author's peer reviewed, accepted manuscript. However, the online version of record will be different from this version once it has been copyedited and typeset.

PLEASE CITE THIS ARTICLE AS DOI: 10.1063/5.0102763

